1-1-2010

Application Of Magnetic Resonance Imaging To Understanding The Pathogenesis Of The X-Linked Leukodystrophy Pelizaeus-Merzbacher Disease

Jeremy Jerome Laukka
Wayne State University,

www.manaraa.com

APPLICATION OF MAGNETIC RESONANCE IMAGING TO UNDERSTANDING THE PATHOGENESIS OF THE X-LINKED LEUKODYSTROPHY PELIZAEUS-MERZBACHER DISEASE

by

JEREMY JEROME LAUKKA

DISSERTATION

Submitted to the Graduate School of

Wayne State University,

Detroit, Michigan

In partial fulfillment of the requirements

for the degree of

DOCTOR OF PHILOSOPHY

2011

MAJOR: MOLECULAR BIOLOGY AND GENETICS

Approved by:

_____
Advisor   **Date**

_____

_____

_____

_____

DEDICATION

This work is dedicated to my father, Warren J. Laukka and to my mother Donna Mae Laukka who served and blessed my life with love, faith and commitment to see that I become an individual of integrity and virtuous principles.

I also wish to dedicate this work to my beloved wife, Nicole L. Laukka for her unwavering support and commitment to our education and personal growth. This PhD is her graduate degree of honor and excellence.

"Along your pathway of life you will observe that you are not the only traveler. There are others who need your help. There are feet to steady, hands to grasp, minds to encourage, hearts to inspire, and souls to save."

 –Thomas S. Monson

ACKNOWLEDGMENTS

I would like to first thank my wife, Nicole L. Laukka for her love, devotion and commitment during the pursuit of this Ph.D. degree.

I would like to give a special and warm thank you to Jim Garbern, M.D., Ph.D. for his commitment to my professional goals of obtaining a Ph.D. It has been an honor and great scholastic opportunity to work under the tutelage of a distinguished scientist and clinician in the study of Pelizaeus-Merzbacher disease. His love and devotion to the families with PMD and those afflicted by other neurological disease will always be remembered and will never be matched. He is an example of a person with a high moral character and in my mind will be regarded as a person of honor and great integrity. I am most grateful for his patience during my own personal challenges and difficulties during the pursuit of this degree and for supporting decisions that will be the foundation for the rest of my life. Thank you!

I would also like to thank John Kamholz, M.D., Ph.D. for being a strong supportive committee member. Every conversation evolved into a learning moment. I walked away with a stronger knowledge and renewed mind set of meeting my next goal. He is a greater mentor, scientist, clinician, teacher and friend who will never be forgotten and will stand as a leading authority in the field of neurology. I would like to thank Bob Skoff, Ph.D. for being a great committee member and for also willing to sit with me and discuss my thesis work. His door was always open and he was a source of great knowledge and advice. He will always be regarding as a superior scientists, colleague and friend in my eyes. I would like to thank Kathy Lovell, Ph.D. for her willingness to serve on my committee. She provided outstanding support and wisdom

from her seasoned knowledge in the field of neuroscience and pathology. I look forward to working and learning from her during the next chapter of my life.

I would like to thank Ander Sima, M.D., PhD. For his Swedish smile and candid personality. He is a tremendous neuropathologist and teacher who took time to study the neuropathology tissue of PMD patients and to set me straight, when I thought I was correct!

I would like to thank Jas Sohi and Susan of Dr. Kamholz's lab for providing me with wonderful technical support and they did it with a smile! I would like to thank Denise from Dr. Skoff's lab for her excellent technical support in the processing and staining of brain tissue. She is always a reliable source of positive feedback…Most of the time! I would like to thank Deniz Altinok, M.D. for assisting in the reading interpretation of PMD neuroimaging. I appreciate his professionalism, out-going and respectful demeanor. He will always have my respect and it was a great honor to have collaborated with a seasoned and experienced neuroradiologists.

A special thank you goes to the Center of Molecular Medicine and Genetics, especially Dr. Grossman for assisting me with my Ph.D. training when times were challenging. Also, I would like to acknowledge Dr. Kapatos for being a great student advisor and for being receptive and understanding.

Finally, I would like to thank all of the PMD families for making it possible for clinicians and scientists to develop a greater knowledge of the pathogenesis and genetics of the disease, so that one day we may provide ways to monitor and investigate ways to improve the quality of life and the overall clinical outcome.

TABLE OF CONTENTS

LIST OF TABLES

LIST OF FIGURES

CHAPTER 1

INTRODUCTION

Interest in central nervous system (CNS) started in the 19th century. Rudolf Virchow (1821-1902), a German physician, was first to suggest the name 'myelin' when he described the sheaths that encircled axons. For several decades research in the field of myelin was dominated by pathology and continued to make instrumental advancement into the clinical and histological description of several demyelinating diseases. Many of the disorders with white matter involvement cannot be placed under the narrow concept of leukodystrophy, which implies inherited demyelinating disorder. The broader term "white matter disorders" and "leukoencephalopathies" are defined as all conditions in which predominantly or exclusively white matter is affected (van der Knaap 2001). Key concepts throughout this dissertation are (1) demyelination, used when there is loss of myelin; (2) hypomyelination, which means that too little myelin is formed and this deficiency is permanent; (3) dysmyelination, used when the process of myelination is disturbed, leading to abnormal, patchy, or irregular myelination.

The underlying genetic involvement is not fully understood in all types of leukodystrophies, and because phenotypic expression of the same genotype can also be variable, diagnosis of many leukodystrophies presents a considerable challenge. Leukodystrophies often express themselves within the first two years of life corroborating with the critical window of normal myelination (Barkovich 2000; Barker and Horska 2004). The diagnostics of cerebral white matter disorders was revolutionized by the advent of magnetic resonance imaging (MRI) in the late 1980s. While leukodystrophies were previously defined based on pathological findings alone, MRI has provided a powerful tool for investigating the cerebral white matter in living patients (van der Knaap, Smit et al. 1997). The previously known "classical"

leukodystrophies have been demonstrated to show characteristic patterns of MRI abnormalities (Cheon, Kim et al. 2002). MRI offers superior soft tissue contrast, multiple contrast mechanisms for improved tissue characterization, and artifact-free imaging of the brain stem and cerebellum. Advanced MR modalities such as diffusion tensor imaging (DTI), magnetization transfer (MTR) and proton magnetic resonance spectroscopy (H-MRS) are evolving as a primary diagnostic tool in the evaluation of leukodystrophies. MRI has changed the field entirely with it now possible to visualize white matter abnormalities in detail in living individuals and to incorporate what is known regarding the pathologic nature to provide a complete diagnostic description of the disease.

This dissertation will examine the role of conventional MRI and DTI to further characterize Pelizaeus-Merzbacher disease (PMD), which is a rare and progressive condition that is an X-linked recessive leukodystrophy of the central nervous system myelin. Furthermore, this work will examine the neuropathology of patients characterized by mutations affecting the *PLP1* gene and is instrumental in describing how CNS white matter pathology complements neuroimaging in characterizing PMD.

Pelizaeus-Merzbacher disease

Pelizaeus-Merzbacher disease (PMD) is a rare and progressive condition that is an X-linked recessive leukodystrophy of the central nervous system myelin. The underlying disturbance of myelination in PMD is attributed to the failure to form myelin (Seitelberger 1970; Seitelberger, Urbanits et al. 1996), rather than to breakdown of preexisting myelin as observed in multiple sclerosis (MS). PMD is caused by mutations of the proteolipid protein 1 (*PLP1*) gene found on chromosome Xq22 and manifests with a clinical heterogeneous phenotype that may

depend upon the location and type of mutation (Garbern, Cambi et al. 1999; Garbern, Cambi et al. 1999; Cailloux, Gauthier-Barichard et al. 2000; Hubner, Orth et al. 2005; Garbern 2007). The functional significance of PLP is its role as a major protein in CNS myelin, making up about half of the total myelin protein mass (Lees, Samiullah et al. 1984). Serving as an integral membrane protein, PLP is a structural protein acting as a strut that maintains the morphology of the intraperiod line of compacted myelin in the CNS (Duncan, Hammang et al. 1987; Boison and Stoffel 1994; Boison, Bussow et al. 1995; Griffiths, Klugmann et al. 1998). The exact type of *PLP1* mutation dictates the onset and severity of PMD and can be classified according to the mutational mechanisms, including the deletion/insertion of the entire gene (Pham-Dinh, Boespflug-Tanguy et al. 1993; Garbern, Cambi et al. 1999; Garbern, Moore et al. 2002), point mutations that affect splicing or regulation of gene expression and increased dosage of the *PLP1* gene (Ellis and Malcolm 1994; Sistermans, de Wijs et al. 1996; Sistermans, de Coo et al. 1998). In PLP1 related defects of myelination, the clinical severity of PMD varies from the severe 'connatal' form (Seitelberger, 1970) that begins during infancy to a much milder variant spastic paraplegia type 2 (SPG2) which has a relatively normal life span (Saugier-Veber, Munnich et al. 1994; Hudson 2003; Inoue 2004). The clinical description exhibits clinical and genetic heterogeneity which reflects X-linked recessive traits and distinct myelin pathology that begins at birth or early in infancy, representing the connatal and classical forms of PMD (Zeman, DeMyer et al. 1964; Seitelberger 1970; Koeppen, Ronca et al. 1987).

The most severe form, connatal PMD, (Seitelberger 1970) presents at birth or during the first few weeks of life with pendular nystagmus, hypotonia, respiratory distress, pharyngeal weakness and stridor. Affected males later develop significant spasticity and have little voluntary

muscle control. Cognitive impairment is likely. Pharyngeal weakness causes swallowing difficulties, and infants can have stridor, optic atrophy and seizures (Garbern 2005).

Classical form (Pelizaeus 1885; Merzbacher 1910) is the most common form of the disease, also present in infancy, usually within the first two to four months of life. Affected males develop nystagmus, hypotonia with lower extremity weakness, trunk and limb ataxia, and head titubation. The motor milestones are delayed, and children develop spastic quadriparesis. Most children never walk independently. Language function can be normal, although dysarthric, and cognitive impairments are common. The affected patients do not exhibit respiratory involvement and can survive at least until the sixth decade of life (Garbern 2005). In classical PMD, *PLP1* duplications comprise of 65-70% of the cases with mild to moderate severity (Inoue, Osaka et al. 1996; Sistermans, de Wijs et al. 1996; Inoue 2004). The *PLP1* gene dosage effect and clinical severity are linearly correlated indicated that the *PLP1* gene is dosage sensitive. Studies have found that three or more copies of the *PLP1* gene in patients have a more severe form of PMD (Wolf, Sistermans et al. 2005), while those that have a deletion of the *PLP1* gene or SPG2 have a relatively mild form of PMD.

A subset of patients with null mutations presents into the first 5 years of life with mild spastic quadriparaesis, mostly affecting the lower extremities (Garbern, Moore et al. 2002). Patients with the null syndrome are able to ambulate despite the increased tone. They have ataxia, but do not exhibit pendular nystagmus. While they have mild to moderate cognitive difficulties, language skills develop initially. The PLP1 null syndrome is further distinguished from other forms of PMD by the presence of a mild demyelinating peripheral neuropathy (Garbern 1999).

White matter

The CNS tissue is comprised of grey matter structures and an extensive array of connecting white matter tracts. The white matter is made up of myelinating axons, a large number of glial cells and vasculature that supply nourishment. The glial cells include oligodendrocytes, which are myelin-forming cells, astrocytes, which are responsible for the blood-brain barrier and other functions, and microglia cells, which have phagocytic function. Understanding the complexity of glial cell function is evolving. On a dry weight basis, 40-50% of white matter is myelin (Baumann and Pham-Dinh 2001).

Myelin is a modified plasma membrane that spirally wraps and insulates the axons (Fig 1). Each myelin sheath is composed of multiple segments which are modified extensions of oligodendrocytes. Myelination in the CNS is differs from that of the PNS in that a single oligodendrocyte can myelinate up to 50 different internodal segments on neighboring axons. The myelinated axons under electron microscopy (Arroyo and Scherer 2000) shows the myelin sheath composed of multiple plasma membrane layers with the opposed membranes forming the intraperiod line with a the thin space between the adjacent myelin leaflets contiguous with the extracellular space (Fig. 1). The myelinated axons are completely covered by myelin except in <1µm gaps known as nodes of Ranvier that contain a cluster of voltage-gated sodium channels essential for saltatory conduction of electrical impulses (Black, Kocsis et al. 1990; Arroyo and Scherer 2000; Arroyo, Xu et al. 2001).

To discriminate between the various mechanisms involved in the sorting and transport of myelin components and how they related to disease pathogenesis, it is relevant to first provide insight into the molecular composition of the myelin sheet. During myelin formation, OLGs mature in a process in which development stages can be identified (Fig 1.1). The cells

differentiate from bipolar progenitor cells (O2A stage) to a cell with branched processes (GalC stage), when the earliest myelin specific protein 2', 3'-cyclic nucleotide 3' phosphodiesterase is expressed (Pfeiffer, Warrington et al. 1993). Maturation into myelin forming OLGs and the assembly of the myelin sheath as such is characterized by the sequential expression of the proteins that make up the myelin, including myelin-associated glycoprotein (MAG), myelin basic protein (MBP), proteolipid protein (PLP) and myelin oligodendrocyte glycoprotein (MOG) Pfeiffer, Warrington et al. 1993).

Myelin can be considered to be subdivided into a compact region, responsible for its physical insulation properties and a non-compact region called the radial component (Arroyo and Scherer 2000). The compact myelin is formed by the apposition of the external faces of the membrane of the myelinating cell, forming the intraperiodic line; the apposition of the internal faces, followed by extrusion of cytoplasm, gives rise to the formation of the major dense line (Fig 1.2). A tight junctional array is located between compact and non-compact myelin, which likely serves as a diffusion barrier between these myelin subdomains (Gow, Southwood et al. 1999; Morita, Sasaki et al. 1999). The compact region is enriched with glycosphingolipid galactocerebroside and sulfatide. In this region, the major myelin proteins are proteolipid protein (PLP) and myelin basic protein (MBP), accounting for 50% and 30% of the total protein mass, respectively (Garbern 1999).

PLP1 **gene and proteolipid protein**

The PLP1 gene is composed of seven exons that extend over 17 kb of genomic sequences located on chromosome Xq22 (Diehl, Schaich et al. 1986). Expression of PLP1 dominates in the CNS OLGs lineage and correlates with the onset of myelination that begins during the 3rd

trimester of pregnancy in humans (Inoue 2004). The alternative splicing of the *PLP1* gene generates two proteins, PLP and DM-20 which lacks amino acids 116-150 of the PLP sequence (Nave, Lai et al. 1987). The proteoplipid protein is the major integral membrane protein of CNS myelin (Griffiths, Klugmann et al. 1998). PLP spans the membrane four times (Fig. 1.3) and is highly hydrophobic with 50% hydrophobic amino acids (Popot, Pham-Dinh et al. 1991; Weimbs and Stoffel 1992). As a structural protein, PLP plays a major role in assembly and stabilization of the myelin sheath in that the proteins brings about the correct apposition of the extracellular myelin leaflets, thereby stabilizing the multilayer membrane structure after compaction (Duncan, Hammang et al. 1987; Boison and Stoffel 1994; Boison, Bussow et al. 1995; Griffiths, Klugmann et al. 1998; Bizzozero, Bixler et al. 2001; Rosenbluth, Nave et al. 2006). Surprisingly, mice lacking PLP1 and DM20 are not critical for oligodendrocyte differentiation and assembly of CNS myelin (Boison, Bussow et al. 1995; Klugmann, Schwab et al. 1997). However, ultrastructural examinations of myelin in both knockout mice and patients with a deletion of the *PLP1* gene have shown myelin to be physically fragile (Boison and Stoffel 1994; Klugmann, Schwab et al. 1997). Furthermore, in hereditary spastic paraplegia and the absence of PLP in mice and PMD patients not only causes structural instability, but causes axonal injury resulting in late-onset axonal swellings and degeneration without any significant reduction in myelin (Garbern, Moore et al. 2002; Deluca, Ebers et al. 2004). PLP1 point mutations results in premature arrest of OLGs differentiation and early death, while overexpression of the normal PLP1 gene in transgenic mice leads to severe dysmyelination (Kagawa, Ikenaka et al. 1994; Readhead, Schneider et al. 1994). In humans, a variety of mutations, including missense mutations (Cailloux, Gauthier-Barichard et al. 2000), deletions (Raskind, Williams et al. 1991; Garbern, Cambi et al. 1997; Garbern, Yool et al. 2002) and duplications (Wolf, Sistermans et al.

2005) are known to cause the dysmyelinating disorder PMD and spastic paraplegia (Saugier-Veber, Munnich et al. 1994; Inoue, Khajavi et al. 2004). Gene duplications of the human PLP locus are responsible for the majority of the cases leading to enhanced expression of the PLP1. Although it is evident that PLP plays a vital role in myelin assembly and maintenance, on a functional and molecular level, its precise role remains undefined.

Trafficking of PLP

PLP and its alternatively spliced isoform DM20 are synthesized in the endoplasmic reticulum (ER) and subsequently transported via vesicles to the Golgi, followed by transport to the compact internodal region of the myelin sheath. Upon removal from the Golgi, PLP1 is now assembled together with cholesterol and galactocerebroside-enriched membrane domains in myelin rafts during transportation to be inserted into oligodendrocytes membrane. Point mutations, mostly resulting from missense amino acid substitutions comprised of 15- 20% of the genetic abnormalities responsible for PMD. Clinical phenotypes are quite variable extending from mild (SPG2) to severe (connatal PMD). Majority of *PLP1* point mutations cause more severe dysmyelinating and demyelinating disease rather than that caused by null mutations that suggest the absence of functional PLP is not involved in the proper maintenance of myelinating axons and not from a cytotoxic effect of mutant protein. Mutant PLP has been demonstrated that misfolded protein accumulates in the ER inducing the unfolded protein response (UPR) (Gow, Southwood et al. 2002; Southwood, Garbern et al. 2002) and not allowing the protein to reach the Golgi to interact with cholesterol and other lipids into myelin rafts (Simons, 2000). Because of the retention and failure to transport PLP the oligodendrocyte cell membrane this mechanism is considered to cause premature oligodendrocyte death (Gow, Southwood et al. 1998). The

trafficking of both PLP/DM20 results in a severe clinical phenotype compared to a milder phenotype (SPG2), which results from an accumulation of PLP1 and not DM20 (Southwood, Garbern et al. 2002). Protein misfolding and activation of the UPR is not an unknown entity unique to just PMD, but it is also found in other neurodegenerative diseae such as Alzheimer's disease and Parkinson disease (Hoozemans, Veerhuis et al. 2005; Hoozemans, van Haastert et al. 2007; Hoozemans, van Haastert et al. 2009). Unlike missense mutations, there are no spontaneous animal models for PLP1 gene duplications, but transgenic mice have been generated by (Kagawa, Nakao et al. 1994; Readhead, Schneider et al. 1994). The homozygous mice with high PLP1 gene dosage exhibit a severe early-onset dysmyelination with increased oligodendrocyte cell death, which maybe due to the accumulation of PLP1 in late endosome/lysosomes. The exact pathogenesis is not fully understood, but the imbalance in transport and assembly of myelin constituents adversely affects myelin assembly in the Golgi (Garbern 2007). The severe dysmyelinating pattern and clinical phenotype found in homozygous mice have also been identified in patients with three or more copies of PLP1 (Wolf, Sistermans et al. 2005). On ther other hand, hemizygous mice with a lower copy number develops normally with no clinical signs until later in life. The clinical signs develop later in life due to the late onset demyelination and axonal shperoids and degeneration (Anderson, Schneider et al. 1998). Taken together, the pathologic and clinical severity is similar to that of PLP1 knockout mice relfecting the sensitivity to changes in gene dosage of 'too much or none at all.'

Magnetic resonance imaging investigation of white matter disorders

MRI is very sensitive in showing signal abnormalities in the white matter. Apart from myelin disturbances (hypomyelination, dysmyelination, and demyelination), damage to other components of the white matter may contribute to the observed signal abnormality. These include edema, seen for

instance in conjunction with increased vascular permeability, and gliosis, which occurs when astrocytes react to diverse forms of injury (van der Knaap 2001).

T_1-weighted images are used to assess the anatomic structures. During the early phases of myelination, small amounts of myelin are better visualized on T_1-weighted images. On these images, normally myelinated white matter appears bright and cerebrospinal fluid (CSF) is black. Pathological white matter gives a decreased signal and appears dark on T_1-weighted images.

T_2-weighted images are superior in showing the pathological processes of white matter. For subjects aged 9-10 months or beyond, T_2-weighted images are more useful in evaluating the stage of myelination. Normal myelinated white matter appears dark and CSF is bright on these images. Pathology in the white matter leads to an abnormally high signal on T_2-weighted images.

FLAIR (Fluid attenuated inversion recovery) is a T_2-weighted sequence, where the signal of the free fluid, e.g. CSF, is nullified. In these images, the CSF is black and myelinated white matter is dark. If white matter is pathologic, it appears hyperintense and especially periventricular lesions are easily distinguished. The cystic nature of the lesions is also revealed by FLAIR images.

As the white matter myelinates, it changes from hypointense (dark) to hyperintense (bright) relative to gray matter on T_1-weighted images and from hyperintense to hypointense relative to gray matter on T_2-weighted images. These changes in signal intensity are caused by increasing brain lipid concentration and decreasing water content (Barkovich 2000). The myelin signal appears earlier on T_1-weighted images. In a newborn, myelin is seen in the posterior limbs of the internal capsules and in the dorsal brainstem (Fig 1.4). During the first year of life, progressive myelination is seen, with sensorimotor and visual pathways maturing first and subcortical association areas maturing last (Fig 1.4) (Barkovich 2005). By the age of 24 months, myelination appears essentially mature in MRI (Barkovich 2000).

Myelination Milestones

Myelination within the CNS begins approximately the fourth month of fetal development at the cervical levels of the spinal cord. In the brain, myelination begins approximately the sixth month of gestation and is known to be limited to the region of the basal ganglia. The trend for myelination evolves more rapidly in areas of the brain linked to functional systems that are utilized during early periods of life, such as motor behavior (Barkovich 2005). Myelination progress is from caudal to cephalad and from dorsal to ventral. Thus, the occipital lobes of the cerebral hemispheres myelinate early while the frontal lobes myelinate late. White matter changes are seen best on T_1-weighted images during the first six to eight months of life and T_2-weighted images are best to evaluate myelination between six and eighteen months of life.

T_1-weighted MRI of maturing white matter found in figure 1.4 shows the striking feature that much of the brain remains unmyelinated in a neonate. However, an increase in white matter signal intensity is observed in the newborn at the level of posterior aspect of the posterior limb of the internal capsule. Around 5 month of age, the corticospinal tracts of the posterior limb of the internal capsule becomes more pronounced expressing hyperintensity of white matter seen throughout both the anterior and posterior limbs of the internal capsule. Continuing on to the 8th month, the deep white matter appears hyperintense, however the subcortical white matter from the frontal to occipital poles remains hypointense (Barkovich 2005). The peak of myelin formation rapidly occurs during the first 24 months of postnatal development, however, myelination can precede slowly through the second decade of life in some cortical fibers, predominately those tailored to associative areas (Baumann and Pham-Dinh 2001).

An understanding of the development and structure of myelin is helpful in explaining the change in white matter signals during brain development and thus in improving the reliability to

differentiate demyelination vs. dysmyelination disorders. Furthermore, the location of myelin disturbances is critically important to disease phenotype. Often abnormal MRI signal intensities may precede clinical signs of the disease. Leukodystophies such as PMD are aggressive and can produce distinct patterns of abnormalities on MRI that can help distinguish them.

The myelination milestones of various white matter structures (Table 1) becomes pivotal in understanding and describing cerebral white matter abnormalities found in many inherited diseases. Among the "classical" leukodystrophies, metachromatic leukodystrophy, Krabbe disease, X-linked adrenal leukodystrophy are lysosomal and peroxisomal diseases in which progressive demyelination occurs in both the CNS and the PNS (Melhem, Barker et al. 1999; Suzuki, Armao et al. 2001; Gieselmann, Franken et al. 2003). Alexander disease is a primary astrocytic disorder caused by dominant mutations of the GFAP gene (Brenner, Johnson et al. 2000). Canavans disease is an organic acid disorder with spongiform leukoencephalopathy (Matalon and Michals-Matalon 2000) and last Pelizaeus Merzbacher disease is an X-linked hypomyelinating disorder that has been well described by (Seitelberger 1970; Ulrich and Herschkowitz 1977; Seitelberger 1995).

MRI characteristics of Pelizaeus-Merzbacher disease

An appreciation of the normal appearance of unmyelinated and myelinated white matter structures on brain MRI is helpful for understanding imaging studies of infants and children with a dysmyelinating leukodystrophy (Barkovich 2005). In normal full-term infants, myelination is usually evident on MRI in the pons and cerebellum, and by the age of three months, normal infants show myelination in the posterior limb of the internal capsule, splenium of the corpus callosum, and optic radiations (Barkovich 2005). Absence of these MRI findings suggests the

diagnosis of a dysmyelinating syndrome such as PMD. The brain MRI of older children with the PMD often reveals diffuse hypomyelination marked by increased signal intensity in the cerebral hemispheres, cerebellum, and brainstem on T_2-weighted or fluid-attenuated inversion recovery (FLAIR) sequences (Fig 1.5). No clear correlation between genotype, clinical phenotype, and MRI phenotype has been established for PMD, but reasonable assessments can be inferred. However, some experts have noted an inverse correlation between the amount of myelin present and the clinical disease severity (van der Knaap, Breiter et al. 1999). As an example, no myelin is present at all in some infants with connatal PMD, the most severe form of PMD (van der Knaap, Breiter et al. 1999). In patients with the classic PMD phenotype, the white matter abnormalities on MRI have been divided into three subtypes (Nezu, Kimura et al. 1998; Nezu, Kimura et al. 1998):

1. Type I: diffuse abnormality in the hemispheres with lesions affecting the corticospinal tracts; this type was found in patients with a PLP1 duplication.

2. Type II: similar hemispheric lesions without corticospinal involvement.

3. Type III: patchy hemispheric involvement. The patchy areas of myelin forming the "tigroid" pattern are not readily apparent on neuroimaging in most patients (Takanashi, Sugita et al. 1999).

Patients with the SPG2 phenotype are said to have less severe abnormalities on brain MRI compared with the PMD phenotype. However, the reported abnormalities on T_2 MRI in SPG2 range from discrete or patchy hyperintensities to more diffuse leukoencephalopathy (Cambi et al., 1995; Hodes et al., 1999).

Significance

The most important clinical tools for investigating white matter disorders in living patients are magnetic resonance techniques to evaluate macroscopic structural changes and the integrity of the microstructural infrastructure. With modern MRI techniques, we can now complement that which is examined pathologically to monitor the pathogenesis and response to therapeutic intervention in white matter disease.

Imaging in living patients can be used to detect and quantify gray- and white-matter abnormalities on both macrostructural and microstructural levels. Conventional structural magnetic resonance imaging (MRI) reveals the size, shape, and tissue composition (gray vs. white matter) of the brain and its constituent parts. Alterations of normal appearing white matter (NAWM) is of great importance because its true patho-physiological significance is not completely understood. An immediate goal is to provide a firmer basis of magnetic resonance techniques as a tool to reveal the integrity of white-matter connectivity.

The primary parameters accessible from DTI, the directional diffusivities, are often combined into summary parameters sensitive to tissue pathology and morphology. DTI can make reasonable assessments into the integrity of white matter connectivity and the associated pathological conditions that perturb the higher organization of the CNS by monitoring the changes in diffusion of water over the course of disease progression. However, such parameters lack specificity to detect and differentiate axon vs. myelin degeneration alone, which warrant the application of MRS. The high sensitivity of DTI to microscopic structural tissue changes can be applied to the development, pathology and monitoring of neurological diseases. The degree of myelination, axonal swelling, microglia proliferation and reduced extracellular matrix will influence the behavior of microscopic water diffusion and therefore, reflect the pathological

changes as they take place in real time. Magnetic resonance imaging techniques can make reasonable assessments into the pathological conditions of PMD. The goal is to provide a basis for the application of magnetic resonance techniques such as DTI as tools to evaluate the microstructural architecture of axonal pathology and myelin degeneration not only in the pathogenesis of PMD, but also in other diverse groups of dysmyelinating and demyelinating disorders.

Hypothesis

The *central hypothesis* is that novel MRI techniques may provide insight into differentiating between axonal pathology & myelin degeneration, *in vivo*, in patients with PMD. In white matter tracts, water diffusion is greater parallel to the axon than perpendicular to it, due to the presence of directional subcellular structures that include axon membranes, cytoplasm filaments that comprise the axonal cytoskeleton and the myelin sheath with act as barriers to diffusion. We propose that axonal damage will cause a decrease in parallel diffusivity and fractional anisotropy caused by a decrease in the lengths of the axons as axons degenerate, but changes may only be measurable at the distal ends of the major neuronal pathways. In addition, dysmyelination may also cause increased radial diffusion if increased free water is present between the normally dehydrated leaflets comprising compact myelin or if the packing density of axons is increased due to the thinning of myelin sheaths.

AIMS OF THE STUDY

One of the objectives in current MRI research of white matter diseases with axonal pathology and alterations in myelin structure and function is to provide more sensitive and

specific markers of the biological effects of the disease as well as better monitor disease progression and response to treatment. There is currently no non-invasive modality capable of assessing the axonal and myelin components explicitly. However, a number of MR techniques are available that allow the study of these structures by indirect methods.

Specific Aim 1: To investigate structural MRI studies to quantify and compare the relative volumetric proportions of white matter of the brain in children and adults with PMD to a functional disability score. Volumetric analysis will provide an important contribution to our understanding of the severity of PLP1 gene mutations correlated with functional disability score assessment of patients. In this MRI study, volumetric analysis is critical to our understanding of the neuroanatomical development in PMD. Region of interest not only includes a global perspective of cerebral white matter, but also to consider focal white matter regions such as the sensorimotor area confined to the pre and post central gyrus. Investigating white matter volumes from a diffuse and focal perspective may provide a correlation to clinical phenotype found in PMD. A further aim will be to measure the intercaudate distance, to validate the whole brain volumetric analysis and to serve as a validation or potential substitution when demarcation of white vs. grey matter become too difficult to discern.

Specific Aim 2: To quantitatively investigate the parameters of DTI in patients with genetically confirmed PMD, characterizing the microstructural changes that may have significant therapeutic implication. The parameters of DTI analysis will validate specific markers of axonal damage and myelin degeneration regarding the pathogenesis of PMD. This method will be instrumental in assessing particular white matter pathways such as the corticospinal tract, a prominent descending motor pathway and the dorsal columns which include assemblies of major ascending sensory fibers. A further aim is the reconstruction of the motor and sensory pathways

using DTI as an in vivo method for mapping white matter fiber trajectories and measuring the density of the axonal fibers. The goal of DTI is to characterize WM tissue such that DTI parameters, unique in their ability to probe tissue microstructure, provide a greater degree of sensitivity and/or specificity for pathologic tissue changes than what conventional MRI is able to provide. The goal of fiber tractography is to map the brain's network of interconnections and establish connectivity patterns between subcortical areas involved in motor movement.

Specific Aim 3. To perform a neuropathologic examination on patients clinically diagnosed with Pelizaeus-Merzbacher disease. Exact type of *PLP1* mutation dictates the onset and severity of PMD and can be classified according to the mutational mechanisms, including the deletion of the entire gene, point mutations that affect splicing or regulation of gene expression and increased dosage of the *PLP1* gene. The objective is to examine in particular the brain pathology of PMD patients that have a range of mutational mechanisms. The white matter structure of particular interest is the corpus callosum. The reason extends from preliminary results of our diffusion tensor imaging analysis demonstrating a 107% increase in radial diffusion compared to age match control subject.
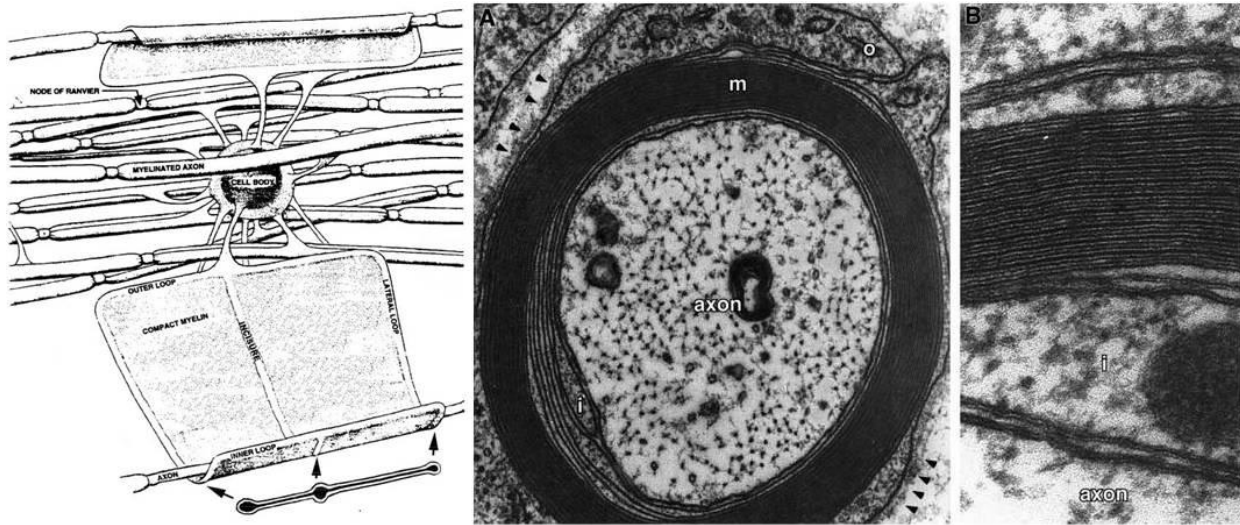
Figure 1. **Left:** The relationship between a oligodendrocytes and myelinated nerve fibers in the CNS. A single oligodendroctye is capable of myelinating up to 50 internodal segments. **Right:** The ultrastructure of a myelinated fiber. (a) The EM shows an axon (a) and its compact myelin sheath (m). (b) This EM shows that the compact myelin sheath is composed of alternating major dense and intraperiod lines (Arroyo and Scherer 2000)
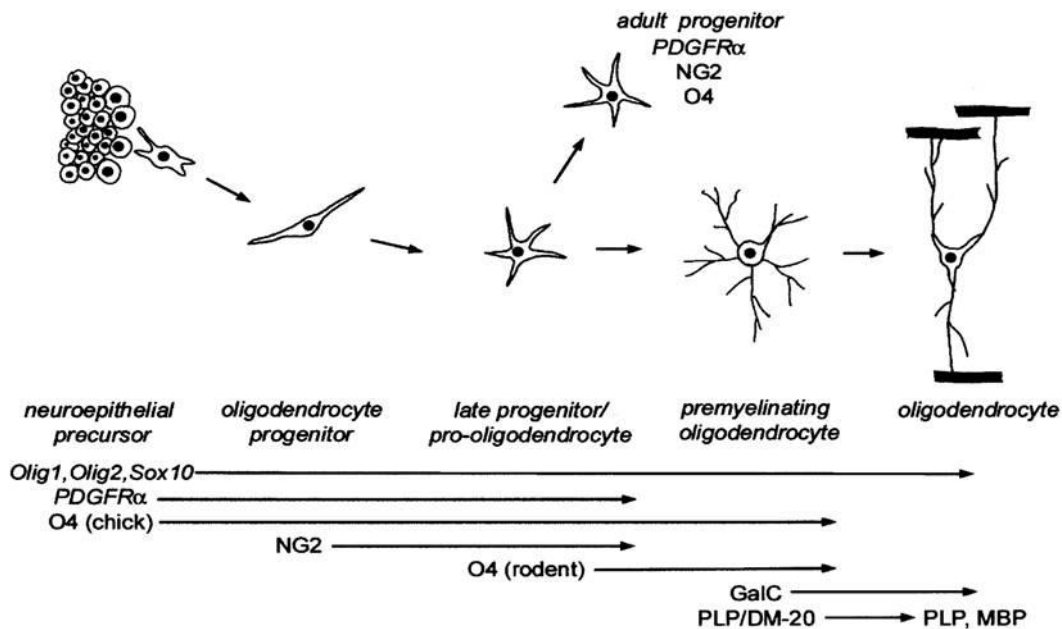
Figure 1.1 Illustrations of the various stages of oligodendrogenesis. (Woodruff, et al. 2001)
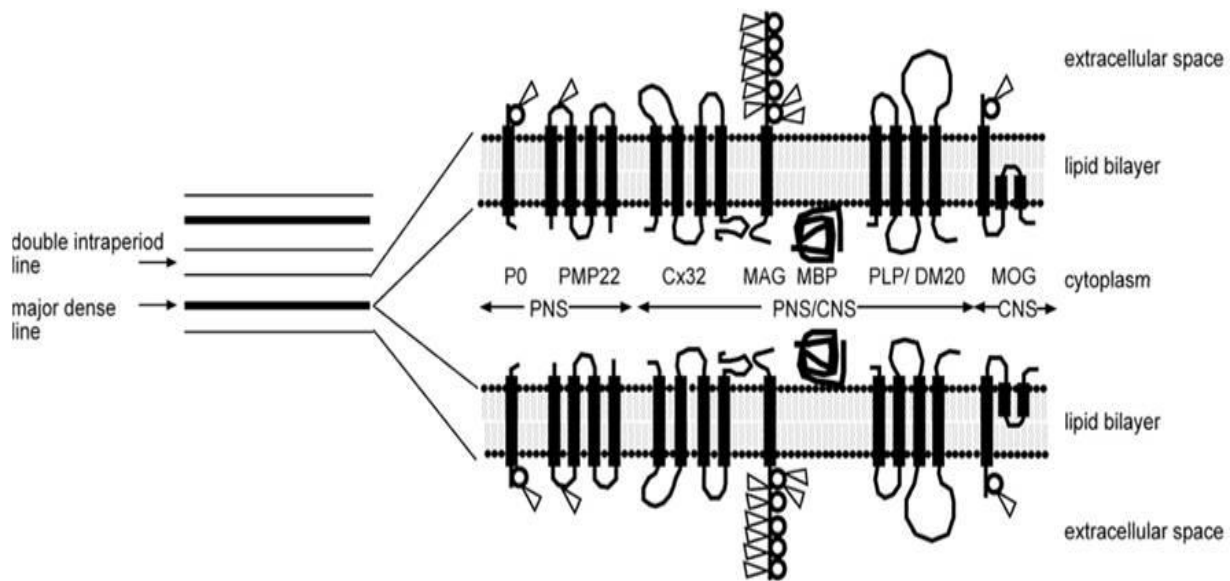
Figure 1.2 Composition of myelin. The myelin membrane is composed of repeated layers with protein-lipid-protein-lipid-protein structure. Glycolipids and cholesterol are located at the extracellular faces and phospholipids at the cytoplasm (intracellular) faces of the lipid bilayer. In compact CNS myelin, MBP and PLP are the major protein and in the PNS P0 and PMP22 are the major proteins. The closely apposed external faces of the membrane form the double intraperiod lines. The fused internal faces of the myelin membrane form the major dense lines. Modified from (Baumann and Pham-Dinh 2001)
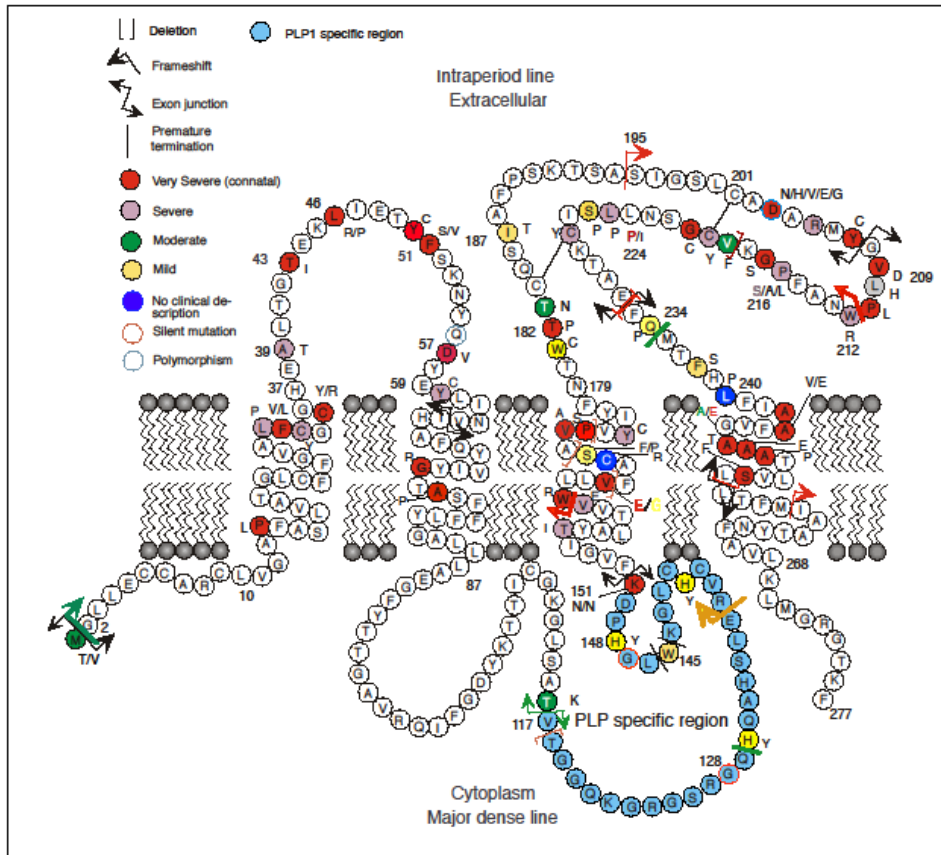
Figure 1.3 Proposed model for the secondary structure of PLP as it lies

in the lipid bilayer. PLP is a transmembrane protein with two

extracellular loops and one intracellular loop with its N- and C- termini

facing the cytoplasm, The PLP specific region (blue) differentiates PLP

from DM20. Known PLP1 mutations are shown with the most severe

phenotype (red) at a single amino acid position. Mutations that lie in the

large second extracellular loop can lead to abnormal crosslinking that

result in retention of the mutated PLP1 in the endoplasmic reticulum

(Garbern 2007).
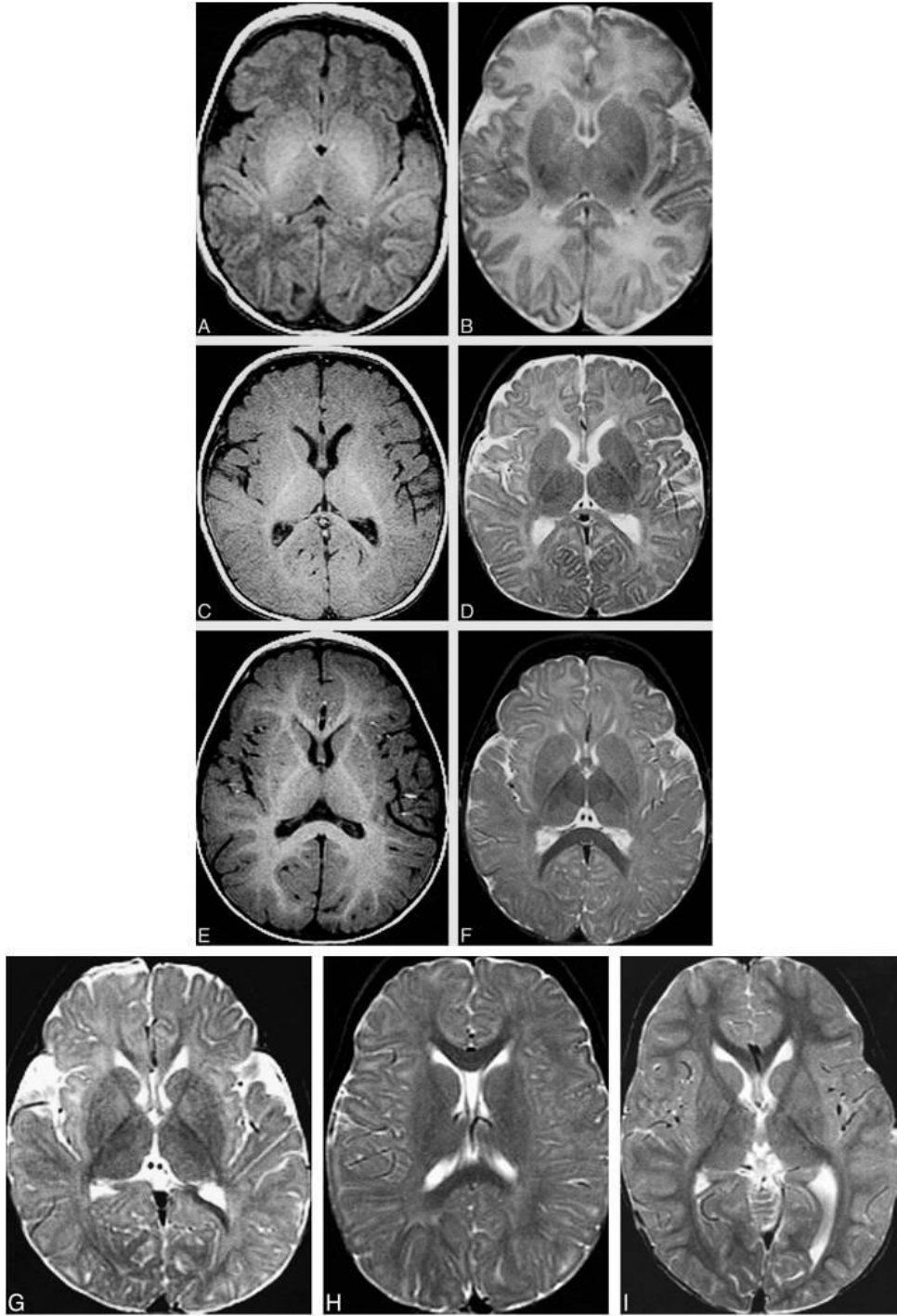
Figure 1.4 MRI changes of a normal pattern of myelination at the level of the basal ganglia. (A, B) Neonate MRI shows that myelination onT1-weighted image (A) and T2-weighted images (B) is limited to the posterior limb of the internal capsule at this level (black arrow). (B) Same patient shown in panel A. (C, D) of a 5-month-old patient shows hyperintensity in the entire internal capsule, optic radiations, and splenium of the corpus callosum. (D) Same patient shown in panel C shows hypointensity limited to the posterior limb of the internal capsule and a portion of the optic radiations. (E, F) 8-month-old patient shows hyperintensity in all white matter except the immediate subcortical regions. (F) Same patient shown in panel (E) shows hypointensity in the entire corpus callosum, the entire posterior limb of the internal capsule, and part of the anterior limb of the internal capsule. (G) 12-month-old patient shows hypointensity in the entire internal capsule, in the subcortical white matter of the motor cortex, and in the subcortical white matter of the visual cortex. (H) 18-month-old patient shows hypointensity in most of the deep white matter but lack of maturity of subcortical white matter. (I) Image of a 24-month-old patient show that essentially all white matter is hypointense. (Barkovich, 2000)

Anatomic Region: Brain	T1	T2
Cerebellar peduncle, middle	0	0-2 months
White matter, cerebral	0-4 months	3-5 months
Posterior limb internal capsule		
Anterior	1 month	4-7 months
Posterior	0	0-2 months
Anterior limb internal capsule	2-3 months	7-11 months
Corpus callosum, genu	4-6 months	5-8 months
Corpus callosum, splenium	3-4 months	4-6 months
Occipital white matter		
Central	3-5 months	9-14 months
Peripheral	4-7 months	11-15 months
White matter, frontal		
Central	3-6 months	11-16 months
Peripheral	7-11 months	14-18 months
Centrum semiovale	2-4 months	7-11 months

Table 1. Modified from Barkovich, AJ. Pediatric Neuroimaging. 3rd ed. Lippincott

Williams & Wilkins Philadelphia 2000 pg. 38
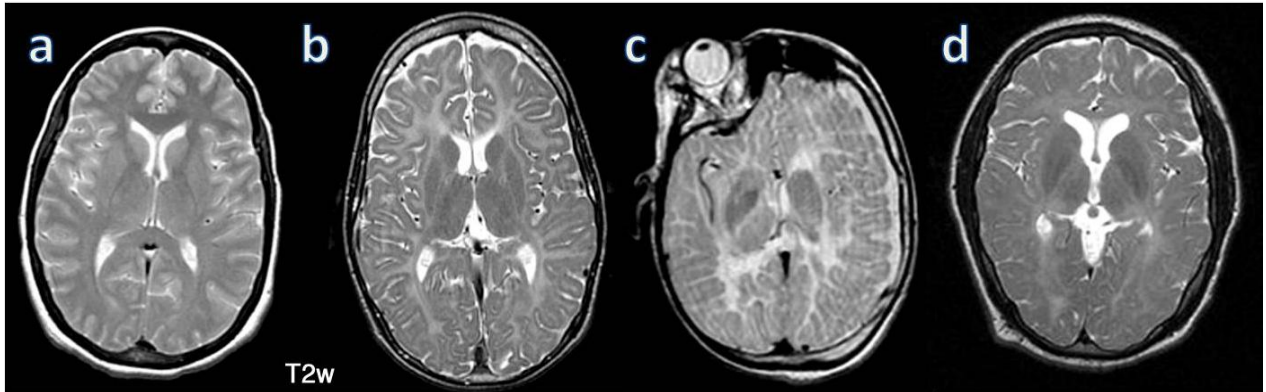
Figure 1.5 (a) Normal. Phenotypic expression is quite variable with the (b) classical form (i.e. duplications) exhibiting a high T_2 signal located periventricularly with small foci of less affected areas of preserved myelin (a "tigroid" pattern). (c) Severe 'connatal' form generally exhibits severe hypomyelination reflecting the reduced T_1 signal and a diffuse high T_2 signal, whereas (d) the mild null mutation consists of a relatively normal T_1 and T_2 signal, although periventricular hyperintensity may persists, but not always evident.

Chapter 2

NEURORADIOLOGIC CORRELATES OF CLINICAL DISABILITY AND PROGRESSION IN PELIZAEUS-MERZBACHER DISEASE

Pelizaeus-Merzbacher disease (PMD), an X-linked dysmyelinating disorder, is caused by mutations in the gene encoding proteolipid protein (*PLP1*), the major structural protein in central nervous system (CNS) myelin. Patients with PMD display a variety of neurological signs and symptoms, including spastic paraparesis, nystagmus, cognitive and visual impairment, and may also have a peripheral neuropathy. The majority of patients with PMD have a variable sized duplication of a region of the X-chromosome containing the PLP1 gene, suggesting that overexpression of PLP1 in oligodendrocytes is the cause of the disease. More than 100 point mutations in the *PLP1* coding region have also been identified in patients with PMD, however, accounting for approximately 15-25% of cases (Hodes,et al. 1993) see **http://www.med.wayne.edu/Neurology/plp.html**), and have been shown to have a variety of deleterious effects on oligodendrocyte function and myelination. Although the disease is both genetically and phenotypically variable in humans, its pathogenesis in rodent, canine, and pig models has been convincing shown to be a result of dysmyelination.

Brain MRI studies in patients with PMD have demonstrated patterns consistent with hypomyelination, both in patients with duplications and in patients with point mutations. A study by Garbern and coworkers has also shown that some patients with PMD caused by a PLP1 null mutation, have decreased levels of N-acetylaspartate (NAA) due to a length-dependent axonal degeneration. In contrast, a study of patients with PLP1 duplications has found increased brain

levels of NAA. These MRI studies have not yet delineated a common pathogenic mechanism in PMD, and have not provided a framework to correlate the clinical phenotype of patients to their underlying genotype.

In our current work we have analyzed the clinical phenotypes and MRI scans of 49 male patients with PMD and 10 female carriers for whom the PLP1 genotype had been determined. Nine patients had PLP1 duplications, two had PLP1 triplications, while the other 50 individuals had one of 29 different PLP1 point mutations. To estimate the clinical severity of these patients we developed a 32-point functional disability scoring system, based on a scale for analyzing patients with ALS, and validated it for inter-rater reliability in 22 patients with PMD. We then quantified total brain volume, white matter volume, inter-caudate ratio, and corpus callosum volume for our cohort of patients using conventional T_1- and T_2-weighted MRI sequences as well as a three-dimensional volumetric radiofrequency spoiled gradient echo (SPGR) series. Taken together, our data demonstrate that decreased white matter volume is a common finding for all the PMD patients in this cohort, regardless of genotype. In addition, clinical severity, measured by our functional disability scoring system, is correlated with white matter volume, inter-caudate ratio and corpus callosum volume. Although there are multiple genetic and molecular mechanisms causing PMD in this cohort, these data imply that white matter atrophy is the major pathological determinant of the clinical disability in most patients.

Materials and Methods

PMD patients

Our study population included 45 males and 10 females with known PLP1 mutations. The patients were analyzed serially from our population of patients with known PMD and selected based on their willingness to participate in this study. The age of each individual at the time of

MRI analysis, their functional disability score, and PLP1 mutation are listed in Table 2.3 Nine patients had PLP1 duplications, two had PLP1 triplications, while the other 50 individuals had one of 29 different PLP1 point mutations. Seven patients were between 4 and 5 years of age, 7 were between 5 and 10 years of age, 12 were between 10 and 20 years of age, 18 were between 20 and 40, and 10 were older than 40 years of age. The age of one patient at the time of analysis was not known.

Inter-caudate Ratio

The inter-caudate distance (ICD) and transverse skull diameter (TSD) were measured from the most caudal axial T_1 weighted MRI image for each of the 55 PMD patients in our study. The ICD was defined as the linear distance on this image between the medial borders of the head of the caudate nucleus; the TSD was defined as the distance separating the inner table of the skull on this same image. The inter-caudate ratio (ICR) was then calculated by dividing the ICD by the TSD at the same axial section level, as described previously by Caon and co-workers (Caon, Zvartau-Hind et al. 2003). NIH image was used to perform all measurements. A set of typical measurements is shown in Figure 2.

MR imaging acquisition and processing for volumetric measurements

Patients were evaluated with routine clinical brain MR image scans (T_1-weighted and T_2-weighted sequences) and three-dimensional volumetric radiofrequency spoiled gradient echo (SPGR) series at Children's Hospital of Michigan on a GE-Sigma 1.5 tesla scanner (General Electric, Milwaukee, WI), and their total brain volume, white matter volume and grey matter volume measured from these scans. Patients were excluded from this analysis because the contrast between grey and white matter was insufficient for volume segmentation. Four examples of coronal sections from SPGR series with varying grey matter-white matter contrast are shown

in Figure 2.4d. Volume segmentation could not be performed from scan is part d of this figure because of lack of contrast. The raw, GE-sigma-formatted image data from these scans were then transferred to Apple Macintosh Power PC workstation, and the SPGR image data were imported into the program NIH 1.62 for visualization, processing, and quantitative analysis. DICOM images were also obtained and were imported into ImageJ (version 1.32j) to partition the series into an ordered 124 contiguous slices. The scale for each slice was set to 10.666 pixels per centimeter, 16 bit unsigned with dimensions of 256 X 256.

To prepare the stacks for volumetric measurements, non-brain structures, including the skull, dura, subarachnoid spaces, ventricles, cerebellum, and brainstem were excluded from the region of interest (ROI) by manually tracing around them using the NIH program 1.62 as shown in Figure 2.1. The color threshold was manually adjusted for each slice to insure accurate segmentation of white and grey matter boundaries. This methodology was used to measure the ROI for each of the 62 slices available for each MRI scan. The brain volumes are expressed in units of cubic centimeter.

Corpus callosum area measurements

The corpus callosum area was analyzed in 36 patients from a mid-sagittal section in which the genu, body, and splenium of the corpus callosum could be visualized. The corpus callosum area was measured using the program NIH 1.62 as described above by manually tracing around the corpus callosum and the area expressed in square centimeters.

Results

White matter atrophy accounts for brain atrophy in patients with PMD

Comparison of total brain volume to white matter volume for 46 patients with PMD, shown in Figure 2.2, demonstrates a linear relationship (Pearson r =.91, P=<0.0001). Since this analysis includes patients with different ages that could confound this relationship, we also plotted white matter volume against patient age. As shown in Figure 2.3, there is no significant correlation between white matter volume and patient age. These data thus suggest that white matter atrophy is the major pathological feature in PMD for patients of all ages and mutation type.

A scoring system to measure functional disability in patients with PMD

In order to determine whether changes in white matter volume are associated with clinical disability in patients with PMD, we developed and validated a simple and reproducible clinical scale adapted from a scale used for patients with ALS (Cedarbaum, Stambler et al. 1999). This functional scale (0 to 32) shown in table 2 (also, see Appendix B), measures the ability of patients to perform routine tasks of daily living, such as feeding, bathing, dressing, and walking. The scoring system does not depend on any specific disease process or neurological sign, and can be assessed from a short interview with the patient's caregiver. Using this scale four neurologists at Wayne State University School of Medicine have estimated the functional disability of a group of 22 patients with genetically confirmed PMD.

The inter-rater reliability of this scoring system, shown in Table 2.1 and 2,2, is greater than 95%, and is thus quite reliable. The scores, however, shown in Table 1 (also, see Appendix B), suggest that functional disability is not equally distributed throughout the possible variable

range, but instead occurs in 3 clusters: 0-10 (severe); 10-20 (moderate); and 20 and above (mild). Interestingly, these clusters probably represent patients with connatal PMD, classic/transitional PMD and progressive spastic paraparesis, similar to the categories originally proposed by Seitelberger, 1970.

The functional disability score (FDS) is correlated with white matter volume in patients with PMD

A comparison of white matter volume to that of the patient's functional disability score (FDS) is shown in Figure 2.5. As can be seen from this data, white matter volume is positively correlated to the FDS (Pearson r= 0.50, P < 0.0001) suggesting that white matter atrophy is a major cause of clinical disability in PMD for patients of all ages and mutation type.

The FDS is correlated with the inter-caudate ratio (ICR) in patients with PMD

To establish a simple MRI metric to follow PMD disease progression, and to confirm the relationship of white matter atrophy and functional disability described above (Fig 2.6), we measured the inter-caudate ratio (ICR) for all 55 PMD patients, and compared it to their functional disability score as shown in Figure 2.7. The ICR has been used previously as an MRI metric in patients with multiple sclerosis (MS), and has been shown to correlate with disability in this disease as measured by the expanded disability scoring system (EDSS), suggesting that it is well suited for analyzing diseases of white matter. As can be seen in the figure the ICR is positively correlated to the FDS (Pearson r=-0.35, P=< 0.0001), further suggesting that white matter atrophy is a cause of clinical disability in PMD for patients of all ages and mutation type (Fig 2.6).

The FDS is correlated with corpus callosum area in patients with PMD

As an additional check on our data relating white matter atrophy to functional disability (Fig 2.9), we measured the area of the corpus callosum at its midpoint for 36 PMD patients for which this MRI section was available (Fig 2.8). Since the corpus callosum is the largest white matter track in the brain, the functional disability of PMD patients should be correlated with demyelination and thus atrophy within this structure.

Discussion

MRI has been proven to be instrumental in the diagnostic work-up in cases of leukodystrophies (van der Knaap and Valk 1995) Most individual leukodystrophies have distinct patterns of MRI abnormalities that maintain white matter region consistency among patients with the same disorder. Distinctive MRI pattern of leukodystrophies have been well documented (André, Monin et al. 1990; van der Knaap 2001; Barker and Horska 2004; Phelan, Lowe et al. 2008; Kohlschutter, Bley et al. 2010). The MRI pattern that exists among patient groups with the same disorder is not applicable to PMD, which expresses a rich heterogeneous pattern among patients with duplications among the (4) descriptive classes of PMD, not including the interfamily heterogeneity.

These results demonstrate the sensitivity that MRI technology imposes in detecting clinically relevant changes or monitoring the progression of the disease or a response to therapeutic treatment. The results show that WM atrophy positively correlates and the ICD negatively correlates with functional disability in PMD patients. Thus conventional MRI provides a reasonable measure that can assist in a predictive outcome and the progressive

development of disability. These findings indicate that this quantitative measure, including the results is clinically relevant, gradable, objective and practical enough for inferring about the pathogenesis of PMD. The presence of WM atrophy in excess of what might be expected for age is well described in several WM disorders, predominately, in multiple sclerosis (MS) studies. Atrophy is a clinically relevant entity in MS (Losseff and Miller 1998) and atrophy in the cerebellum (Davie, Barker et al. 1995) has been correlated with ataxia. Studies that involve WM, GM or both have shown a corroborating trend in the correlation with clinical measurements of motor and cognitive disability. Volumetric atrophy, global or localized, have been shown to correlate with clinical disability and cognitive scales in Alzheimer's disease temporal lobe atrophy (Visser, Verhey et al. 2002), GM atrophy associated with cerebellar function (Anderson, Fisniku et al. 2009), and thalamic atrophy observed in MS (Houtchens, Benedict et al. 2007).

These findings are reproducible and relevant to PMD and can provide constructive relationships between clinical disability and a non-invasive approach to monitoring progressive changes as well as responses to therapeutic treatments. This study shows evidence that during the natural progression of PMD; WM atrophy is a clinically relevant entity and is responsible in part for the decline in functional disability in PMD. The severity of dysmyelination and atrophy of pre-existing WM is dependent upon the type of *PLP1* gene mutation, as it is a factor in assessing the severity of myelin loss. It is naive to ignore the role axonal fibers play in the clinical and pathological outcome in PMD and their impact on clinical disability. Most patients with PMD lack primary axonal degeneration (Mar and Noetzel 2010), but some axonal loss has been found in completely demyelinated areas (Gencic, Abuelo et al. 1989). Axonal damage has been reported in patients with a null mutation (Garbern, Yool et al. 2002), as well as in PLP knockout

mouse model (Griffiths 1998; Griffiths, Klugmann et al. 1998; Edgar, McLaughlin et al. 2003). These studies exemplify the importance of interpreting WM pathology in the context of mutation type with additional support that the absence of PLP, the major CNS protein is instrumental in maintaining axonal integrity. Furthermore, animal models that experience natural occurring and spontaneous mutations may show an occasional axonal spheroid, but the majority show well preserved axonal fibers (Griffiths 1996). Transgenic mice engineered to carry extra copies of the *PLP1* gene serve as an experimental model for patients with duplications and reports show that axonal degeneration is a significant pathological feature (Anderson, Schneider et al. 1998). The cluster of PMD patients with duplications and triplications who exhibit the greatest decrease in WMV and decline in FDS may reflect the involvement of axonal injury found in the transgenic models. The findings are further supported by the observation found in patients with three and five copies of the *PLP1* gene that the level of expression is related to increased clinical severity (Wolf, Sistermans et al. 2005).

As the disease progress to a more severe clinical phenotype, axonal injury may contribute and become a contributing variable responsible for the decline in disability. Axonal loss is widely accepted as contributing to the cause of neurological disability in MS (De Stefano, Matthews et al. 1998) and correlates with the degree of inflammatory demyelination (Trapp, Peterson et al. 1998; Trapp, Bo et al. 1999). Together, the lack of mature myelin, late stage demyelination and axonal damage are variables that should be accounted for in white matter pathologies and should all be evaluated to explain the strong linear correlation between WM atrophy and FDS. Axonal pathology is well documented in CNS pathologies, most notably MS, but is also observed in variety of myelin disorders (Bjartmar, Yin et al. 1999; Bjartmar and Trapp 2001; Mar and Noetzel 2010). In PMD, the extent of axonal injury increases with age and

coexists with the infantile onset of PMD, thus accounting for the progressive neurologic signs in PMD. Some axonal loss is evident; especially those axons that have undergone complete loss of the very little existing myelin that originally encircled the axons, due to a lack of functional PLP (Gencic, 1989). Most patients do not demonstrate signs of primary axonal pathology, however, in both the *PLP1* knockout mouse model and patients with a null mutation experience axonal pathology that manifest in a length-dependent pattern (Garbern, Yool et al. 2002).

The simple linear measurement of the intercaudate distance may act as a surrogate measure of cerebral atrophy, especially in PMD patients that have a severe dysmyelinated CNS that causes the white-grey matter segmentation nearly impossible to differentiate. This simple method has been utilized in monitoring and understanding the pathology of MS by measuring brain atrophy as a marker for neuroaxonal loss and disease progression (Bermel, Bakshi et al. 2002; Caon, Zvartau-Hind et al. 2003) and is not only applicable to PMD, but other form of leukodystrophies that have strictly a demyelinating pathogensis.

Conclusion

The clinical severity measurements and MRI volumetric findings are consistent with the idea that white matter volume is inversely correlated with PMD severity. The correlation was moderate, although highly significant. The diagnoses of cerebral white matter disorders was revolutionized by the advent of MRI. Leukodystrophies were previously defined based on autopsy pathological findings alone, but MRI has provided a powerful tool for investigating and monitoring disease progression in living patients. The MR imaging findings in our patients are compatible with diffuse hypomyelination of the cerebral hemispheres. Although significant advances in the understanding and diagnosis of leukodystrophies using MRI have been made in

the last decade, many problems remain. A substantial number of leukodystrophies remain unclassified despite multiple investigations using clinical, genetic, biochemical, or imaging studies. In addition, the common observation of abnormal white-matter signal on MRI (T_2 hyperintensity) can reflect multiple different underlying pathologic changes, including acute or chronic demyelination, inflammation, edema, or gliosis. Therefore, conventional MRI studies might lack specificity. Because of this issue, there has been interest over the last few years in alternative advanced magnetic resonance methodologies (in particular magnetic resonance spectroscopy) that might provide more specific or complementary information regarding brain structure and composition particularly to examine the role of axonal injury in a vast array of white matter diseases.

Our data demonstrate that reduced white matter volume is likely one determinant of neurological disability in PMD patients, while axonal dysfunction or loss correlates with clinical progression, which is a late (typically post-adolescent) phenomenon. The findings in this study, explicitly shows how the degree of WM atrophy appears to be dependent on the type of *PLP1* mutation.

The use of MRI as a clinical tool to follow the natural history of PMD and incorporate its application in the evaluation of future therapies is instrumental making this study and the functional disability score assessment applicable to other forms Leukoencephalopathies.

Inter-caudate Distance

Transverse Width of the Inner Skull Table
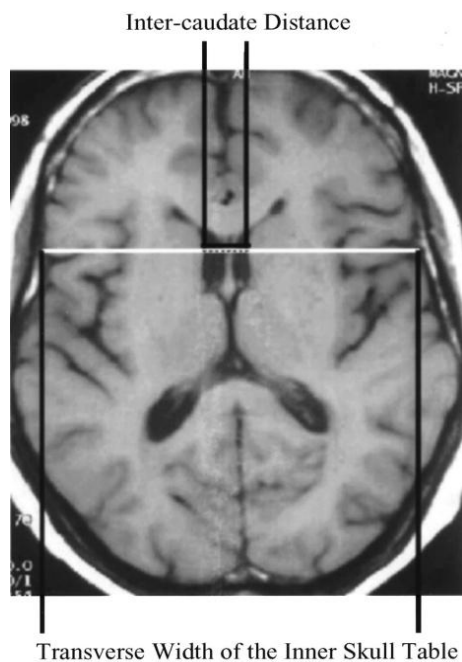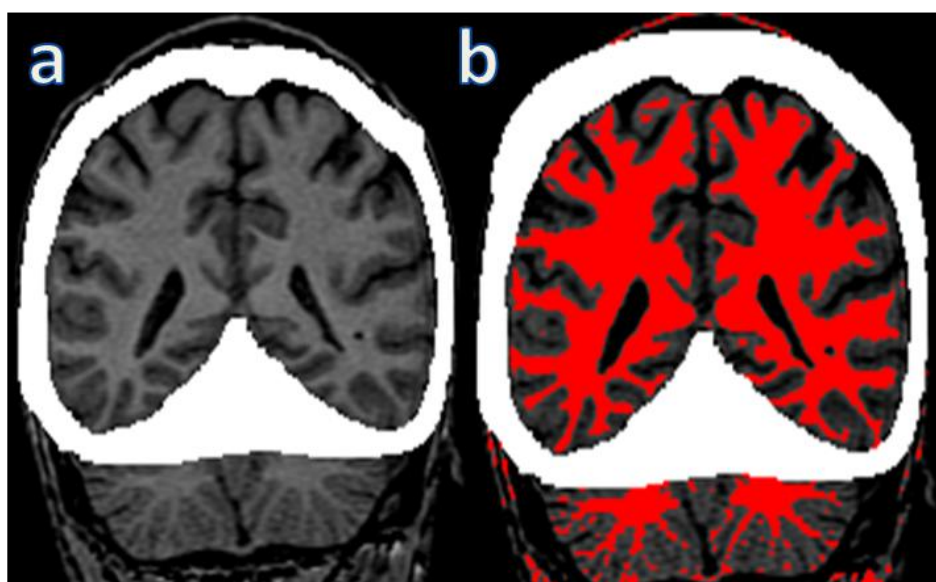
Figure 2.

Figure 2.1 (a) SPGR MRI outlining the brain parachyma excluding non-brain

structures (i.e. bone and dura matter), cerebellum and brainstem. (b)

Application of the color threshold highlighting the WM to be quantified. In

addition to subtracting CNS tissue and non-brain structures from the analysis,

the lateral ventricles and subarachnoid spaces also were excluded.
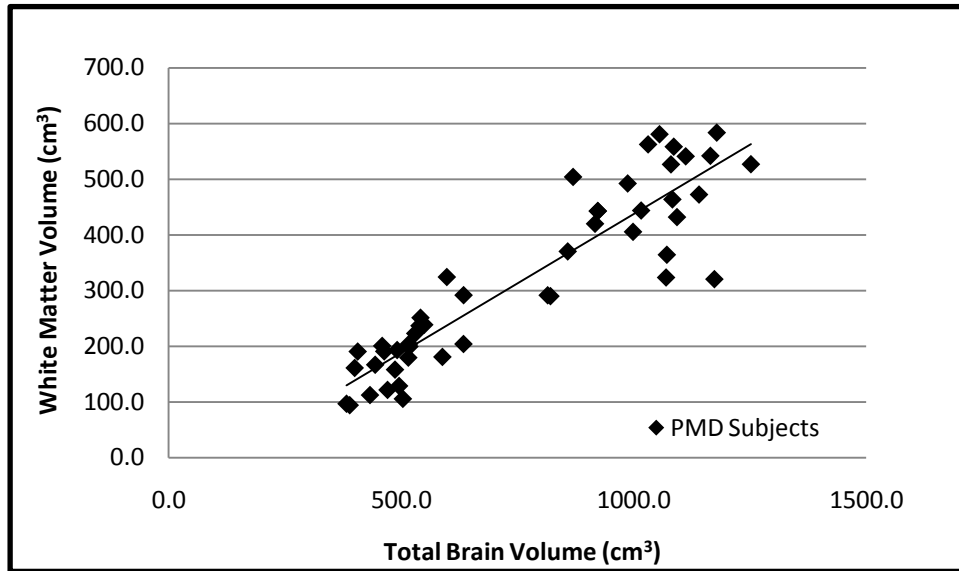
Figure 2.2 Changes in white matter volume account for the change in

total brain volume.
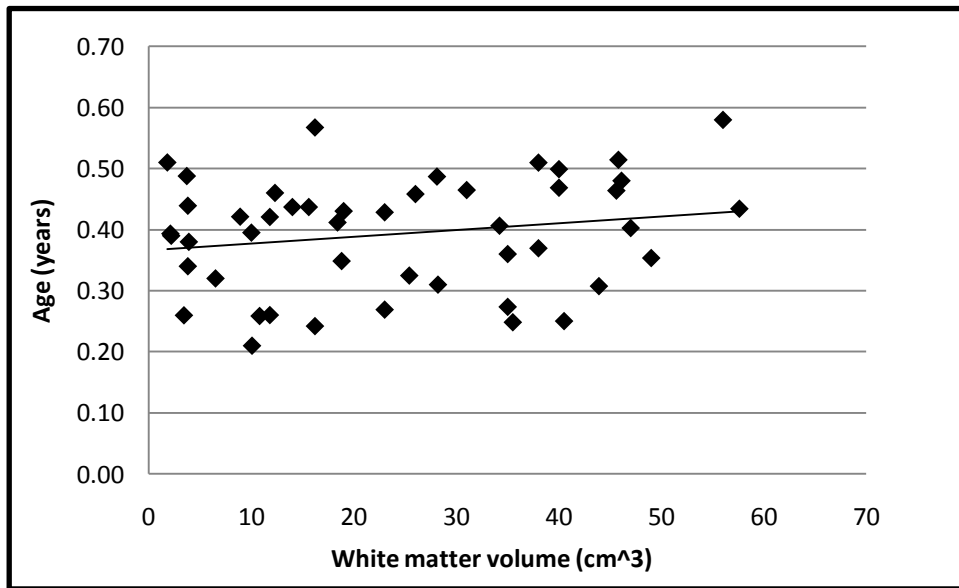
Figure 2.3 Changes in white matter volume is not confounded by the

patient's age.

Ability	Score range
*Education	0 - 3
*Employment	0 - 3
Speech	0 - 4
Feeding	0 - 4
Dressing	0 - 3
Toileting	0 - 3
Writing	0 - 5
Sitting	0 - 2
Walking	0 - 5
Breathing	0 - 3
Best possible score: 32	

Table 2. Functional disability score.

Patient	Phys. #1	Phys. #2	Phys. #3	Phys. #4	Mutation	Deletion size (kb)
BD	13	12	12	10	Duplication	330-890
BC	27	27	27	27	DelG4 heterozygote	
KB	7	7	6	6	Del G4 male	
JB	9	10	9	9	Del G4 male	
MB (#0007)	20	20	20	20	Del G4 male	
S	14	14	13	12	unknown	
AD (#0017)	4	4	4	4	Pro14Leu	
JS	5	5	5	5	Lys150Asn	
A1	27	27	27	27	Ile186Thr (rsh)	
A2	27	27	27	27	Ile186Thr (rsh)	
JR	14	14	16	16	duplication	1320-2013
MR1C	16	15	15	15	duplication	1320-2013
CM	20	17	17	20	Del 19 bp intron 3	
ST	16	14	16	15	Duplication	1020-1440
MS	2	2	2	2	+3 IVS 6 (skips exon 6)	
SC	4	4	4	3	Duplication	220-740
DC	6	7	6	6	Duplication	220-740
PC	16	16	16	16	Duplication	220-740
HB	27	27	27	27	unknown	
GK	9	8	8	7	Duplication	630-860

Table 2.1 Functional disability scores used for interrater reliability estimate

Pairwise Rater	Pairwise Correlation	Average Spearman Correlation
R1-R2	0.99467	
R1-R3	0.99086	
R1-R4	0.95802	
R2-R3	0.98935	
R2-R4	0.99164	
R3-R4	0.99696	
	5.9215	0.986916667

Table 2.2 Interrater reliability estimates
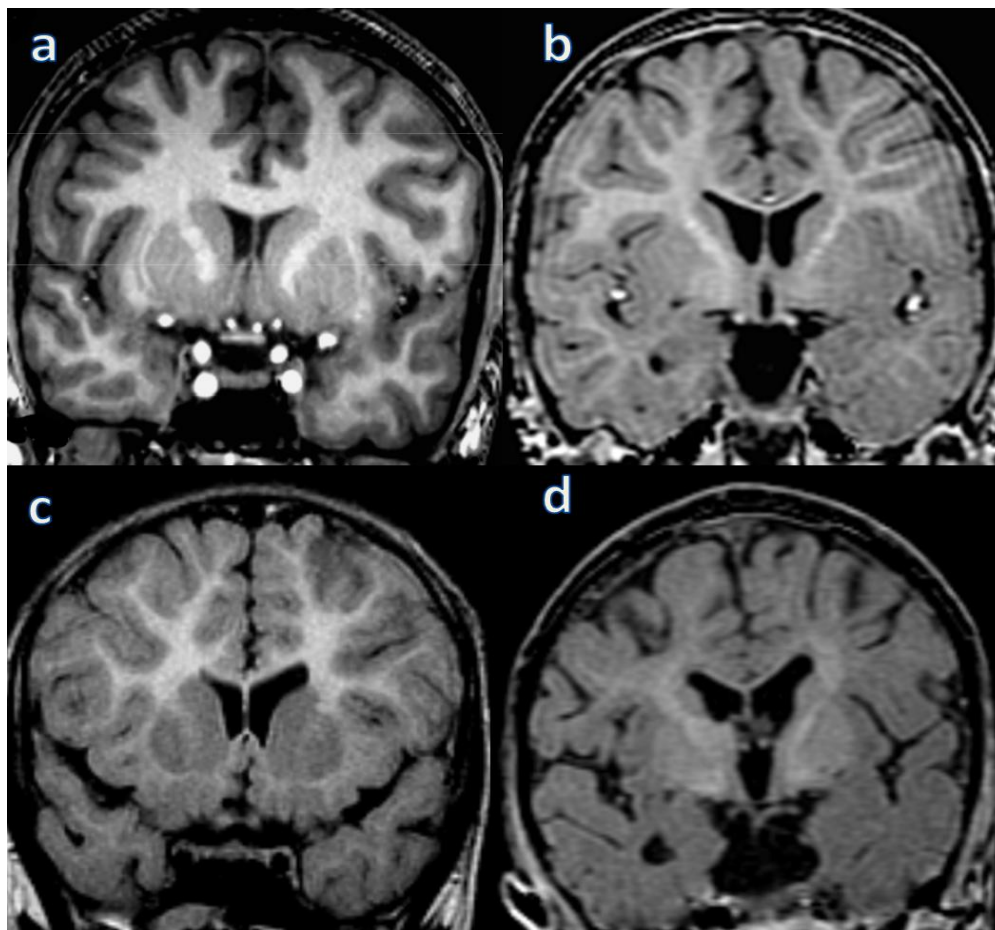
Figure 2.4 SPGR MRI of three PMD patients with duplications of the *PLP1* gene. (a) normal myelination of the subcortical WM and internal capsule. (b) Subcortical WM is isotense with a gradual decrease in hyperintensity of the internal capsule. Patients FDS = 20. (c) Moderate thinning of the subcortical WM with notable reduction in the temporal lobe. The internal capsule exhibits significant hypointensity reflective of a substantial reduction to absent of WM. Patients FDS = 12. (d) Diffuse reduction to absence of myelinated fibers with moderate enlargement of the lateral ventricles and periventricular hyperintensities representing preserved islands of myelin fibers. Patients FDS = 5.
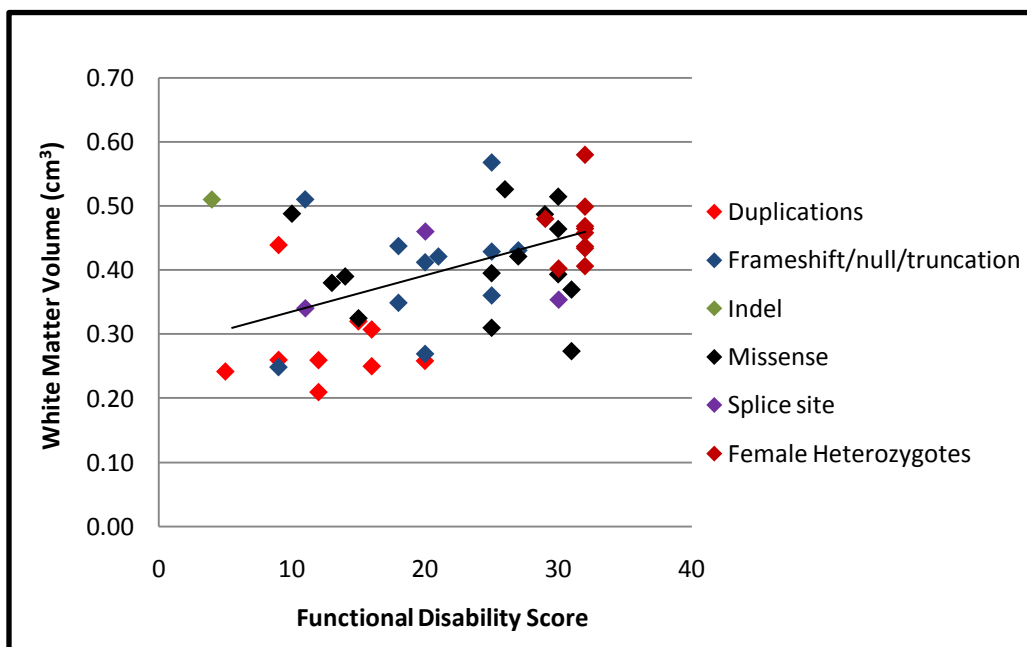
Figure 2.5 Change in white matter volume account for the changes in overall functional disability in patients with PMD.
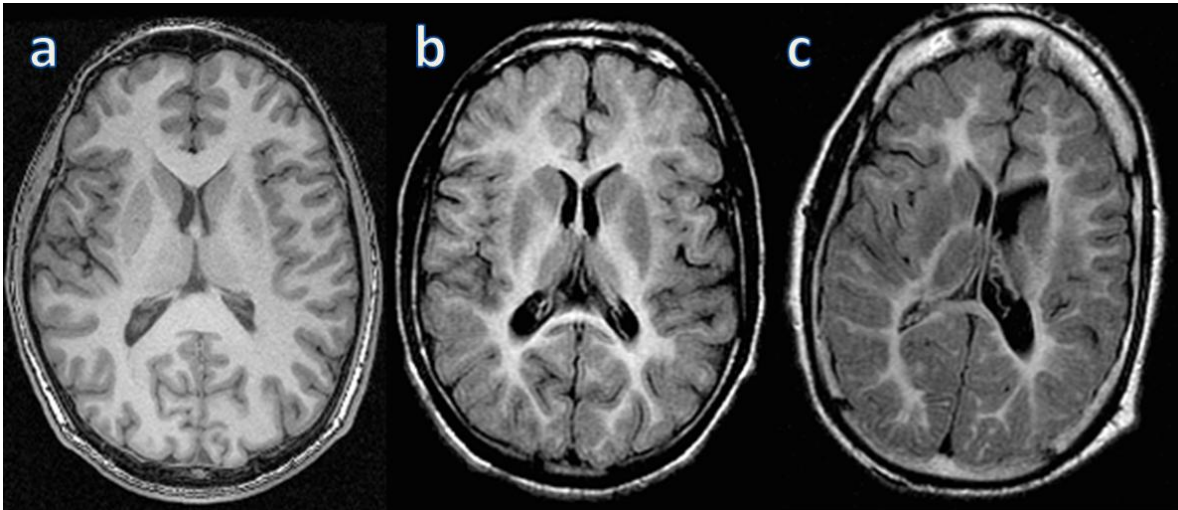
Figure 2.6 (a) Axial T_1-weighted MRI of a normal myelinated brain. (b) FLAIR MRI of a PMD patient with a delC279 frameshift mutation resulting in a nonfunctional truncated PLP. The WM of the internal capsule is relatively normal with a slight reduction to thinning of the subcortical WM. Patients FDS = 20. (c) Axial T1-weighted MRI of a PMD patient with a P14L missense mutation. A uniform and diffuse reduction of cerebral WM exemplified by a decrease in T_1 signal intensity and marked reduction of the posterior limb of the internal capsule with a corresponding increase in ventricular enlargement.
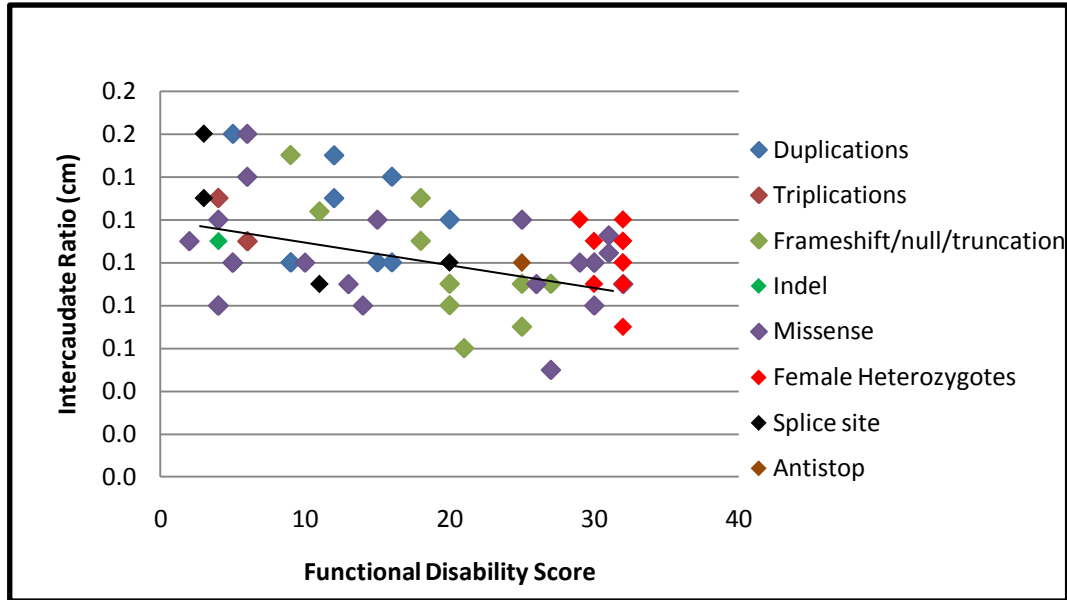
Figure 2.7 The inter-caudate ratio increases as white matter volume decreases in

PMD and is a linear measure that changes in respect to a decrease in functional

disability.
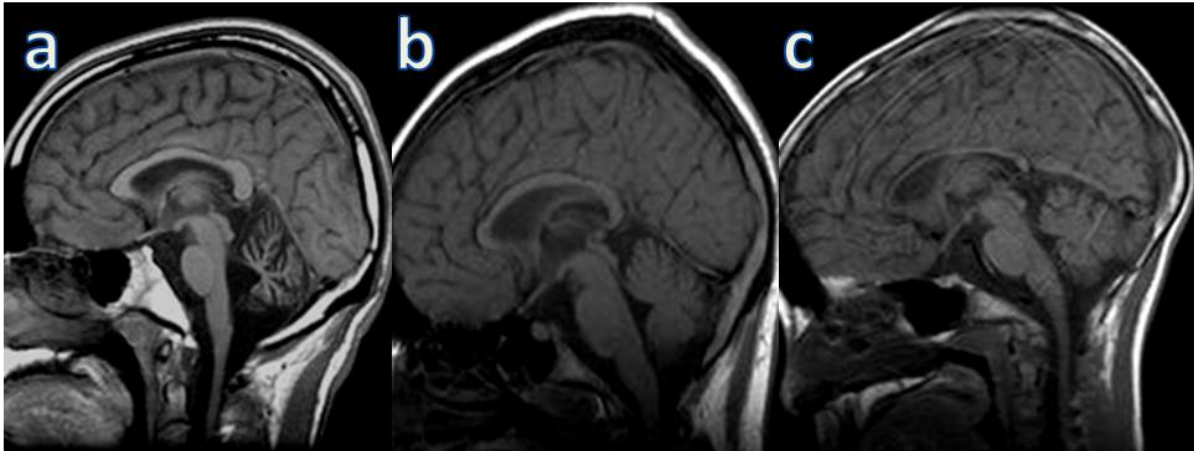
Figure 2.8 Sagittal T_1-weighted MRI of corpus callosum in PMD. (a) Normal myelination. (b) PMD patient with a complete deletion of the *PLP1* gene. The corpus callosum WM is relatively normal with a uniform thickness. Patients FDS =18. (c) Patient with a duplication of *PLP1* gene exhibits a severe reduction to absence of WM fibers of corpus callosum. Patients FDS =9.
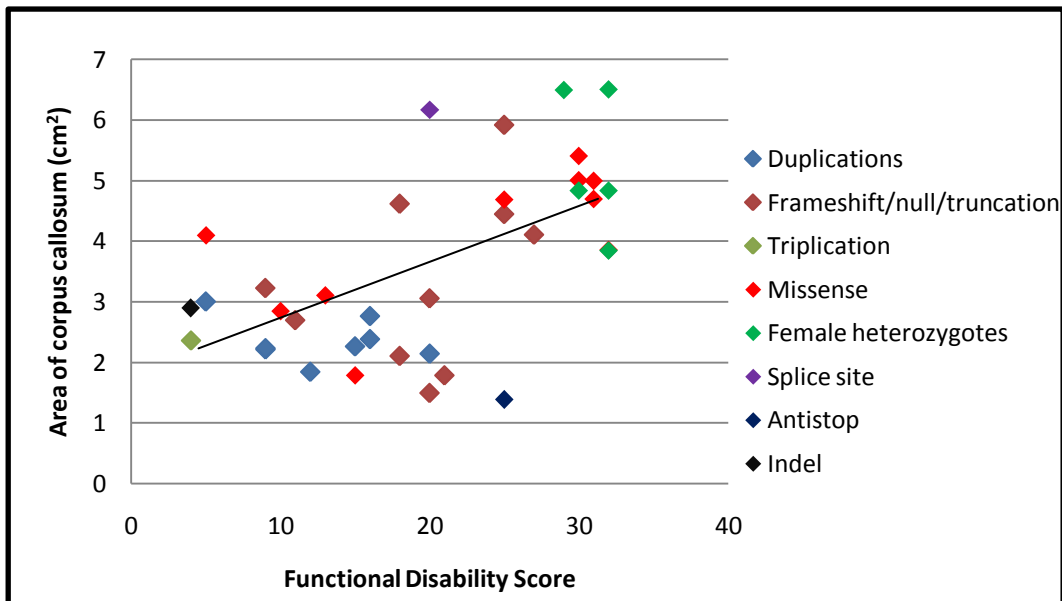
Figure 2.9 Corpus callosum area positively correlates with a decrease in patient functional disability. Atrophy of the corpus callosum is an indirect measure of a large white matter fiber bundle that is affected by dys/demyelination and axonal loss.

Table 2.3

PMD Patients	PLP1 Mutation	Age	Sex	FDS	ICD	WMV	CCV
B.D.	Duplication	10	M	12	0.09	.21	NA
B.W.	Duplication	3.5	M	12	0.15	.26	1.84
J.E.	Duplication	11.9	M	9	0.10	.26	2.21
J.H.	Duplication	10.8	M	20	0.12	.26	2.14
J.S.	Duplication	16.2	M	5	0.16	.24	3.06
J.J.	Duplication	6.5	M	15	0.10	.32	2.26
N.C.	Duplication	3.8	M	9	0.10	.44	2.23
P.C.	Duplication	43.9	M	16	0.14	.31	2.38
T.B.	Duplication	40.5	M	16	0.10	.25	2.76
B.S.	X276W	10	M	25	0.09	.40	1.39
C.E.	delC279	23	M	20	0.09	.27	1.5
S.P.	delC279	11.8	M	21	0.06	.42	1.79
B.H	K143X	16.2	M	25	0.09	.57	5.92
J.R.	del403-419	18.9	M	18	0.13	.35	2.11
T.B.	del403-419	35.5	M	9	0.15	.25	3.23
T.B.	del403-419	35	M	25	NA	.36	NA
C.G.	Deletion	14	M	18	0.11	.44	4.62
T.F.	DelG1/hetero	40	F	32	0.12	.47	4.83
J.F.	DelG1/hetero	15.6	F	32	0.11	.44	3.84
J.F.	DelG1	18.5	M	20	0.08	.41	3.06
C.B.	delG1/hetero	47	F	30	0.11	.40	4.83
T.K.	W144X/hetero	46.1	F	29	0.12	.48	6.49
M.K.	W144X	23.4	M	25	0.07	.43	4.11
T.D.	c.454-322G>A	NA	M	11	.12	.55	2.7
J.H.	Del 37E	1.8	M	4	0.11	.51	2.9
J.H.	F50V	2.9	M	5	0.10	NA	4.1
A.S.	C34R	8.2	M	2	0.11	NA	NA
G.W.	G245W	4.7	M	6	0.14	NA	NA
A.W.	H139Y	8.9	M	27	0.05	.42	NA
W.M.	I186T	45.6	M	30	0.08	.46	5.01
J.L.	L80R	5.2	M	4	0.08	NA	NA
M.G.	L80R	7.9	M	4	0.12	NA	NA
C.R.	L84R	3.7	M	10	0.10	.49	2.85
J.T.	L86P	1	M	5	0.10	NA	NA
A.D.	P14L	23.1	M	4	0.08	NA	NA
M.E.	R136W	12	M	32	0.1	NA	3.86
P.D.	P14L hetero	40	F	32	0.08	.50	6.5
H.B.	P172S	4.1	M	6	0.16	NA	NA
C.M.	R136G	12	M	14	0.08	.39	3.86
J.E.	X277W hetero	26.4	M	32	0.09	.46	NA
R.S.	Y156H	NA	M	13	0.09	.38	3.11
A.S.	Y206H	2.1	M	30	0.10	.39	5.41
C.J.	Y206H	28.3	M	25	0.10	.39	4.69
J.S.	V218F	25.5	M	15	0.12	.32	1.79

A.J.	Y206H/hetero	57.6	F	32	0.11	.43	NA
C.S.	Y206H/hetero	34.2	F	32	NA	.41	NA
J.H.	p.226S>P	56.6	F	32	0.10	.58	NA
M.H.	p.226S>P	31.1	F	32	0.12	.47	NA
R.H.	p.226S>P	45.8	M	30	0.10	.51	NA
T.H.	p.226S>P	28.1	M	29	0.10	.49	NA
P.G.	X278C	35.2	M	31	.11	.27	5.0
S.G.	X278C	38.4	M	31	.10	.37	4.7
C.S.	IVS6+3G>T	49	F	30	0.1	.35	NA
M.S.	IVS6+3G>T	23	M	3	.16	NA	NA
P.S.	IVS6+3G>T	25	M	3	.13	NA	NA
Z.B.	IVS6-1G>T	3.8	M	11	.09	.34	5.14
C.M.	IVS3 del+28-+46	12.3	M	20	0.10	.46	6.17
J.S.	Triplication	NA	M	6	0.11	NA	NA
N.T.	Triplication	1	M	4	0.13	NA	2.36
H.B.	NOT PMD	51.4	M	31	0.10	.55	5.68
M.P.	NOT PMD	25.4	M	32	0.10	.40	5.84

CHAPTER 3

ALTERED WHITE MATTER MICROSTRUCTURAL INTEGRITY REVEALED BY DIFFUSION TENSOR IMAGING IN PELIZAEUS-MERZBACHER DISEASE

The central nervous system (CNS) undergoes profound developmental changes during the first few years of life that provide the structural and functional elements necessary for normal neurological development. The maturation of white matter (WM) pathways, which are dependent on the process of myelination, is critical towards the development of the nervous system(van der Knaap, Valk et al. 1991). Dysmyelinating disorders or leukodystrophies comprise those disorders in which myelin is not formed properly, or when myelin formation is delayed or arrested (van der Knaap and Valk 1995). Failure to myelinate produces deficits in motor, sensory and cognitive function due to impairment, or interruption, in the connectivity of WM pathways to various gray matter regions. The underlying pathology of a neurological disease may involve axonal injury, myelin degeneration, or both. An accurate and non-invasive evaluation of the underlying WM pathology is crucial for diagnosing and monitoring clinical disease progression and responses to therapeutic intervention.

Owing to its high sensitivity, magnetic resonance imaging (MRI) is the primary neuroimaging modality used to detect and characterize white matter abnormalities in patients with leukodystrophies (Cheon, Kim et al. 2002) but has not been shown to provide insight into the underlying WM pathology and provide an examination of the microstructural properties of the CNS tissue. The development of diffusion tensor – magnetic resonance imaging (DTI-MRI)

allows a greater degree of sensitivity towards characterizing the effects of the neurological disease on the cytoarchitecture of the CNS tissue. Because patients serve as their own baseline reference, DTI makes it possible to follow subjects longitudinally to determine how the microstructural properties change over time.

The diffusion tensor describes the magnitude, the degree of anisotropy, and the orientation of diffusion anisotropy voxel by voxel, providing a unique way to study WM architecture in vivo. Although this MR technique may be of diagnostic utility, it is currently applied most often to characterize fiber tracts and serves as a biomarker for fiber integrity (Werring, Clark et al. 1999; Ciccarelli, Werring et al. 2001; Le Bihan, Mangin et al. 2001). Diffusion represents the translational motion of *in vivo* water molecules and is dominated by the cytoarchitecture to probe the integrity and organization of the static neuroanatomy. In the CNS, the diffusive properties of water depend on the local molecular and biochemical environment and are restricted by microstructures, such as cell membranes, axons, myelin sheaths, extracellular matrix and sub-cellular organelles, which include microtubules, microfilaments and proteins. In particular, and unique to the CNS, is the compartmentalization of intra- and extra-cellular water by the formation and cylindrical packing of the longitudinal array of axonal fibers. The pattern of diffusion is dependent on the water's anatomical localization. In organized bundles of nerve fibers, the net motion of water is greater parallel to the longitudinal axis than perpendicular to them. This preferential directionality of diffusion is attributed to cell membranes of both axons and the numerous lipid bilayer's of myelin. The relative effects of the different intra- and extra-cellular compartments on water diffusion in CNS white matter is still uncertain and debated, but generally presumed to be dominated by the water within axons and that in the extracellular spaces, which are also constrained by axonal and myelin membranes (Song, Sun et al. 2002;

Peled 2007). The relative contributions of intramyelinic water and the periaxonal space to the magnitude of water diffusivity is not fully established (Laule, Leung et al. 2006). Canavan disease represents a global disturbance of cerebral water homeostasis with the development of intramyelinic edema resulting from N-Acetyl Aspartoacylase accumulation in neurons increasing water diffusion into the periaxonal space (Baslow 2000; Engelbrecht, Scherer et al. 2002; Patay 2005).

Many of the animal models of neurologic disease, in particular those of still unknown cause, such as multiple sclerosis, Alzheimer disease, Parkinson disease and epilepsy are of uncertain relevance to human disease although they may share some similarities with the human conditions that they are meant to recapitulate. Induction of disease in these animals has potentially non-specific and widespread effects that confound analysis and interpretation of experimental results. For example, experimental autoimmune encephalitis (Gold, Hartung et al. 2000), regarded as the best model for multiple sclerosis, typically involves treatments that result in variable degrees of inflammation, generation of reactive oxidative compounds, edema, demyelination (Song, Yoshino et al. 2005) and axonal damage (Onuki, Ayers et al. 2001).

The analysis of animals with mutations affecting defined subcellular components of the CNS, in contrast, provides powerful insights into the understanding the more important effects on the diffusion of water in normal myelinated pathways as well as into changes in water diffusion caused by disease pathology. Pelizaeus-Merzbacher disease (PMD) is an X-linked disorder of the central nervous system (CNS), caused by a wide variety of mutations affecting proteolipid protein 1 (PLP1), the major protein in CNS myelin (Hudson, Puckett et al. 1989; Trofatter, Dlouhy et al. 1989; Raskind, Williams et al. 1991; Inoue, Osaka et al. 1999). PLP1 is the major structural protein in CNS myelin, and is believed to form 'adhesive struts' that bind

adjacent lamellae of myelin membrane. (Boison and Stoffel 1994; Boison, Bussow et al. 1995). The *PLP1* gene is alternatively spliced and, in addition to PLP1, also encodes the internally truncated DM20 protein, which lacks 35 amino acids from the intracellular loop (Nave, Bloom et al. 1987). These proteins are targeted to the oligodendrocyte cell membrane. Although the precise molecular and cellular functions of PLP1 and DM20 remain incompletely understood, they are thought to be important for maintaining compaction of the myelin sheath in the CNS (Boison, Bussow et al. 1995; Klugmann, Schwab et al. 1997). Since PLP1/DM20 are restricted to oligodendrocytes, the myelin forming cells of the CNS, PMD and its excellent animal models (Nave, Schneider et al. 1995; Yool, Edgar et al. 2000) provide highly specific systems with which to evaluate the effects of disturbance of a single cell type on the structural and functional integrity of the nervous system.

A wide variety of *PLP1* mutations, both naturally occurring and experimentally generated, have been reported in humans and a variety of other mammalian species (Yool et al, 2000). Somewhat surprisingly, complete lack of PLP1 results in a relatively mild phenotype, both in rodents and in humans. Targeted inactivation of the murine *PLP1* gene results in little neurologic abnormality until adulthood, and morphologically is characterized by a subtle increased spacing between adjacent lamellae of myelin membranes (Boison and Stoffel 1994; Klugmann, Schwab et al. 1997; Rosenbluth, Nave et al. 2006), presumably due to loss of interlamellar adhesion mediated by PLP1/DM20. PLP1-null human patients, have a surprisingly mild phenotype characterized by relatively good early neurologic development which is followed by progressive neurologic deterioration during adulthood (Klugmann, 1997; Garbern, 1997; Garbern, 2002). In both mice and humans lacking PLP1, the late deterioration is characterized most strikingly by axonal degeneration rather than by loss of myelin.

The most common mutation that causes PMD is complete duplications of the *PLP1* gene, which is presumed to cause overexpression of *PLP*1 and DM20. In experimental systems, *PLP*1 overexpression results in aberrant *PLP*1 processing, with ectopic compartmentalization of Plp1 with cholesterol and disturbed assembly of myelin membrane (Simons, Kramer et al. 2002; Karim, Barrie et al. 2007). *PLP1* missense mutations, in contrast, span the full clinical range of syndromes, from very mild 'pure' spastic paraparesis to fatal 'connatal' PMD. Severity of the missense mutations is thought to arise in part from accumulation of unfolded PLP1/DM20 that leads to varying degrees of oligodendrocyte apoptosis that is triggered by activation of the so-called unfolded protein response pathway (UPR) (Gow, Friedrich et al. 1994; Gow and Lazzarini 1996; Gow and Lazzarini 1996; Southwood, Garbern et al. 2002). Although there are currently no disease-specific therapies for PMD, there are several strategies that are hoped to lead to effective treatment of this severe disorder (Garbern 2007), and evaluation of future clinical trials will require robust clinical and laboratory tools with which to evaluate patients.

In most cases, conventional MRI shows an arrest of myelination. T_2-weighted images present a high signal intensity of unmyelinated white matter structures, whereas these structures have low signal intensity on T_1-weighted images. In 'severe' connatal PMD due to missense mutations, the brain is severely hypomyelinated which suggests thin to complete absence of myelin. Classical PMD cases exhibit a less pronounced myelin deficiency. There is a patchy absence of myelin with preservation of myelin islets giving the white matter the classical 'tigroid pattern'. Mild PMD involves patients with a null mutation, where relatively a normal amount of myelin develops with the abnormalities involving the intraperiod line.

The objective of this study was to perform DT-MRI and to quantify separately the parallel and perpendicular diffusivities of major white-matter tracts and to compare these values

to those of age-matched normal control subjects. We hypothesize that patients with PMD experience severe dysmyelination of white-matter structures without significant axonal damage at least initially and the severity of this disease correlates positively with degree of dysmyelination.

Furthermore, to supplement our study, we categorized the 12 PMD patients into three groups [i.e. null (3), mild (5) and severe mutations (4)] representing the degree of mutation severity affecting the *PLP1* gene. This supplemental investigation is on-going and the analysis of additional patients with genetically confirmed PMD will strengthen the principle that correlating the known *PLP1* gene mutation, which dictates the onset and severity of PMD, with the diffusivity markers are instrumental in our understanding of the pathogenic mechanism of the disease. The objective is to use DT-MRI and quantify the parameters or indices (i.e. parallel and radial diffusivities) to examine the six white matter structures and to correlate the quantified results to the pathogenic pattern observed in *PLP1* mutations.

Methods and Materials

Subjects and clinical evaluation

Twelve male patients with PMD, aged 2 to 45 years of age, were compared to a group of twelve age-matched healthy subjects free of neurological disease. Genetic analysis of their *PLP1* genes revealed: #1: Y206H; #2: IVS6-1G>T (causing exon 7 skipping); #3: L84R; #4: P173S; #5: G245W; #6: L80R; #7: Deletion; #8: del 403-419 (causes frame shift at residue 135); #9: P.226S>P; #10: X278C; #11: X278C; #12: P.226C.

Image Acquisition

MRI studies were performed on a GE 1.5 Tesla Sigma Excite (GE Healthcare, Milwaukee, Wisconsin) and standard head coil. The MRI exam includes (1) volumetric T_1-weighted images utilizing a 3D magnetization preparation spoiled gradient echo (SPGR) sequence, (2) Coronal fluid attenuation inversion recovery (FLAIR) images, (3) high resolution morphologic axial T2W fast spin echo series, and *4)* diffusion weighted spin-echo echo planar images. The DT-MRI sequence consists initially of an image volume with no diffusion weighting ($b = 0$ [s/mm^2]) followed by the acquisition of image volumes in 6 gradient in non-collinear directions with a b-value of 1000 [s/mm^2]. For each b-value and gradient direction, 6 images were acquired and magnitude averaging was used to reduce artifacts and to increase signal to noise ratio. The total imaging time for the entire DT-MRI sequence is 9 minutes.

Diffusion tensor image data processing and analysis

Six brain white matter structures were chosen for analysis: anterior-limb of internal capsule (ALIC), posterior-limb of internal capsule (PLIC), genu of corpus callosum (GCC), splenium of corpus callosum (SCC), base of the pons (PO), and cerebral peduncle (CP). The PLIC, PO and CP represent proximal to distal components of the major motor pathway, the corticospinal tract. This approach of parallel and perpendicular diffusivity components have been used to evaluate myelin loss and axonal injury (Song, 2002; Song, 2003; Budde, 2007). Regions of interest (ROI) were manually drawn on directionally color-encoded (DCE) maps at the edge of each structure to minimize partial voluming effect (Fig 3). Subsequently, these ROIs were automatically copied on the three axial views of main, middle and minor eigenvalues maps because approaches that exploit the ADC or FA have not resulted in improved specificity for the underlying pathology in WM disorders (Budde, 2007). After identifying the structures, areas of

interest were selected over at least 3 adjacent slices and averaged to obtain mean and standard deviation (SD) values of all *eigenvalues* λ_1, λ_2, and λ_3. Values of parallel diffusion ($\lambda_1 = \lambda_{//}$), radial diffusion ($\lambda_{\perp} = (\lambda_2 + \lambda_3)/2$), ADC and FA were then calculated on each ROI for the patients and normal controls and averaged to obtain a mean value for each group.

In these selected white matter structures, the diffusion parallel to the neural tracts and the mean of the two other eigenvalues that is related to the diffusion perpendicular to the tracts, which reflects the water movement across the fibers were recorded. Maps of λ_1, λ_2, λ_3, ADC and FA were obtained after tensor diagonalization using DTI studio software (H. Jiang and S. Mori; Department of Radiology, Johns Hopkins University, Baltimore, MD) ROI based measurements of these were analyzed separately to provide a more direct assessment of the directional diffusion changes associated with white matter of PMD patients. Based on previous DT-MRI evidence demonstrating that derived parallel and perpendicular diffusivities can detect and separate axonal from myelin damage (Song, Sun et al. 2002; Harsan, Poulet et al. 2006; Harsan, Poulet et al. 2007), we measured separately the three *eigenvalues.*

For the ALIC, PLIC and CP since the side-to-side differences were not significant at *p < 0.05* using a simple Pearson correlation test, the left and right sides were combined.

The between-two-groups statistical comparison was carried out separately for each structure with a post-hoc repeated measures with multiple analysis of covariance (MANCOVA) using age as covariate, and Boneferroni correction. Group differences with *p < 0.002* were considered significant. Age of the subjects was included as a covariate, because previous studies have reported age-related increases in FA and decreases in ADC (Schmithorst, Wilke et al. 2002; Snook, Paulson et al. 2005; Bonekamp, Nagae et al. 2007).

Results

In this study of twelve patients with genetically confirmed PMD, the quantitative difference among the six white matter structures between the two groups (PMD vs. NC subjects) validates the supportive and sensitive role of DTI-MRI to probe and characterize the microstructural changes that accompany the pathogenic process found in PMD. Detailed measurements of diffusion tensor characteristics demonstrated that the most sensitive parameter to measure myelin pathology is radial diffusion and to a much lesser extent axial diffusion (Table 3; Fig 3.1). The percentage increase (Table 3) demonstrated that the most sensitive DT-MRI parameter to measure microstructural abnormalities was the radial diffusion that showed an increase in values ($\lambda_\perp$ = 76%, 109%, 25%, 43%, 36%, and 17% respectively) and were higher than those in the axial direction ($\lambda_{//}$ = 8%, 13%, 8%, 6%, 11%, and 6% respectively). As expected from the ROI-based analysis the increase freedom of radial diffusion due to the dys/demyelinated axonal fibers was proven to be significantly higher (P=<0.001) in the studied white matter structures in PMD. Axial diffusion is the descriptive parameter in describing the architectural integrity of CNS tissue, particularly the myelin component which is the most discriminating parameter for identifying myelin pathology.

The magnitude of water axial parallel to the axonal fibers in PMD patients showed a relative mild to small significant difference when compared to normal control subjects (Fig 3.1). This relatively insignificant change could be accounted for by the influence of the PMD subjects who express a milder phenotype. Despite the overall non-significant change in parallel diffusivity of water diffusion in the WM structures studied we noticed a significant increase in the overall ADC values (Fig 3.2) in the patient group compared to control subjects. This observation demonstrates the overwhelming increase of the radial component in water diffusivity

and highlights the structural role of the myelin sheath as a sensitive marker to monitor the progression of myelin pathology.

The tissue microstructure and architecture expressed by FA was significantly lower in the ALIC, PLIC, GCC and SCC ($p < 0.002$) (Fig 3.2). Decreased FA was most marked in the SCC and mildly significant in the ALIC, GCC and CP of *PLP1* null mutations (Fig 3.4). These observations suggest that abnormalities lie within the myelin, but do not exclude the proliferative influences of the astroglial processes that become activated. Furthermore, the reduction in FA is also driven by the significant increase in radial diffusion rather than axial diffusion where mild to no significance was observed.

Deletion of the PLP1 gene causes a 'mild' form of PMD.

To further examine the overall impact myelin has on the diffusion markers, patients with null mutations (Table 3.1) share an increase in radial diffusion (Fig. 3.3) in the studied WM structures ($\lambda_\perp = 33\%$, 55%, 98%, 207%, 1.8%, and 58% respectively) and were higher than those in the axial direction ($\lambda_{//} = 11\%$, .31%, 13%, 20%, -4%, and .68% respectively). This finding provides a supportive explanation into the known pathogenesis suggesting that these types of mutations which include either a compete deletion of the *PLP1* gene or by frameshift mutation causing a truncated PLP disrupt the ultrastructural integrity of the myelin sheath. Although myelin is relatively spared early in the disease pathogenesis, the ultrastructural abnormalities are due to the relaxed diffusional barriers imposed by the adjacent myelin leaflets creating a barrier free extracellular space. This 'pathologic space' resulting in a 'radial component' allows the aqueous fluid to flow where imposed barriers are relaxed and the myelin sheath is unable to provide a unidirectional aqueous environment, consistent with compact myelinated fibers.

The overall ADC was markedly increased (Fig 3.4) in the ALIC, PLIC, SCC (P=<0.01) and is driven by the overwhelming increase in radial diffusion. The reduction in the FA was also significant (Fig 3.4) in the ALIC, GCC, SCC and CP (P=<.05). The relaxed diffusion barriers that exist between the adjacent myelin leaflets in null or functionally null mutations may also explain the decrease in FA. PMD patients expressing mild mutations expressed little difference in FA, indicating that myelin thickness is not a major contributor, but may involve minor influences to anisotropy.

PLP1 missense mutations causes a 'severe' form of PMD

Patients with 'severe' missense mutations share an increase in radial diffusion in the studied WM structures (Table 3.2; Fig 3.6). The percentage increase demonstrates that the most sensitive DT-MRI parameter to interpret myelin architecture is radial diffusion, which showed an increase in values ($\lambda_\perp$ = 35%, 55%, 78%, 139%, 44%, and 74% respectively) and were substantially higher than those in the axial direction ($\lambda_{//}$ = 15%, 16%, 25%, 25%, 24%, and 27% respectively) (Fig 3.7). As expected from the ROI-based analysis the increase freedom of radial diffusion is due to the thinning to absence of myelin and was proven to be significantly higher (P=<0.001) in the studied white matter structures in PMD (Fig 3.5; Fig 3.6). Furthermore, consistent with the findings of those with a null mutation ADC also increased particularly in the ALIC, PLIC, Po (P=<.01) SCC and CP (P=<.05), whereas FA decreased markedly in the ALIC (P=<0.01) and more mildly within the PLIC and CP (P=<0.05) (Fig 3.7).

Discussion

A number of neurological disorders involve white matter pathology leading to myelin and axonal dysfunction. Determining whether a particular disease is a result from myelin pathology alone or involves axonal changes that encompass degeneration and/or spheroid abnormalities cannot be depicted from a neurological examination alone. The advent of magnetic resonance imaging has become the principle imaging modality in patients with inherited neurodegenerative disorders and is instrumental in the identification, localization and characterization of white matter abnormalities. A particular MR imaging technique that demonstrates an elevated sensitivity towards monitoring the natural progression of various leukodystrophies is DTI. Diffusion imaging has been found to be superior to conventional anatomical MRI in differentiating dysmyelinating disorders, such as Pelizaeus- Merzbacher disease from demyelinating disorders, such as globoid cell leukodystrophy and Alexander's disease (Ono, Harada et al. 1995; Ono, Harada et al. 1997) and provides a unique insight into tissue structure and organization, potentially providing information about the size, orientation and tortuosity of both the intra and extracellular spaces. Due to its inherent sensitivity to the disruption of microstructural architecture, DTI complements conventional MRI methods in the evaluation, progression and monitoring of therapeutic intervention of neurological disorders regardless of etiology.

The present DTI investigation is the first in-vivo study, to our knowledge performed on twelve PMD subjects that have *PLP1* mutations ranging in clinical severity, providing a direct characterization and assessment of myelin loss of brain white matter tracts. The cylindrical packed axons and associated myelin affects diffusion anisotropy of water molecules; therefore, we monitored its effect on brain axons using DTI to correlate the complexity of the effects of

structural modifications in the white matter that cannot be obtained from conventional relaxation-based T_1-weighted, T_2-weighted or FLAIR MRI. Our study examined the DTI sensitive markers $\lambda_{//}$ and $\lambda_{\perp}$, as well as ADC and FA parameters to assess the integrity of white matter in this patient population.

In the developing brain, water molecules in the cerebral cortex move more radially than horizontally (McKinstry, Mathur et al. 2002). This anisotropy disappears with maturation and increases as the axons myelinate. Measurements assessing the radial component of ADC are instrumental in assessing normal brain maturation and the early manifestations if an inborn error is disrupting the normal pattern of myelination. Our analysis revealed findings that involved a significant increase in water diffusivity perpendicular to the axon of six selected white matter structures (ALIC, PLIC, CP, GSS, SCC, and Po) as measured by ($\lambda_{\perp}$). This result yielded a significant increase in the overall mean diffusivity quantified by ADC along with a significant decrease in the fractional anisotropy expressed by FA index. The radial diffusion index in this study corroborates with previous reported literature exhibiting the inverse correlation with the amount of CNS myelin (Song, Sun et al. 2002; Song, Sun et al. 2003; Song, Yoshino et al. 2005; Harsan, Poulet et al. 2006). Our results of increased $\lambda_{\perp}$ in PLIC (43%), ALIC (25%), CP (36%), GCC (76%), SCC (109%) and Po (17%), are in agreement with the increased $\lambda_{\perp}$ observed in other white-matter diseases such as the early phase of MS (Henry, Oh et al. 2003), white-matter lesions (Budde, Kim et al. 2007), dysmyelinated animals (Song, Sun et al. 2002; Harsan, Poulet et al. 2006), and *ex vivo* study on demyelinated cuprizone-treated mice (Song, Yoshino et al. 2005).

Perpendicular (radial) diffusivity

Reduction of radial diffusivity during maturation is suggested to be attributed to myelination as this modulates the diffusion anisotropy originating from cell membranes by creating an additional barrier (Beaulieu 2002). Furthermore, the lack/disruption of myelin sheath has been found to increase radial diffusivity without affecting axial diffusivity. These findings, along with the histological observation of continuing white matter myelination into adulthood support the fact that decrease in radial diffusivity reflects the myelination process (Bonekamp, Nagae et al. 2007).

Radial diffusion contributes to two-thirds of the overall ADC value, and the remaining 1/3 is attributed to the parallel diffusion. Although there was a relatively small increase in parallel diffusion in the white matter structures analyzed a significantly higher mean diffusion (ADC) values in these structure was observed and this is a consistent finding within across the *PLP1* mutation subtypes. This means that despite a reduction of $\lambda_\perp$ by a factor of two-thirds, the overall diffusion increased significantly, suggesting the severe dysmyelinated white matter in PMD overcomes the small change observed in parallel diffusion. Radial diffusion increased in patients with deletion of the *PLP1* gene due to the relaxed barriers. Studies involving *PLP1* null mice and the addition of ferricyanide (FCN), an aqueous extracellular tracer demonstrated that in thick myelin sheath, FCN filled the interlammelar spaces irregularly, whereas the thinly myelinated fibers the inter-lamellar spaces are filled across the full length of the sheaths, with no FCN present in normal myelin (Rosenbluth, Nave et al. 2006). The results of this study demonstrating the tendency of the extracellular fluid to leak into the interlammellar space demonstrating the existence of a "radial component" to myelin in the rodent model expressing the null syndrome.

Of the white matter structures studied, the genu and splenium of the corpus callosum which serves as the major conduit of the white matter connecting the homologous cortical areas exhibited an even greater increase in radial diffusivity compared to the other significant white matter structures. Our study shows radial diffusion to be mildly reduced in patients with *PLP1* null mutations, but still overwhelmingly significant compared to *PLP1* missense mutations. This finding may indicate that *PLP* null mutations retained an appreciable amount of myelin forming a resistant barrier to the properties of radial diffusivity, whereas the marked loss to complete absence of myelin *PLP1* missense mutations allows the water molecules to cross the fibers perpendicularly with more freedom, resulting in an increase in $\lambda_\perp$ values.

Modifications of the intracellular or extracellular spaces, as well as the abnormalities contributed by astrocytic activation and may influence the radial component of water diffusivity. The increase in radial diffusivity in the white matter and cerebellum in experimentally demyelinated mice and in MS supports the correlation of $\lambda_\perp$ with of myelin pathology (Ciccarelli, Werring et al. 2001; Filippi, Cercignani et al. 2001; Cassol, Ranjeva et al. 2004).

Parallel (axial) diffusivity

Our study showed a mild increase in parallel diffusion ($\lambda_{//}$). The destruction of neurofibrils has been found to increase parallel diffusivity (Kinoshita, Ohnishi et al. 1999). Other factors which have been proposed to affect parallel diffusivity include fiber coherence (Dubois, Dehaene-Lambertz et al. 2008), and axonal injury, which in animal studies is associated with reduction in axial diffusivity(Kim, Budde et al. 2006). Therefore, it is likely that changes in axial diffusivity reflect complex interactions of multiple biological factors that drive it in different directions.

The increase in parallel diffusivity was observed in the ALIC, GCC, SCC in patients with deletion of the *PLP1* gene and the ALIC, PLIC, GCC and CP in severe mutations and maybe related in principal to the relaxed diffusion barriers imposed by PLP and the dysmyelinating pattern that is found in connatal PMD due to *PLP1* missense mutations. The thinning to absence of myelin modeled in connatal PMD most likely involves the progressive axonal pathology that contributes to the neurological severity in PMD (Fig 3.5). These findings also are consistent with the results of (Harsan, Poulet et al. 2007), showing an increase in parallel diffusion in the corpus callosum and anterior commissure in the white matter in jimpy mice brains compared to dysmyelinated oligo-TTK transgenic mice. These findings and those of this study reflect the contribution of astrocytic hypertrophy to the elevation of these diffusion coefficients. Axon fibers are relatively preserved during the initial phases of the pathogenesis for patients with classical and connatal forms of PMD, but will eventually undergo late-onset changes similar to patients that lack PLP1 as oppose to those that lack a functional PLP1. The majority of the PMD population accounting for the 'mild' classical form and 'severe' connatal form in that order, the complex structural three-dimensional cytoskeleton make-up of axons is intact and composed of longitudinal arrays of oriented neurofibrils (i.e. microtubules and neurofilaments) that presumably account for the anisotropic diffusion and presents a sufficient barrier to hinder the radial component of water diffusion. It should not go without mention that the late-onset axonal pathology is evident in duplications and point mutations and would intrinsically impose stress and disrupt the arrays of neurofibrils. In cases that involve patients with deletion of the *PLP1* gene, axonal pathology has been reported in patients and rodent models exhibiting focal axonal swellings causing impairment of the anterograde and retrograde transport mechanisms (Griffiths 1998; Garbern, Griffiths et al. 2000; Garbern 2005) and may influence the parallel coefficient by

decreasing the flow of water due to an increase in the intra-axonal hindrance imposed by the enrichment of neurofilaments in swellings, accumulation of dense bodies, multivesicular bodies and mitochondria (Bjartmar, Yin et al. 1999).

The respective contribution of the extracellular and intracellular compartments to the measured ADC remains unclear. The cylindrical and parallel organization of the fibers explains the presence of anisotropy prior to myelination, but to a lesser degree following myelination. The diffusion coefficients have been shown to be influenced by several factors including the axonal morphology (Brady, Witt et al. 1999; Harsan, Poulet et al. 2006), myelin integrity (Song, Yoshino et al. 2005) as well as intra-axonal composition (Harsan, Poulet et al. 2006). An amplification of parallel diffusion coefficients was found in *Jimpy* mice brain and are thought to be contributed by hypertrophic astrocytes, because cytoplasm extensions of astrocytes follow the axonal pathway longitudinally (Skoff 1976), and also in axonal injury and normal appearing white matter of experimental autoimmune encephalomyelitis animal model (Budde, Kim et al. 2007).

Fractional Anisotropy

Most patients with PMD lack signs of primary axonal changes, but axonal injury is a characteristic feature in a small number of cases and is suggestive to be specific to the nature of the *PLP1* gene mutation. Axonal pathology has been demonstrated to exist in a length-dependent and late-onset pattern in PMD patients and animal models exhibiting the null mutation. The severity of axonal injury increases with disease progression contributing to the decline in neurological ability in PMD (Garbern, Cambi et al. 1999). Our DTI results indicate that changes in axonal integrity are reflected by the decreased FA and are likely to be replaced by large

structures with a higher degree of isotropism, which may either be axonal spheroids or edematous spaces.

Prior to myelination, cerebral white matter development consistently demonstrates an increase in isotropy followed by an increase in the degree of anisotropy with white matter maturation as seen in neonates and infants. The diffusion changes are tightly linked to the degree of cohesiveness and cylindrical packing of axonal fibers and reduced extra-axonal space, due to the natural thickness of myelin as the white matter matures over time. In white matter, any change in tissue orientation patterns inside the MRI voxel will result in a change in degree of anisotropy (Le Bihan, Mangin et al. 2001). The FA estimated by the DT-MRI method provides information about the arrangement of local tissue cytoarchitecture. The ability to evaluate the separate contribution of the directional diffusivities to the assessed anisotropy gives information about the factors that contribute to the abnormal fiber development or myelination abnormalities. Furthermore, the decrease in FA reflects the nature of an intact CNS from a microstructural view that describes the health and viability of the cytoarchitecture.

Our study found a disruption in WM microstructural organization as reflected by the lower FA index (Table 3) in the anterior limb internal capsule (-14%), posterior limb internal capsule (-19%), pons (-13%), cerebral peduncle (-16%), genu (-26%) and splenium (-32%) of corpus callosum in the PMD group when compared to the healthy control group (Table 3). The low FA observed in the white matter and cerebellum in dysmyelinated mice confirms the FA sensitivity of myelin pathology (Filippi, Cercignani et al. 2001; Ciccarelli, Werring et al. 2003; Cassol, Ranjeva et al. 2004). Detectable changes in FA of these structures indicate a disturbance of developing fibers that project through these white matter areas (Huppi 2001; Drobyshevsky, Song et al. 2005). The amplified decrease in FA may arise from the severe astrocyte hypertrophy

detected in the brains of PMD patients. Astrocyte hypertrophy and oligodendrocyte death accompanying the myelin deficit was shown to play a role in the amplification of water diffusion coefficients in jimpy brains because cytoplasm extensions of astrocytes follow the axonal pathway longitudinally (Skoff 1976). The degree of anisotropy that has been reported in previous literature has shown how FA progressively increases with remyelinatioin after experimental demyelination (Harsan, Poulet et al. 2006) and in remyelinated MS lesions (Tievsky, Ptak et al. 1999).

Conclusion

Inherited leukodystrophies represent a heterogeneous group of disease with a wide spectrum of distinctive causes and the underlying genetic involvement is not fully understood due to the variable phenotypic expression that one gene may express. Together, this adds a considerable challenge in the diagnosis of leukodystrophies and is associated with substantial morbidity and mortality in children. Significant advances and the understanding of inherited leukodystrophies such as PMD have propelled the importance of neuroimaging techniques in monitoring disease progression. The role of neuroimaging modalities in probing into the microstructural substrate is not limited to DTI-MR alone, but also includes MRS which is instrumental in deciphering the biochemical composition of the tissue. Neuroimaging applications complement each other by highlighting the direct insight into the physical properties and architectural organization of the CNS tissue. Diffusion imaging can make reasonable assessments into the integrity of white matter connectivity and the associated pathological conditions that perturb the higher organization of the CNS by monitoring the changes in diffusion of water over the course of disease progression.

Diffusion tensor imaging is particular adapted for analyzing white matter structures and changes in water content associated with maturation or perturbed maturation as evident in leukodystrophies. In the severe 'connatal' form of PMD, the maturation process is perturbed as a result of cytotoxic insults of misfolded PLP causing premature cell death of oligodendrocytes resulting in their inability to myelinate axons. Our results provide supporting evidence that axon fibers lack or have a thin layer of myelin creating a barrier free environment amplifying the diffusion in a radial direction, due to a reduction in myelinating cells. In the mild form of PMD, null mutations demonstrated a similar result, concluding that abnormalities involve the myelin sheath, but the pathologic disturbances are found between the myelin leaflets marked by increased distance between intraperiod lines that should be adhered together forming compact myelin by PLP. This interlamellar space created as a result of a lack of PLP enables diffusion to proceed in a radial direction.

Although elevated, axial diffusion was not a diffusion parameter that provided direct insight into a particular subtype of pathology, but it did exhibit a strong correlation with the observed astrogliosis and the enlarged extracellular space as a result of hypomyelination (reviewed in Chapter 4). The results also provide concluding evidence that the density of axon fibers is reduced resulting, thus amplifying axial diffusivity.

The decrease in FA which is a measure of white matter organization that commonly asses the connectivity of the rich fiber bundles in PMD among other forms of leukodystrophies demonstrated that the fibers were disintegrated. The results obtained from all the white matter structures analyzed excluding the Pons demonstrated the accuracy of FA as a measure of the multidimensional diffusion profile, but the regions of complex fiber-crossing may have a lower FA than those areas of a predominant unidirectional white matter structure as in the corpus

callosum. With this knowledge, interpretation must be carefully analyzed to reflect the complex nature of the white matter structure of interest.

The interpretation of DTI must incorporate the specific *PLP1* genetic mutation, which is a definitive component that alters the pathologic characterization of the individual PMD subtypes. Early detection of subtle changes in brain microstructure and the accurate assessment of dys/demyelination of the CNS tissue using DTI have an important contribution towards the diagnosis, monitoring and therapeutic treatment of PMD.

	λ_1 [10^{-3} mm^2/s]	λ_2 [10^{-3} mm^2/s]	λ_3 [10^{-3} mm^2/s]	ADC [10^{-3} mm^2/s]	FA
GCC					
C	1.533 ± 0.153	0.482 ± 0.110	0.260 ± 0.062	0.758 ± 0.077	0.722 ± 0.060
P	1.616 ± 0.157	0.754 ±0.215	0.550 ± 0.150	0.974 ± 0.150	0.533 ± 0.111
SCC					
C	1.533 ± 0.178	0.450 ± 0.132	0.258 ± 0.080	0.747 ± 0.110	0.738 ± 0.052
P	1.713 ± 0.226	0.836 ± 0.264	0.630 ± 0.244	1.059 ± 0.206	0.495 ± 0.149
ALIC					
C	1.072 ± 0.078	0.531 ± 0.062	0.330 ± 0.061	0.644 ± 0.055	0.608 ± 0.073
P	1.166 ± 0.073	0.644 ± 0.062	0.460 ± 0.081	0.757 ± 0.058	0.514 ± 0.078
PLI					
C	1.156 ± 0.128	0.436 ± 0.098	0.227 ± 0.075	0.607 ± 0.068	0.770 ± 0.145
P	1.241 ± 0.123	0.617 ± 0.053	0.416 ± 0.096	0.758 ± 0.070	0.588 ± 0.086
Po					
C	1.008 ± 0.060	0.620 ± 0.063	0.332 ± 0.088	0.653 ± 0.057	0.481 ± 0.078
P	1.079 ± 0.132	0.712 ± 0.102	0.441 ± 0.112	0.744 ± 0.107	0.410 ± 0.072
CP					
C	1.246 ± 0.104	0.594 ± 0.074	0.394 ± 0.074	0394 ± 0.081	0.745 ± 0.061
P	1.377 ± 0.140	0.794 ± 0.183	0.547 ± 0.180	0.906 ± 0.158	0.502 ± 0.118

	λ_1		λ_{23}		ADC		FA	
	%	P	%	P	%	P	%	P
ALIC	8	0.004	25	<0.001	16	<0.001	-14	0.001
PLIC	6	0.10	43	<0.001	20	<0.001	-19	<0.001
GCC	8	0.04	76	<0.001	30	<0.001	-26	<0.001
SCC	13	0.01	109	<0.001	43	<0.001	-32	<0.001
Po	6	0.14	17	0.01	11	0.02	-13	0.03
CP	11	0.01	36	0.001	22	0.001	-16	0.01

Table 3. The top panel, represent the mean and standard deviation (SD) values of all

eigenvalues λ_1, λ_2, and λ_3. Values of parallel diffusion ($\lambda_1 = \lambda_{//}$), radial diffusion ($\lambda_\perp = (\lambda_2 +$

$\lambda_3)/2$), ADC and FA were then calculated on each ROI for the patients and normal controls

The bottom panel, exhibits the percentage change and P-value between the patients and

normal control for each of the selected white matter ROI. Anterior limb of the internal

capsule (ALIC), Posterior limb of the internal capsule (PLIC), Genu of corpus callosum

(GCC), Splenium of corpus callosum (SCC), Pons (Po), Cerebral peduncles (CP).

Figure 3.1 Left: Perpendicular (radial) diffusion $10^{-3} mm^2/s$. The patients demonstrate a significant increase (<0.05) compared to the normal control subjects. Right: Parallel (axial) diffusion $10^{-3} mm^2/s$. Parallel diffusion exhibited a mild increase compared to normal controls subjects.
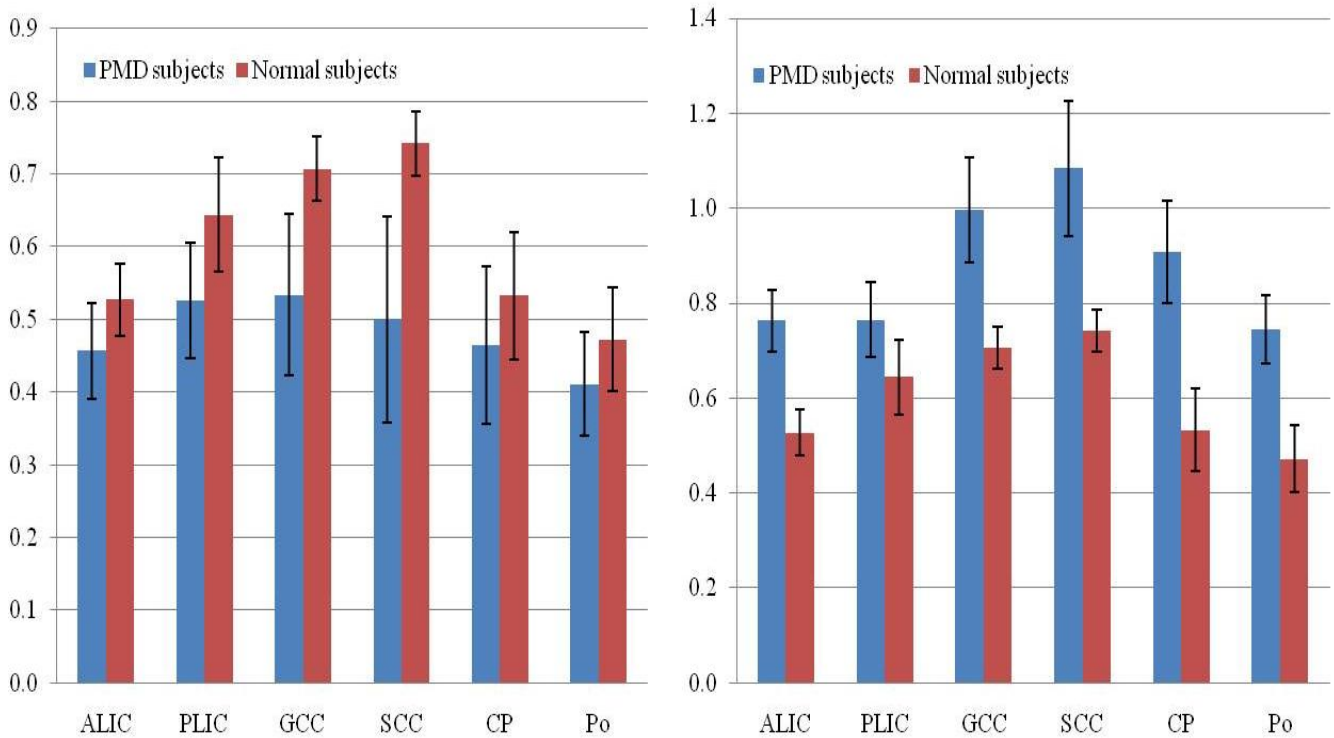
Figure 3.2 Left: Fractional aniostropy 10^{-3}mm^2/s. The patients demonstrate a significant decrease (<0.05) compared to the normal control subjects. Right: Apparent diffusion coefficient 10^{-3}mm^2/s.

	λ_1 [10^{-3} mm^2/s]	λ_2 [10^{-3} mm^2/s]	λ_3 [10^{-3} mm^2/s]	ADC [10^{-3} mm^2/s]	FA
ALIC					
C	1.035 ± 0.083	0.513 ± 0.120	0.339 ± 0.124	0.629 ± 0.102	**0.604 ± 0.141**
P	1.147 ± 0.061	0.664 ± 0.020	0.503 ± 0.043	0.772 ± 0.08	**0.467 ± 0.018**
PLIC					
C	1.170 ± 0.100	0.367 ± 0.144	0.212 ± 0.130	0.583 ± 0.124	**0.853 ± 0.153**
P	1.173 ± 0.081	0.628 ± 0.051	0.449 ± 0.049	0.750 ± 0.032	**0.531 ± 0.085**
GCC					
C	1.578 ± 0.180	0.458 ± 0.063	0.249 ± 0.053	0.762 ± 0.033	**0.739 ± 0.066**
P	1.508 ± 0.034	0.779 ± 0.099	0.563 ± 0.079	0.950 ± 0.056	**0.481 ± 0.069**
SCC					
C	1.494 ± 0.085	0.369 ± 0.036	0.280 ± 0.120	0.714 ± 0.053	**0.749 ± 0.061**
p	1.703 ± 0.070	0.968 ± 0.216	0.763 ± 0.221	1.145 ± 0.164	**0.415 ± 0.131**
Po					
C	0.981 ± 0.051	0.615 ± 0.103	0.369 ± 0.158	0.655 ± 0.095	**0.447 ± 0.143**
P	1.037 ± 0.052	0.680 ± 0.040	0.433 ± 0.033	0.717 ± 0.036	**0.400 ± 0.026**
CP					
C	1.250 ± 0.064	0.584 ± 0.116	0.401 ± 0.118	0.745 ± 0.061	**0.627 ± 0.159**
P	**1.282 ± 0.061**	**0.761 ± 0.053**	**0.542 ± 0.074**	**0.862 ± 0.057**	**0.466 ± 0.043**

	λ_1		λ_{23}		ADC		FA	
	%	P	%	P	%	P	%	**P**
ALIC	11	<0.01	33	<0.001	22	<0.001	-16	**0.04**
PLIC	.31	0.9	55	0.01	21	<0.01	-28	**0.1**
GCC	13	0.04	98	0.04	35	0.04	-35	**0.04**
SCC	20	0.01	207	<0.01	77	<0.01	-53	**<0.01**
Po	-4	0.6	1.8	0.8	-1.1	0.8	-10	**0.2**
CP	**.68**	**0.9**	**58**	**0.01**	**-22**	**0.01**	**-31**	**0.01**

Table 3.1: Null mutations. The top panel, represent the mean and standard deviation (SD) values of all *eigenvalues* λ_1, λ_2, and λ_3. Values of parallel diffusion ($\lambda_1 = \lambda_{//}$), radial diffusion ($\lambda_\perp = (\lambda_2 + \lambda_3)/2$), ADC and FA were then calculated on each ROI for the patients and normal controls The bottom panel, exhibits the percentage change and P-value between the patients and normal control for each of the selected white matter ROI. Anterior limb of the internal capsule (ALIC), Posterior limb of the internal capsule (PLIC), Genu of corpus callosum (GCC), Splenium of corpus callosum (SCC), Pons (Po), Cerebral peduncles (CP).
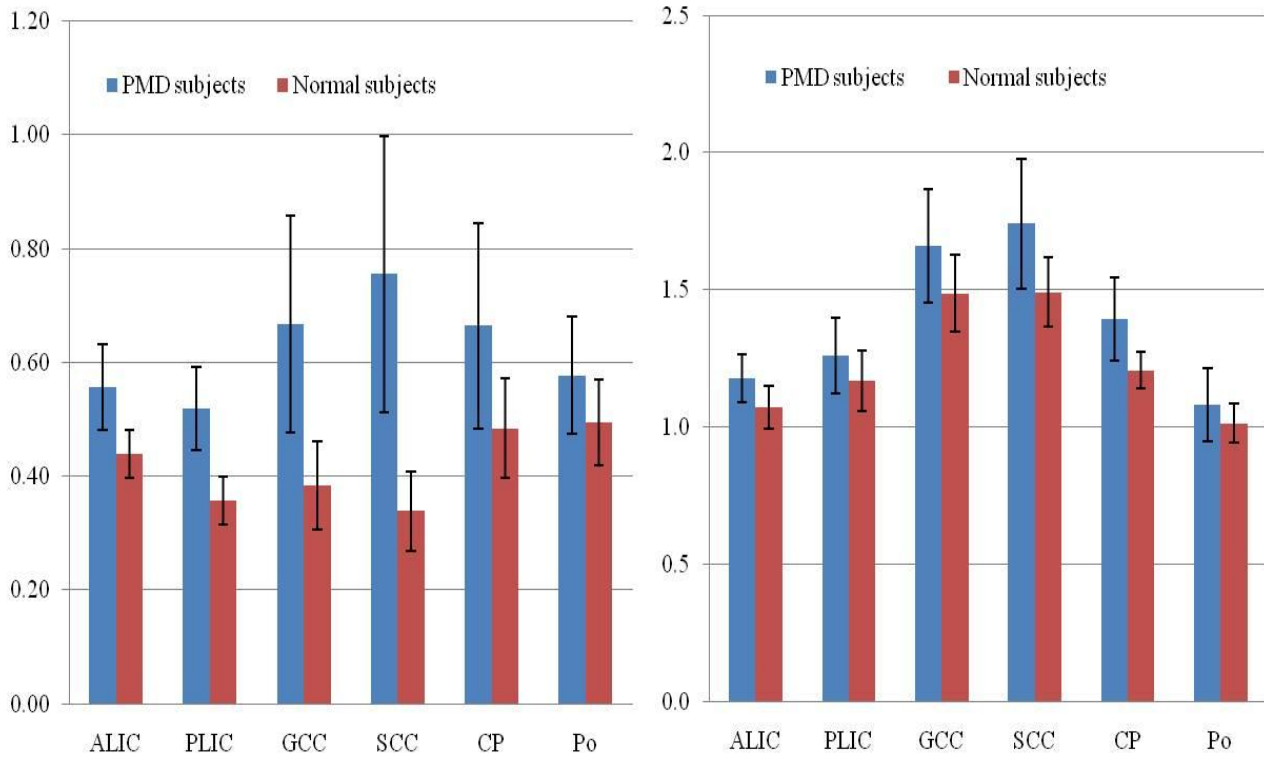
Figure 3.3: Null mutations. Left: Parallel (axial) diffusion 10^{-3}mm^2/s. Parallel diffusion

exhibited a mild increase (ALIC, GCC, SCC) and decrease (Po) compared to normal

controls subjects. This finding may suggest the role of axonal pathology, particularly the
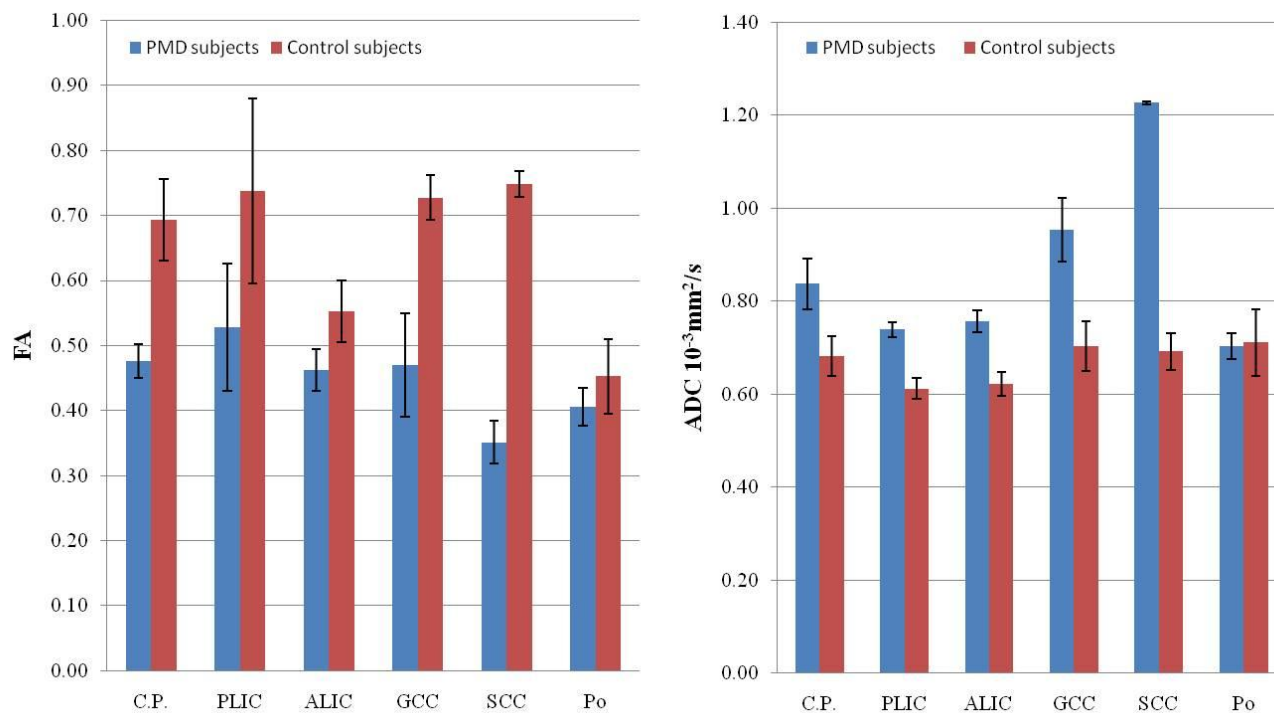
Figure 3.4: Null mutations. Left: Fractional Anisotropy (FA) 10^{-3}mm^2/s exhibited an increase compared to normal controls subjects. This finding supports the disruption of the cytoarchitecture and arrangement of fiber Right: Apparent diffusion coefficient (ADC) 10^{-3}mm^2/s. The patients demonstrate a significant increase (<0.05) compared to the normal control subjects.
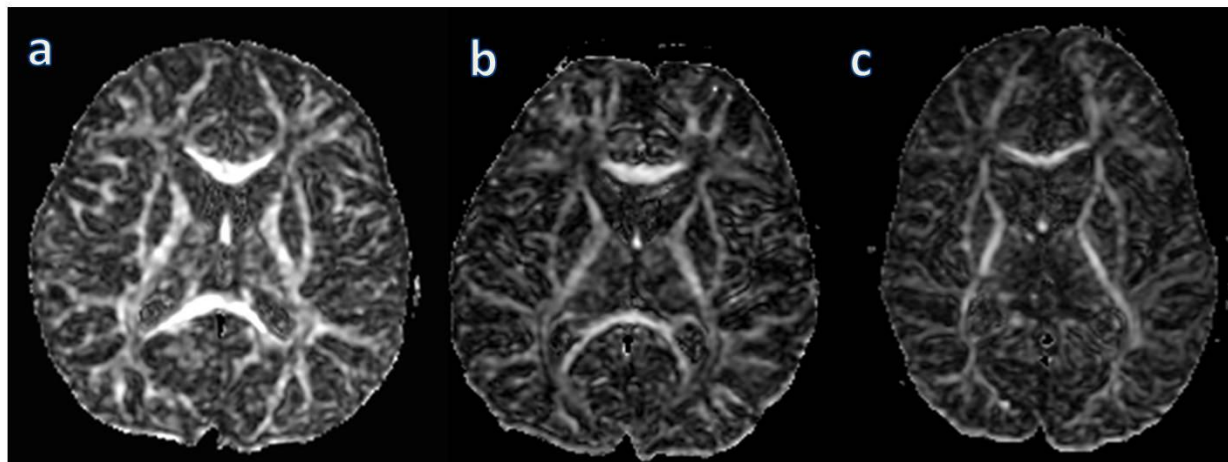
Figure 3.5 Axial FA diffusion maps of PMD patients with 'severe' *PLP1* mutations. (a) 2 year 1 month-old patient with a Y206H mutation and a FDS (30). (b) 3 year 7 month-old patient with a L84R mutation and a FDS (10). (c) 3 year 7 month-old patient with a L80R mutation and a FDS (4). The FA maps in these three cases exhibit a high degree of anisotropy diffusion (a) as expressed by the hyperintense areas in the white matter of the corpus callosum, although a significant reduction in the thickness of the white matter fiber bundle was observed and paralleled the regression in FDS. The posterior and anterior limb of the internal capsule in case (b) and moderately in case (c) demonstrates a low signal intensity reflecting areas of isotropic diffusion. The reduction in FA is most likely related to disintegration of fibers, but a significant increase in water content (edema) without any effect on the fibers themselves can give the same FA reading.

	λ_1 $[10^{-3}\,mm^2/s]$	λ_2 $[10^{-3}\,mm^2/s]$	λ_3 $[10^{-3}\,mm^2/s]$	ADC $[10^{-3}\,mm^2/s]$	FA
ALIC					
C	1.032 ± 0.034	0.536 ± 0.020	0.359 ± 0.019	0.642 ± 0.018	**0.564 ± 0.032**
P	1.192± 0.084	0.693 ± 0.023	0.519 ± 0.028	0.801 ± 0.030	**0.467 ± 0.047**
PLIC					
C	1.186 ± 0.047	0.440 ± 0.009	0.279± 0.022	0.635 ± 0.017	**0.759 ± 0.027**
P	1.379± 0.057	0.640 ± 0.062	0.475 ± 0.068	0.832 ± 0.056	**0.614 ± 0.058**
GCC					
C	1.462 ± 0.036	0.481 ± 0.008	0.298 ± 0.010	0.747 ± 0.014	**0.692 ± 0.011**
P	1.802± 0.062	0.740 ± 0.379	0.647 ± 0.267	1.063 ± 0.212	**0.556 ± 0.187**
SCC					
C	1.448 ± 0.081	0.423 ± 0.061	0.248 ± 0.062	0.706 ± 0.031	**0.734 ± 0.040**
p	1.822 ± 0.185	0.873 ± 0.327	0.731 ± 0.210	1.142± 0.127	**0.487 ±0.184**
Po					
C	0.980 ± 0.020	0.617 ± 0.023	0.373 ± 0.053	0.657 ± 0.028	**0.436 ± 0.037**
P	1.214 ± 0.175	0.844 ± 0.063	0.584 ± 0.031	0.880 ± 0.071	**0.339 ± 0.070**
CP					
C	1.188 ± 0.054	0.600 ± 0.033	0.402 ± 0.034	0.730 ± 0.034	**0.582 ± 0.033**
P	**1.513± 0.095**	**0.993 ± 0.226**	**0.750 ± 0.187**	**1.085 ± 0.162**	**0.390 ± 0.122**

	λ_1 %	λ_1 P	λ_{23} %	λ_{23} P	ADC %	ADC P	FA %	**P**
ALIC	15	0.01	35	<0.001	25	<0.01	-17	**<0.01**
PLIC	16	<0.001	55	<0.01	31	<0.01	-19	**0.02**
GCC	25	<0.01	78	0.2	42	0.05	-19	**0.3**
SCC	25	0.02	139	0.03	62	<0.01	-34	**0.08**
Po	24	0.1	44	<0.001	34	<0.01	-22	**0.1**
CP	**27**	**0.02**	**74**	**0.02**	**48**	**0.02**	**-39**	**0.02**

Table 3.2: Severe mutations. The top panel, represent the mean and standard deviation (SD) values of all *eigenvalues* λ_1, λ_2, and λ_3. Values of parallel diffusion ($\lambda_1 = \lambda_{//}$), radial diffusion ($\lambda_\perp = (\lambda_2 + \lambda_3)/2$), ADC and FA were then calculated on each ROI for the patients and normal controls The bottom panel, exhibits the percentage change and P-value between the patients and normal control for each of the selected white matter ROI. Anterior limb of the internal capsule (ALIC), Posterior limb of the internal capsule (PLIC), Genu of corpus callosum (GCC), Splenium of corpus callosum (SCC), Pons (Po), Cerebral peduncles (CP).

Figure 3.6: Severe mutations. Left: Parallel (axial) diffusion 10^{-3}mm^2/s. Parallel diffusion exhibited a mild increase (ALIC, GCC, SCC) and decrease (Po) compared to normal control subjects. This finding may suggest the role of axonal pathology, particularly the presence of axonal swellings providing a diffusion barrier. Right: Perpendicular (radial) diffusion 10^{-3}mm^2/s is significantly increased (<0.05) excluding the Pons.
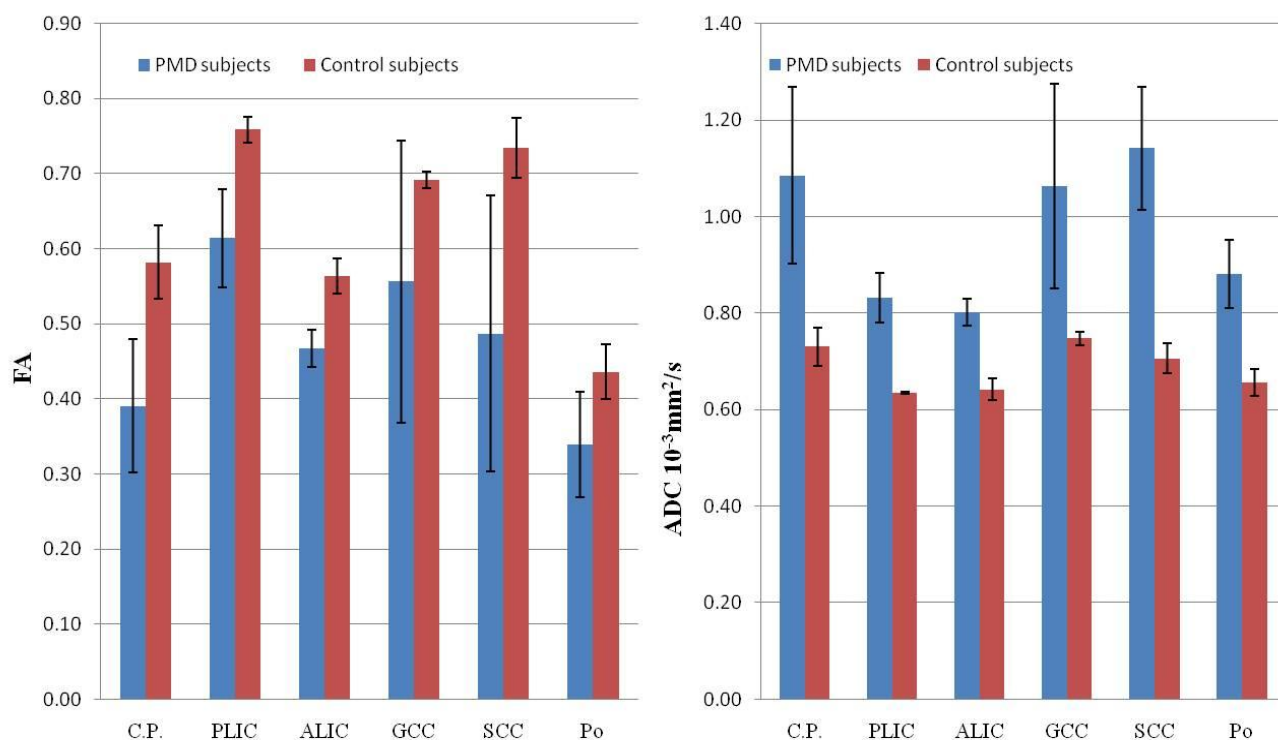
Figure 3.7: Severe mutations. Left: Fractional anisotropy $10^{-3}mm^2/s$. FA, exhibited a

mild increase (ALIC, GCC, SCC) and decrease (Po) compared to normal controls

subjects. This finding may suggest the role of axonal pathology, particularly the presence

of axonal swellings providing a diffusion barrier. Right: Apparent diffusion coefficient

$10^{-3}mm^2/s$ is significantly increased (<0.05) excluding the Pons.

CHAPTER 4

NEUROPATHOLOGY INVESTIGATION IN PELIZAEUS-MERZBACHER DISEASE IN VARIOUS MUTATIONS OF THE *PLP1* GENE

In 1885, Friedrich Pelizaeus first identified a genetic disorder causing spasticity and developmental delay (Pelizaeus 1885). Twenty-five years later in 1910, Ludwig Merzbacher further described the neuropathology of 12 affected individuals related to the proband (Merzbacher 1910). Together, Pelizaeus and Merzbacher identified the X-linked inheritance, the neonatal features, and the hypomyelination of the central nervous system that characterize the disease.

Pelizaeus-Merzbacher disease (PMD; MIM 312080) is classified as a dysmyelinating disorder, in which normal myelination never occurs, as opposed to a demyelinating disorders that often are the basis of other forms of leukodystrophies, in which normal myelin is later destroyed. Over the years, comprehensive surveys of PMD and autopsy reports have provided valuable insights into the clinic-neuropathologic understandings that have led to a distinct classification (classical, connatal, transitional and variants) of PMD that is dependent upon the mutation in the *PLP1* gene (Seitelberger 1954; Zeman, DeMyer et al. 1964; Seitelberger 1970; Seitelberger 1995). At the present time, although valuable contributions have been made in describing the neuropathologic pattern and pathogenic mechanisms underlying the distinct PMD classification, nosological problems regarding PMD still remain. To minimize the problems and to continue moving forward with a greater understanding of the heterogeneity pattern of the PMD, the best diagnosis is accomplished by neuropathologic findings at autopsy in addition to a comprehensive

genetic analysis. As described by (Seitelberger 1984), leukodystrophies are caused by different morphological changes of the CNS. The pathological changes observed in PMD, consists of a diffuse reduction and alteration of CNS myelin. The extent of myelin deficiency differs among the individual subtypes or classifications highlighting the unknown influence imposed by diverse mutational mechanisms of PLP. PMD is the most striking of the leukodystrophies particularly at early ages showing the reduction of developing myelin that is characteristic of dysmyelinating disorders.

The different *PLP1* mutational mechanisms have different effects on oligodendrocyte viability causing the reduction and alteration to CNS myelin. The understanding of the exact mutational mechanism that is responsible for causing the underlying pathology of each PMD subtypes is evolving, but a full understanding still remains. *PLP1* duplications result in overexpression of *PLP1* and the excess protein and its assembled associates, cholesterol and lipids, accumulate in late endosomes and lysosomes reducing the viability of oligodendrocytes effecting myelination (Woodward and Malcolm 2001; Simons, Kramer et al. 2002). *PLP1* point mutations are associated with the severe form of PMD that causes misfolding of PLP resulting in the failure to transport functional PLP to the oligodendrocyte cell membrane. The misfolded PLP accumulates in the rough endoplasmic reticulum (RER), and activates an unfolded protein response (UPR) which modulates the disease severity and includes the transcriptional activation of chaperone genes and apoptosis (Gow, Friedrich et al. 1994; Gow, Friedrich et al. 1994; Gow, Southwood et al. 2002). The ER stress is considered fatal for oligodendrocytes causing premature cell death exerting a downstream 'severe' effect on the ability to myelinate internodal axonal segments (Gow and Lazzarini 1996). *PLP1* null mutations are a complete opposite to PLP1 duplications and many missense mutations, in which myelination proceeds as normal,

oligodendrocytes are preserved forming relatively normal amounts of myelin. Patients with a null mutation experience a relatively mild clinical phenotype during childhood that is classified as mild PMD or complicated SPG2 (Raskind, Williams et al. 1991; Garbern, Cambi et al. 1997; Inoue 2004). Mice with a functionally null *PLP1* gene have functionally normal oligodendrocytes that develop and assemble relatively normal thick myelin, however a late and rapid progression characterized by length-dependent axonal degeneration of motor and sensory tracts along with axonal spheroids are likely responsible for the rapid decline. Although the underlying mechanisms, as previously mentioned, are not fully understood, evidence does support the structural role of PLP in maintaining axonal integrity and compaction of the adjacent myelin leaflets. Absence of PLP paradoxically does not affect myelination. The variability in disease severity is most likely the result of the difference in PLP processing, trafficking of mutant PLP and gain-of-function mechanisms. Examining the neuropathology in conjunction with the clinical history and genetic analysis will provide the infrastructure for piecing together the pathogenesis that is characteristic of a heterogeneous disease such as PMD.

This chapter will focus on results obtained from brain autopsy cases of 4 male PMD patients with confirmed *PLP1* mutations that include: (1) duplication (overexpression), (2) Null (complete deletion), (3) W144X (PLP-specific domain; mild clinical phenotype), (4) IVS6+3G>T (severe clinical phenotype).

Material and Methods

Case reports

***PLP1* duplication case**

Case 1 is from a family previously described clinically, and died at 47 years of age, respectively. He had classical PMD syndrome with understandable but dysarthric speech, spastic

quadriparaesis and never ambulated independently. Voluntary movements were slow with rigidity compromised by severe spasticity.

PLP1 null mutation

Case 2 had a complete deletion of the *PLP1* gene and flanking genes on the X-chromosome as described in (Raskind, Williams et al. 1991). He was wheelchair confined from late adolescence and developed progressive spasticity and dysarthria. He had severe spastic quadriplegia during the last 5 years of life and lost speech 2 years before be expired at age 47 from aspiration pneumonia.

PLP1 point mutations

Case 3 was 50 years old male, respectively with a W144X mutation who had been previously been described (Osaka, Kawanishi et al. 1995) and is considered to have mild PMD or SPG2. This mutation resides in the later part of exon 3 (exon 3b), an internal splice donor site, which is alternatively spliced out of DM20 (Nave, Lai et al. 1987).

Case 4 was a 25 year old male, respectively, who subsequently was discovered to have a PLP1 point mutation that disrupts splicing, causing in-frame exon 6 skipping, with loss of 22 residues (Southwood, Garbern et al. 2002).

Pathological analysis

Histological staining and immunohistochemistry

Corpus callosum (CC) tissue was extracted from each of the 4 male PMD patients brain tissue and a male control patients and tissue sections were embedded in paraffin blocks and the remaining tissue was stored in 4% fresh paraformaldehyde solution. The paraffin-embedded tissue was sectioned at 4μ stainined with routine hematoxylin-eosin (H&E), Luxol-fast blue (LFB), Bielschowsky silver stain and glial fibrillary acidic protein (GFAP)

immunocytochemistry. Tissue was also prepared for 1μ semi-thin sections for toludine blue staining (TB). Immunocytochemistry was performed using immunoperoxidase staining techniques to detect myelin basic protein (MBP), proteolipid protein (PLP-AA3), GFAP, and non-phosphorylated neurofilament (NF-SM32).

Immunoperoxidase staining

The paraffin-embedded tissue was cut into 5μm thick sections and mounted on (+) charged slides and dried for 1hr at 60°C. The tissue was deparaffinized with Xylene (3 changes) and rehydrated through a series of graded ethanol (100, 95, 70 and 50%) to distilled water. The tissue was blocked with endogenous peroxidase activity with 3% H_2O_2 for 5 minutes at room temperature. Epitope antigen retrieval was required, so the tissue was treated with 0.1M citrate buffer and cooked in the microwave for 10 minutes on high power than cooled to room temperature for approximately 20 minutes. The tissue was rinsed briefly in distilled water then blocked with non-specific antibody binding by incubating in 5% serum/0.5% BSA in 1X PBS [(Goat for monoclonal GFAP and MBP and Horse for polyclonals PLP and NF]. The primary antibody [(PLP 1:200), (SMI32-NF 1:1000), (MBP 1:500) and (GFAP 1:1000)] was diluted to the optimal concentration in 1X PBS and incubated overnight at 4°C. The tissue was washed (3 changes) over 5 minutes with distilled water. Biotinylated secondary antibody (Vector Labs) was diluted in 1X PBS and applied [(1:200 for GFAP and SMI32-NF(Mouse)] and [(1:500 for MBP and PLP (Rat)]. Applied 500μl of AEC substrate (Vector labs) was applied and tissue was incubated for 30 minutes or until the tissue turned red which occurred at times after 15 minutes. The tissue was washed in distilled water (3 changes) and then counterstained in Mayer's Hematoxylin for 1 minute and washed in tap water. The tissue was then rinsed once in 0.2%

100% NH₄OH and then briefly in tap water. The tissue was then coverslipped using a water-based mounting media.

Immunohistochemistry – Monoclonal Rat anti-AA3/PLP

Specimens were fixed in 10% Neutral Buffered Formalin followed by processing, embedding in paraffin and sectioned on a rotary microtome at 5µ thickness. Sections were placed on slides coated with 2% 3-Aminopropyltriethoxysilane and dried at 56°C overnight. The slides were subsequently deparaffinized in Xylene and hydrated through descending grades of ethyl alcohol to distilled water. Slides were placed in Tris Buffered Saline pH 7.4 (Scytek Labs – Logan, UT) for 5 minutes for pH adjustment. Epitope retrieval was performed using Citrate Plus Retrieval Solution pH 6.0 (Scytek) in a vegetable steamer for 30 minutes followed by a 10 minute countertop incubation and rinsed in several changes of distilled water. Endogenous Peroxidase was blocked utilizing 3% Hydrogen Peroxide / Methanol bath for 30 minutes followed by running tap and distilled water rinses. Following pretreatment, standard avidin-biotin complex staining steps were performed at room temperature. All staining steps were followed by rinses in Tris Buffered Saline + Tween 20 (Scytek). After blocking for non specific protein with Normal Goat Serum (Vector Labs – Burlingame, CA) for 30 minutes; sections were incubated with Avidin / Biotin blocking system for 15 minutes each (Avidin D – Vector Labs / d-Biotin – St. Louis, MO). Primary antibody slides were incubated for 60 minutes with the Monoclonal Rat anti-AA3/PLP diluted at 1:200 in Normal Antibody Diluent (NAD) (Scytek). Tissue was incubated in biotinylated Goat anti-Rat IgG (H + L) prepared at 11.0µg/ml in NAD incubated for 30 minutes; followed by R.T.U. Vectastain Elite ABC Reagent incubation for 30 minutes. Reaction development utilized Vector Nova Red peroxidase chromogen incubation of 15 minutes followed by counterstain in Gill Hematoxylin (Thermo Fisher – Kalamazoo, MI) for

15 seconds, differentiation, and dehydration, clearing and mounting with synthetic mounting media.

Immunohistochemistry – Polyclonal Rabbit anti-Glial Fibrillary Acidic Protein (GFAP)

Specimens were fixed in 10% Neutral Buffered Formalin followed by processing, embedding in paraffin and sectioned on a rotary microtome at 4µ thickness. Sections were placed on slides coated with 2% 3-Aminopropyltriethoxysilane and dried at 56°C overnight. The slides were subsequently deparaffinized in Xylene and hydrated through descending grades of ethyl alcohol to distilled water. Slides were placed in Tris Buffered Saline pH 7.4 (Scytek Labs – Logan, UT) for 5 minutes for pH adjustment. Endogenous Peroxidase was blocked utilizing 3% Hydrogen Peroxide / Methanol bath for 30 minutes followed by running tap and distilled water rinses. Following pretreatment standard avidin-biotin complex staining steps were performed at room temperature . All staining steps are followed by rinses in Tris Buffered Saline + Tween 20 (Scytek). After blocking for non specific protein with Normal Goat Serum (Vector Labs – Burlingame, CA) for 30 minutes; sections were incubated with Avidin / Biotin blocking system for 15 minutes each (Avidin D – Vector Labs / d-Biotin – St. Louis, MO). Primary antibody slides were incubated for 60 minutes with the Polyclonal Rabbit anti-GFAP diluted @ 1:300 (Dako North America – Carpentaria, CA) in Normal Antibody Diluent (NAD) (Scytek). Biotinylated Goat anti-Rabbit IgG (H + L) prepared at 11.0µg/ml in NAD incubated for 30 minutes; followed by R.T.U. Vectastain Elite ABC Reagent incubation for 30 minutes. Reaction development utilized Vector Nova Red peroxidase chromogen incubation of 15 minutes followed by counterstain in Gill Hematoxylin (Thermo Fisher – Kalamazoo, MI) for 15 seconds, differentiation, and dehydration, clearing and mounting with synthetic mounting media.

Luxol Fast Blue-Hematoxylin & Eosin staining

The 5µ paraffin sections of corpus callosum were deparaffinized in Xylene and rehydrated to 95% alcohol. The sections were placed in Luxol fast blue solution overnight in oven at 56°C. The Luxol fast blue, 0.1% solution was made using 5.0g of Luxol fast blue dissolved in 1L of distilled water and 10% Glacial acetic acid. The tissue was then rinsed in 95% alcohol to remove excess stain. The tissue was washed well in running tap water for approximately 2-3 minutes. Slides were immersed in lithium carbonate solution (0.05% solution) for approximately 20 seconds to begin differentiation. 0.25g of lithium carbonate was diluted in 500ml of distilled water. The tissue continued in 70% alcohol solution until white matter could be distinguished. The tissue was then rinsed briefly in lithium carbonate solution and then put through several changes of 70% alcohol solution until the blue of the white matter appears sharply. Rinse thoroughly in distilled water followed by the immersion in Mayer's hematoxylin for 3 minutes. Slides were washed in tap water for 5 minutes and washed in .025% ammonia water for 1 minute for a blue nucleus. The tissue was washed will in running tap water for 5 minutes and then in distilled water. The tissue was stained in Eosin solution for 8 minutes, following by dehydration in 2 changes of 95% alcohol and 3 changes of absolute alcohol.

Luxol Fast Blue staining

The 5µ paraffin sections of corpus callosum were deparaffinized in Xylene and rehydrated to 95% alcohol. The sections were placed in Luxol fast blue solution overnight in oven at 56°C. The sections were then rinsed in 95% alcohol to remove excess stain. The tissue was washed well in running tap water for approximately 2-3 minutes. The tissue was immersed in lithium carbonate solution for approximately 20 seconds to begin differentiation and continued

in 70% alcohol solution until white matter can be distinguished. The tissue was then rinsed briefly in lithium carbonate solution and then put through several changes of 70% alcohol solution until the blue of the white matter appears sharply. The tissue was dehydrated in 2 changes of 95% alcohol and 3 changes of absolute alcohol.

Hematoxylin and Eosin staining

The 5µ paraffin sections of corpus callosum were deparaffinized in 2 changes in Xylene at 10 minutes each. The tissue was rehydrated in 2 changes of absolute alcohol at 5 minutes each, 95% alcohol for 2 minutes and 70% alcohol for 2 minutes. The tissue was washed briefly in distilled water and then staining with Mayer's Hematoxyln solution for 3 minutes. The tissue was then washed in tap water and then place in .25% ammonia water until the slides turned blue. The tissue was then washed in tap water for approximately 1 minute following by a rinse in distilled water for 2 minutes. The tissue was rinsed in 70% alcohol and then counterstained in Eosin solution for approximately 1 minute and then dehydrated in 95% alcohol for 2 changes and then 3 changes for absolute alcohol for 1 minute each. The tissue was then cleared in 2 changes of xylene, 3 minutes each. The slides were then cover slipped with mounting medium.

Bielschowsky Silver stain

The corpus callosum was fixed in 10% neutral buffered formalin. The paraffin embedded corpus callosum tissue was cut at 5µ sections. The slides were deparaffinized with xylene and hydrated to distilled water, following by 3 washings at 3 minutes each in distilled water. The sections were placed in 20% working silver nitrate solution for 15 minutes at 37C. The remaining silver nitrate was poured off at the end of the 15 minutes into a clean container and saved. The tissue was washed in several changes of distilled water for 10 minutes.

To the silver nitrate that was saved from Step #4, ammonium hydroxide (concentrated 58%) was added drop by drop while agitating the container continuously until the precipitate which forms is completely dissolved. Since approximately 7.0 to 7.5 mls are required, 6.0 mls was added at once; thereafter, the ammonium hydroxide was added drop by drop until the end point is reached.

The tissue was placed in ammoniacal silver solution for 8 minutes at 37C, followed by placing the solution in to a clean container. The slides were placed in the working 1% ammonium hydroxide solution for 3 minutes. To the ammoniacal silver, add 4 drops of developer followed by microwaving for 40 seconds + 20 seconds and agitate at 70°C in water bath for 2 - 3 minutes. Sections are to be agitated until they turn a golden brown color. The tissue was washed in 1% ammonium hydroxide solutions for 2 minutes and then washed in distilled water for 1 minute. The tissue was placed in 5% sodium thiosulfate for 3 minutes and then washed in 3 changes of distilled water at 5 minutes each. The tissue was dehydrates through graded ethyl alcohols and cleared in several changes of Xylene. The slides were then coversliped with permanent mounting media.

Results

Myelin and axonal pathology

PLP1 duplication case (case 1)

This case showed a similar appearance of dysmyelinated tissue to that found in other cases with PMD. The corpus callosum was grossly thin, markedly dysmyelination reflecting a substantial reduction of myelin. The staining pattern for myelin basic protein (MBP) (Fig. 4.1b), proteolipid protein (PLP) (Fig. 4.1c) and toludine blue (Fig. 4.1d) showed a progressive decrease in myelin composition. The primary defect in PMD is the myelin abnormalities, referred as dysmyelinating, but the relatively thin myelin that has formed most likely breaks down

undergoing the process of demyelination. In this particular case, demyelination of preexisting myelin resulted in a characteristic pattern not reported in previous literature and is described here as discreet aggregates or clumps of degenerative myelin products (Fig. 4.1b-f). The deposits of myelin products appear to be concentrated within the extracellular space with a few found intracellular as marked by a solid membrane surrounding the content. Most of the degraded myelin products did not appear to be found within microglia or macrophages representing types of scavenger cells. Furthermore, it appears on H&E staining that no other cells are proliferating or congregating near the region of these aggregates (Fig 4.1f). This finding most likely marks the time period during the pathogenesis that precedes the invasion of scavenger cells to engulf the debris by phagocytosis. Axonal spheroids were not observed, but should not be excluded as an occasional feature, as reported in Sima et al., (2009). Moderate to severe loss of oligodendrocytes and marked astrogliosis were observed. Although axonal injury is not a consistent finding across the PMD spectrum, it is reported in patients and mice as previously discussed and may be influenced by the heterogeneity of PLP1 mutations.

Null mutation case (case 2)

The case showed a similar pattern of myelin loss, but not due to disturbances in myelin formation caused by glial dysgenesis resulting in the classical dysmyelinating pattern. Thinning and density of the myelinated fibers were less pronounced than that of the duplication and missense mutations. The staining of myelin with HE-LFB (Fig. 4.2c) and toludine blue (Fig. 4 .3c) was not severely reduced, although fiber density appeared to be reduced. Axons that did not have any appreciable amount of myelin sheaths most likely experienced late demyelination associated with axonal injury. In contrast to the duplication patient, the products that reminisce that of the structural decomposition of myelin sheath was not observed. The white matter displayed numerous spheroids (Fig. 4.2) and mild astrogliosis (Fig. 4.5e). Activated microglia were occasionally observed as exemplified by their characteristic elongated cigar shape cell morphology, but the only definitive way to identifying the state of microglia is using specific antibodies to label such cells.

Missense mutation cases (case 3 & 4)

Both cases exhibited a severe loss to thinning of myelin consistent of a diffusely dysmyelinated tissue with reduced oligodendrocytes (Fig. 4.2d-e). Both cases exhibited marked astrogliosis (Fig 4.5c-d), but case 4 demonstrated an extensive network of astroglial process acting as a space occupying lesion between the reduced dys/demyelinated axonal fibers (Fig 4.5d). Both cases exhibited a mark reduction in axonal density with an occasional spheroid being found in case 4. Case 3 exhibited a diffuse pattern of numerous spheroids similar to the findings of the null mutation in case 2. Microglia were occasionally observed suggestive of a mild inflammatory response associated with active demyelination particularly in case 3 were appreciable amounts of degenerative myelin sheaths were found clustered.

Discussion

In the present study, results was examined in white matter pathology of the corpus callosum in brain autopsy cases of 4 male PMD patients with confirmed *PLP1* mutations that include: (1) duplication (overexpression), (2) Null (complete deletion), (3) W144X (PLP-specific domain; mild clinical phenotype), (4) IVS6+3G>T (severe clinical phenotype). The observations collected from this neuropathology study supports previously reported findings of the progressive myelinopathy (Zeman, DeMyer et al. 1964; Seitelberger 1970; Seitelberger 1984; Seitelberger 1995) and axonopathy that is characteristic of PMD (Anderson, Schneider et al. 1998; Griffiths 1998; Garbern, Yool et al. 2002; Deluca, Ebers et al. 2004; DeLuca, Ebers et al. 2004).

The classical form of PMD includes duplications of the entire gene accounting for 60-70% of the patient base (Sistermans, de Wijs et al. 1996). Depending on the degree of PLP1 overexpression, experimental evidence involving transgenic mice indicates that gene expression is dosage sensitive and can cause dysmyelination and a late-onset demyelination (Kagawa, Ikenaka et al. 1994; Readhead, Schneider et al. 1994). These findings translate to human patients with three or more copies of the PLP1 gene who exhibited a more severe form of PMD (Wolf, Sistermans et al. 2005). The findings from these and other studies, implies that more than one pathogenic mechanism is responsible for the disease process and clinical severity.

Seitelberger's seminal work that uncovered the neuropathologic characteristics of the PMD subtypes described the classic form of PMD as a patchy appearance of relatively conserved, but thinner than normal myelin with preservation of the axon structure (Seitelberger 1970). These findings are consistent in case 1 of a PMD patient with PLP1 gene duplication reported in this study. LFB, MBP and PLP immunostaining exhibited axons that were moderately myelinated with several fibers experiencing late-onset demyelination in the presence

of numerous 'myelin balls' representing degraded myelin products. As a result of this diffuse pattern of 'myelin balls,' robust microglia were observed discreetly as an enlarged elongated nucleus suggesting the onset of an inflammatory response to the structural changes resulting from the myelin pathology. These findings are also in concert with (Edgar, McCulloch et al. 2010) of *PLP1* transgenic mouse optic nerve that showed high level microglia activation in areas of demyelination and a low level of microglia activation in areas of dysmyelination, furthermore (Tatar, Appikatla et al. 2010) also demonstrated that a large influx of microglia reactivity in PLP transgenic mice. An occasional axonal spheroid and degenerative axons were observed, but was not a regular consistent finding which may suggest that the robust activation of microglia, as reported in inflammatory demyelinating lesion of MS, may influence the late-onset axonal pathology found in PMD (Trapp, Ransohoff et al. 1999).

Early manifestations of pathologic changes begins at birth for the connatal form interfering with the process of myelin formation caused by premature oligodendrocyte cell death due to cytotoxic accumulation of misfolded PLP retained in the ER causing a reduced number of mature oligodendrocytes. LFB, toludine blue, MBP and PLP all showed a significant decrease in staining for myelin in PMD patients with a mild missense mutation (case 3) and severe missense mutation (case 4). Case 3 and case 4 exhibited a marked increase in GFAP-positive staining for reactive astrocytes as previously reported by (Ulrich, Kohler et al. 1983; Ulrich, Matthieu et al. 1983; Koeppen, Barron et al. 1988) and is a marker of CNS white matter injury. An overwhelming proliferation of glial processes in case 4 appeared to occupy the vast extracellular space that maybe described as a space occupying lesion, due to the reduced density of the severely dysmyelinated axons. Myelin degradation products were more frequently identified in case 3 suggesting that the axons were moderately myelinated preceding the active process of

demyelination. Furthermore, the axons in case 4 were severely dysmyelinated with areas of no appreciable amount of myelin detected.

Axonopathy was a common recurring observation found in case 3 that had a PLP-specific nonsense mutation in exon 3B (W144X) and classified as a mild form of PMD or SPG2 (Hodes, Blank et al. 1997; Cailloux, Gauthier-Barichard et al. 2000) and in case 2 of the patient with a deletion of the *PLP1* gene that is also classified as having a mild form of PMD. Both cases exhibited numerous axonal spheroids and thinning of fibers. The axon abnormalities are not a cause of demyelination, since myelin is intact and oligodendrocytes are viable, but the defect lies in the oligodendrocyte-axonal interaction. Consistent with this finding, Garbern and colleagues reported a significant reduction in NAA/Cr ratio in mice and patients using MRS and is indicative of neuronal integrity (Garbern, Moore et al. 2002). These findings echoes prior reports of axonopathy in PMD null mutations and in transgenic mice with low level increase in *PLP1* expression (Anderson, Schneider et al. 1998) and explains the late-onset and relative rapid decline in clinical disability compared to the early onset severe manifestation by *PLP1* missense mutations and the severity of high levels of increase *PLP1* expression.

The inflammatory response imposed by the activated microglia found in case 3 may explain the thinning of axons and numerous spheroids as mentioned previously, whereas the complete absence of PLP1 has been reported not to cause CNS inflammation supporting the maintenance role of PLP in maintaining axon integrity. Axonal injury is most likely a consequence of the inflammation around the axons in case 3, but the alternative view should be considered as well suggesting that that demyelination is also a variable responsible for axon pathology.

Activated microglia were occasionally observed by their characteristic elongated euchromatic nucleus in both *PLP1* missense mutations marking the presence of an inflammatory reaction that has been well documented in EAE mice and MS patients with inflammatory demyelination (Bradl and Linington 1996; Bar-Or, Oliveira et al. 1999; Trapp, Bo et al. 1999; Bradl and Hohlfeld 2003). The Inflammatory response detected in MS has been well described as having a strong influence in controlling axonal pathology found in MS lesions and are responsible for the irreversible neurological disability (Trapp, Peterson et al. 1998; Bjartmar and Trapp 2001; Bjartmar, Wujek et al. 2003). These findings may have strong implications in describing axonal pathology as it relates to neurologic impairment in PMD particularly in the mild cases of PMD that express an appreciable myelin thickness and density of axons that are now susceptible to demyelination marking the end-point in the pathologic progression.

Conclusion

Merzbacher originally described the absence of myelin sheaths specific to the CNS without axonal involvement and preserved myelin islets around blood vessels. These patchy areas of myelin islands give the tissue a "tigroid" appearance (Takanashi, Sugita et al. 1999). Gross sections of the PMD brain reveal atrophy, pallor, and sclerosis of white matter in the cerebrum, cerebellum, and brainstem (Gencic, Abuelo et al. 1989). The axons of the central nervous system lack the typical myelin sheath. In addition, there is a profound loss of oligodendrocytes, which produce myelin. The pathologic pattern of diffuse degraded myelin aggregates, found in duplications is not a new finding as (Seitelberger 1970) described a similar pathology in PMD called "myelin balls." However, beyond the written description the exact pathologic appearance has not been observed to my knowledge.

Axonal damage is variable and found remarkable in particular cases of the PMD subtypes. Axonal damage has been demonstrated, particularly in the null mutation and the mild point mutation found within the PLP1 specific domain cause aberrant trafficking of PLP and not DM20. The presence of axonal spheroids was observed diffusely in both cases with an occasional spheroid found in the severe missense and duplication patients that is likely due to impaired axonal transport from altered proteolipid protein-mediated oligodendrocyte-axonal interactions. This finding follows the pathologic thinking that white matter volume is a clinical manifesting determinant, but axonal play an equal role that exhibits in a late-onset phenomenon. Furthermore, the presence of microglia in the duplication patient, but also found in the mild and severe point mutations suggest a causative role in regulating axonal viability as seen in MS inflammatory demyelination lesions. This was not a prominent finding in the null mutation, although should not be discounted as potential variable, but the late-onset axonal pathology exhibited by degeneration and spheroids are caused by the dosage sensitivity of the *PLP1* gene. The results from this study, corroborates and supports the previous findings documented PMD pathology, but this study also brings new information providing insight into the pattern and progression of the disease pathogenesis.
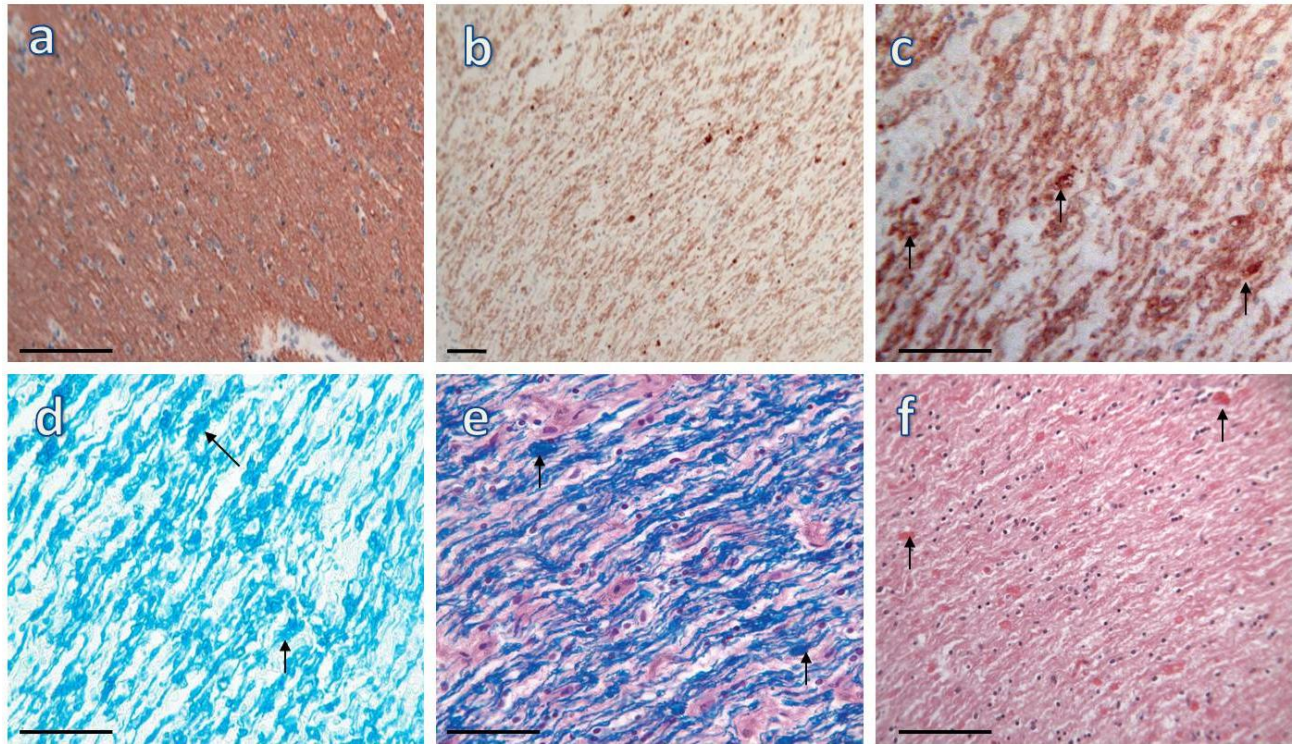
Figure 4.1 Pathologic changes in PLP1 duplication patient (case 1). (a) 60 year-old

control subject, who exhibits a normal density of myelinated fibers and distribution of

oligodendrocytes by immunoperoxidase-MBP staining. (b) Thinning of myelin and reduced

axonal fiber density with an increase composition of myelin degradation products using an

immunoperoxidase staining for MBP. (c) immunoperoxidase stain for PLP exhibiting

irregular non-uniform aggregates (arrows) of PLP a degradation product of myelin. (d)

Luxol-fast blue, (e) HE-LFB and (f) H&E staining provide conclusive insight into a window

a time of the pathologic product of demyelination (arrow) of the very thin pre-existing

myelin that formed. Scale 50 µm.

Figure 4.2 *PLP1* gene deletion. Numerous axonal spheroids (arrows) could be detected by light microscopy under Bielschowsky silver stain (a, b) and H&E-LFB staining (black arrow) (c) and were diffusively observed in the corpus callosum. Plate (a): scale10µm. Plate (b, c): scale 50µm.

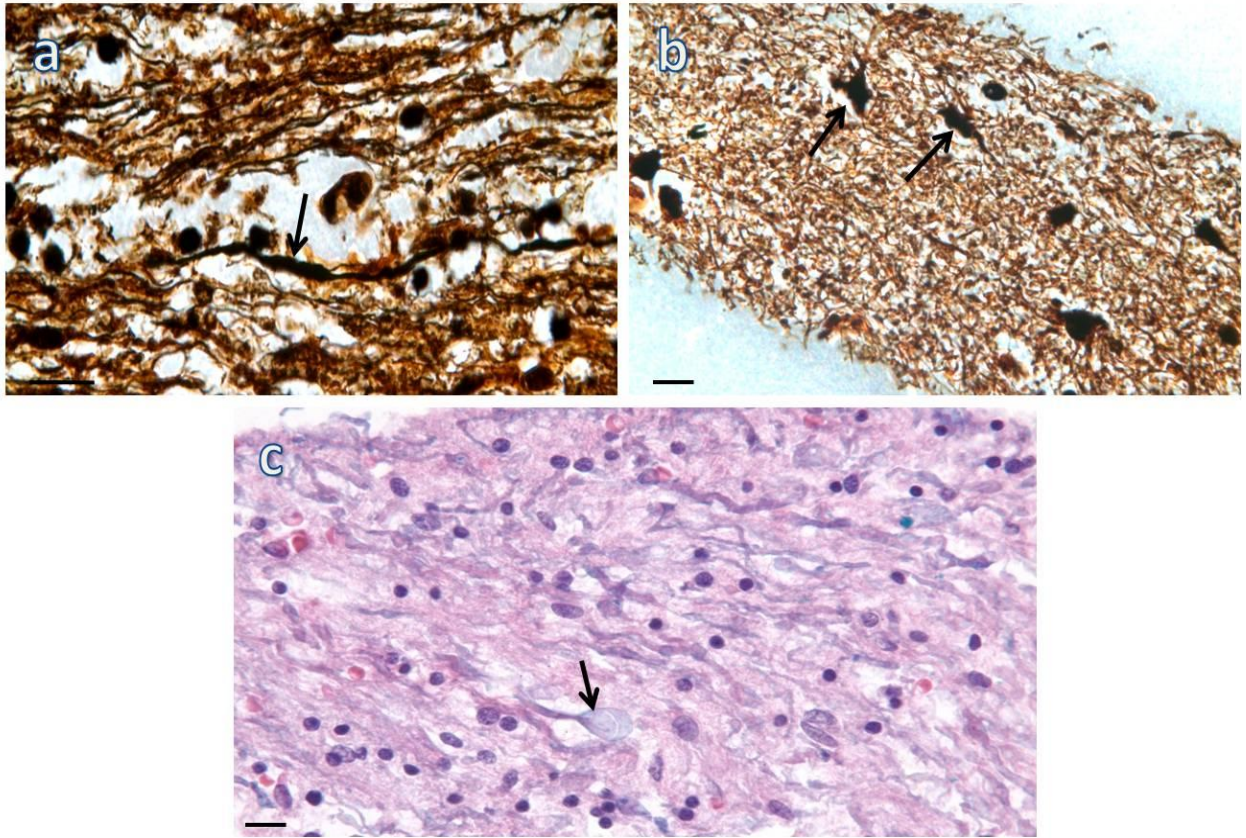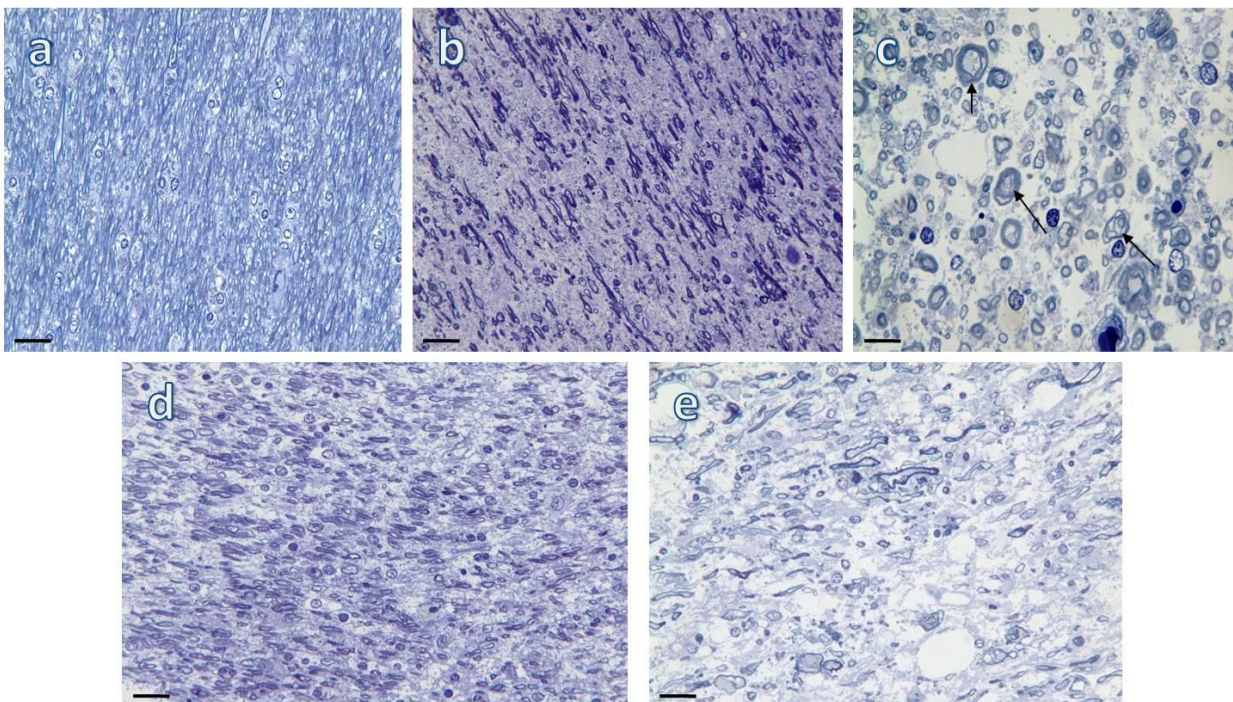**Figure 4.3** Toludine blue staining. (a) 60-year-old control subject with normal thickness and distribution of axonal fibers. (b) Duplication (case 1): Diffuse dysmyelinating and decrease in axon density. (c) Null mutation (case 2): Axons demonstrate relatively thick myelin sheaths with structural abnormalities reflected in the 'unraveled' morphology (artifact) due to the absence of PLP and its innate ability to form compact myelin (black arrows). Axon diameter appears relatively large and may suggest that some of the axons are swollen and actively undergoing demyelination. (d) Severe missense mutation, IVS6+G>T (case 4) and (e) Mild missense mutation, W144X (case 3) exhibits a uniform reduction to absence of myelin and oligodendrocytes. Activated microglia are observed in the 4 cases suggesting an ongoing inflammatory response to the pathologic changes of the white matter, particularly during the destruction of myelin. Scale 50µm.
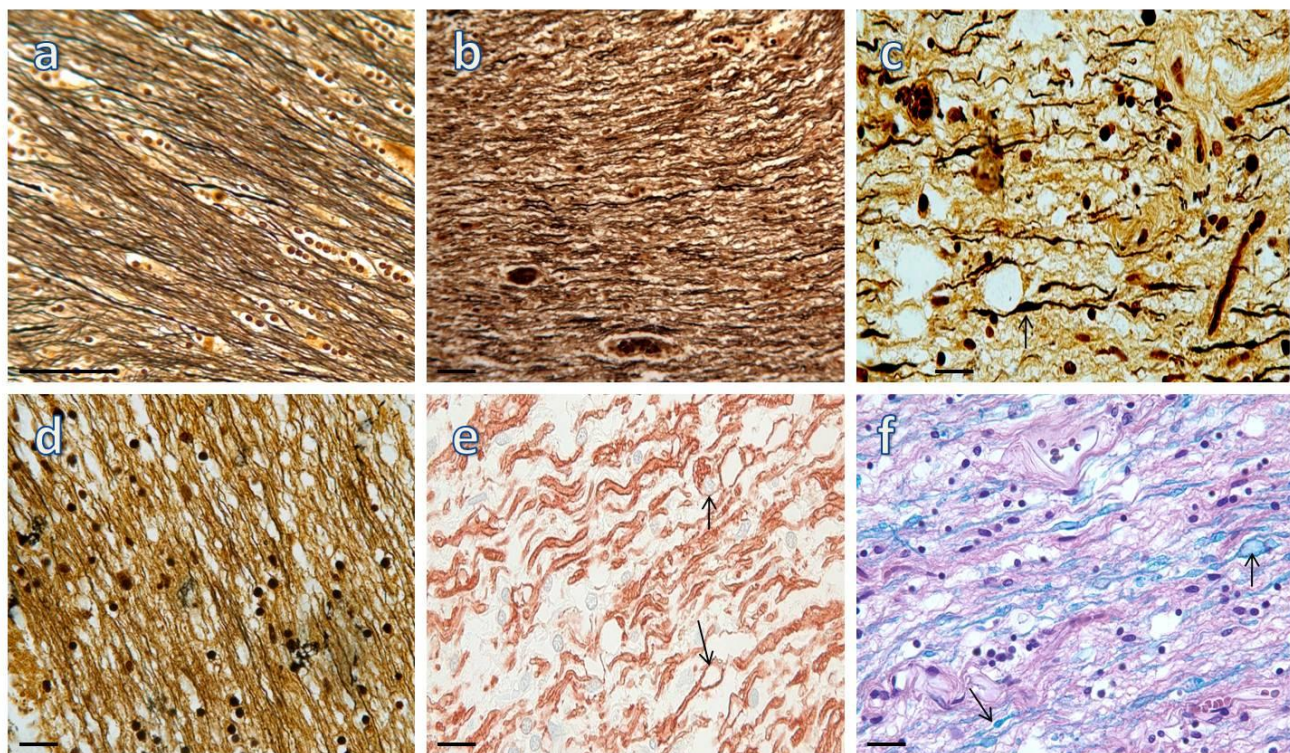
Figure 4.4. Axonal pathology. (a) Bielschowsky silver staining of a normal subject with normal distribution and density of axons. (b) Duplication (case 1). The density of axonal fibers is relatively normal although axonal degeneration is likely to contribute towards the disease pathogenesis. (c) Mild missense mutation, W144X (cases 3) and (d) severe IVS6+G>T (case 4) exhibited a moderate reduction in axon density. The mild mutation W144X (plate c; case 3), exhibited numerous swollen axons (arrows) with Bielschowsky silver stain, (e) immunoperoxidase-MBP staining and with (f) H&E-LFB staining (arrows). Scale 50µm.
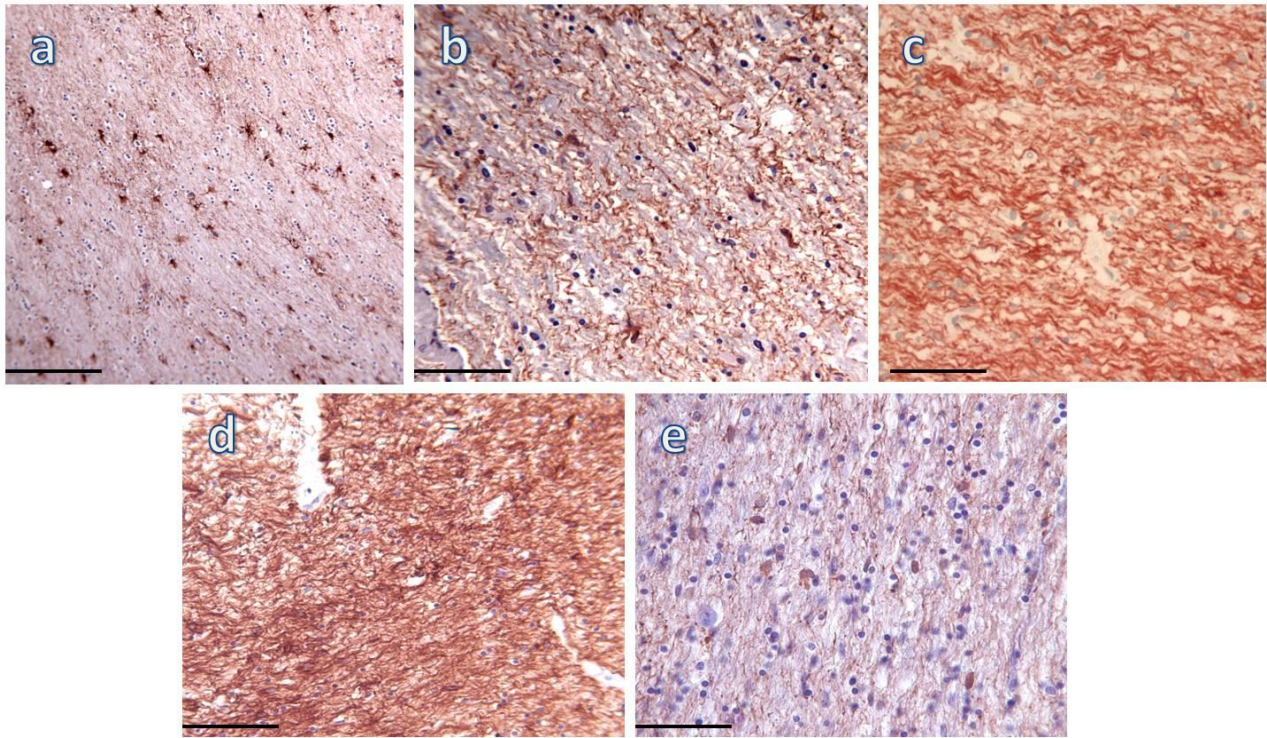
Figure 4.5. GFAP stain. The characteristic and vigorous response of astrocytes to white matter injury is a prominent feature observed in the 4 cases as reflected in the GFAP staining. (a) 60 year-old normal control subject with non-reactive astrocytes. (b) Duplication (case 2) has moderate gliosis, whereas, (c) the mild W144X missense mutation and (d) severe IVS6+G>T missense mutation reflects an extensive array of gliosis occupying the space of the substantially hypomyelinated corpus callosum. (e) Null patient (case 2) exhibits a mild form of gliosis due to the presence of relatively normal thickness of myelin that was sustained through the course of the disease. Scale 50μm.

CHAPTER 5

CONCLUSION

Pelizaeus-Merzbacher disease is a dysmyelinating disorder, in which normal myelination never occurs. Mutations of the PLP1 gene result in a range of phenotypes that form a clinical spectrum, from the more severe PMD at one end, to the relatively mild X-linked spastic paraplegia 2 (SPG2) at the other. Most cases (60-70%) of PMD are caused by duplication of the PLP1 gene, which most likely causes overexpression of PLP, resulting in compromise of the myelin sheath structure. Protein misfolding caused by PLP1 missense mutations is a second likely pathogenic mechanism of PMD. A third mechanism involves null-mutations leading to a loss of function in which no protein is produced. These cause relatively mild disease. The major clinical features of PMD are nystagmus, spasticity, athetosis, tremor, and ataxia. The symptoms vary in onset and severity, thereby producing a clinical spectrum of disease. Various forms or phenotypes of PMD are distinguished by severity of disease and other clinical features.

The results of this study demonstrates that reduced white matter volume is likely one determinant of neurological disability in PMD patients, while axonal dysfunction or loss is a late post-adolescent phenomenon that contributes to the clinical and pathologic progression. The clinical severity measurements and MRI volumetric finds are consistent with the speculation that white matter is inversely correlated with PMD severity. The correlation was moderate, although highly significant. Reduction in white matter volume may result not only from the hypomyelination but also axonal loss. The surrogate marked to measuring the distance between the caudate nucleus is a reliable method to implement when grey white matter segmentation is not possible to delineate.

Since the degree of myelination is relatively preserved in *PLP1* null myelin, the increased radial diffusion found using diffusion imaging is not the result of thinner myelin sheaths per se, but the increased radial diffusion is more likely due to increased myelin water, due to decreased compaction, which described the existence of a "radial component" to myelin, described in *Plp1* null mice, created by aqueous channels that span the myelin sheath. Additional factors, such as astrocytosis, may also contribute to the increased radial diffusion. It should also be mentioned that a slight and insignificant increase in parallel diffusion may be accounted for by the parallel arraignment of the glial processes of astrocytes that occupying the vast extracellular space due to myelin loss. The results indicated that radial and parallel indices are sensitive markers of WM pathology and the parameters may be sensitive to abnormalities that are not apparent on the histological markers. The decrease in FA supports the pathologic findings that the architectural arraignment is completely disrupted due to thinning to degenerative axons. This loss compromised the density and sophisticated pattern that describes the trajectory of neural fibers throughout the white matter. With previous knowledge and current findings, it is not a surprise that an astounding decrease in FA was found across the heterogeneous nature of PMD. This data supports the use of MRI as a clinical tool to follow the natural history of PMD, and potentially for its application in evaluation of future therapies.

APPENDIX A

ABBREVIATIONS INCLUDED IN THIS DISSERATIONS

PMD	pelizaeus-merzbacher disease
PLP	proteolipid protein
CNS	central nervous system
UPR	unfolded protein response
MS	multiple sclerosis
ER	endoplasmic reticulum
ECM	extracellular matrix
MBP	myelin basic protein
IPL	intraperiod line
MAG	myelin associated glycoprotein
GFAP	glial fibrillary acidic protein
NF	neurofilament
GalC	galactocerebroside C
FDS	functional disability score
PNS	peripheral nervous system
PMP22	peripheral myelin protein
WM	white matter
WMV	white matter volume
ALIC	anterior limb internal capsule
PLIC	posterior limb internal capsule
Po	pons
SCC	splenius corpus callosum
GCC	genu corpus callosum
CP	cerebral peduncles
DCE	direction encoded map
FLAIR	fluid attenuated inversion recovery
MRI	magnetic resonance imaging
DTI	diffusion tensor imaging
MRS	magnetic resonance imaging
DT-MRI	diffusion tensor magnetic resonance imaging
ADC	apparent diffusion coefficient
FA	fractional anisotropy
FCN	ferric cyanide
OLG	oligodendrocyte

APPENDIX B

Functional Disability Rating Scale   Patient name: _____

Age: _____   Date of birth:_____   Date of exam: _____

*Education   ☐ 0   ☐ 1   ☐ 2   ☐ 3   0 – no formal schooling; 1 – special school or special education classes; 2 – regular classes, but not at grade level; 3 – regular school, grade appropriate for age (within 2 years)

* If beyond school age:
Employment   ☐ 0   ☐ 1   ☐ 2   ☐ 3   0 – unable to work/homebound; 1 – sheltered workshop (i.e. works at institution dedicated to disable employees); 2 – special job (i.e. works at conventional workplace, but requires special supervision); 3 – regular job

Speech   ☐ 0   ☐ 1   ☐ 2   ☐ 3   ☐ 4   0 – no verbal communication; 1 – rare understandable words with nonverbal communication; 2 – speech understandable with difficulty; 3 – detectable speech disturbance but readily understood; 4 – normal speech

Feeding ☐ 0   ☐ 1   ☐ 2   ☐ 3   ☐ 4   0 – tube feedings only; 1 – some oral feeding, with supplemental tube feedings; 2 – oral feedings with consistency changes to diet; 3 – normal diet with occasional choking; 4 – normal swallowing

Dressing   ☐ 0   ☐ 1   ☐ 2   ☐ 3   0 – total dependence; 1 – Can assist with dressing but dependent on others 2 – independent, but with decreased efficiency; 3 – normal

Toileting   ☐ 0   ☐ 1   ☐ 2   ☐ 3   0 – total dependence; 1 – needs assistance; 2 – independent, but with decreased efficiency; 3 – normal

Writing ☐ 0   ☐ 1   ☐ 2   ☐ 3   ☐ 4   ☐ 5   0 – cannot reach for and grasp writing utensil; 1 – can point to correct letters on computer screen with hand or mouse; 2 – can reach for and grasp writing utensil, but cannot scribble; 3 – can scribble, but cannot draw or write letters; 4 – can draw or write letters, but difficult to read; 5 – normal for age

Sitting ☐ 0   ☐ 2   0 – cannot sit without support; 2 – can sit without support

Walking ☐ 0   ☐ 1   ☐ 2   ☐ 3   ☐ 4   ☐ 5

0 – wheelchair or bedbound; 1 – can crawl/bunny hop; 2– can walk a few steps, but needs adaptive aids or other support; 3 – needs adaptive aids to walk 20 feet;   4 – impaired gait, but uses no assistive devices; 5 – normal gait

Breathing □ 0   □ 1   □ 2   □ 3   0 – ventilator or constant respiratory support; 1 – intermittent use of non-invasive respiratory support; 2 – has respiratory symptoms but does not use ventilatory support; 3 – normal breathing

Total Functional Disability Score:

Percentile (of scorable items) scores:

REFERENCES

1. Aalfs, C. M., J. H. Koelman, et al. (1993). "Posterior tibial nerve somatosensory evoked potentials in slowly progressive spastic paraplegia: a comparative study with clinical signs." Journal of Neurology **240**(6): 351-356.

2. Anderson, V. M., L. K. Fisniku, et al. (2009). "MRI measures show significant cerebellar gray matter volume loss in multiple sclerosis and are associated with cerebellar dysfunction." Mult Scler **15**(7): 811-817.

3. Anderson, T. J., A. Schneider, et al. (1998). "Late-Onset Neurodegeneration in Mice with Increased Dosage of the Proteolipid Protein Gene." Journal of Comparative Neurology **394**: 506-519.

4. André, M., P. Monin, et al. (1990). "Pelizaeus-Merzbacher disease. Contribution of magnetic resonance imaging to an early diagnosis." Journal de Neuroradiologie **17**(3): 216-221.

5. Arroyo, E. J. and S. S. Scherer (2000). "On the molecular architecture of myelinated fibers." Histochem Cell Biol **113**(1): 1-18.

6. Barker, P. B. and A. Horska (2004). "Neuroimaging in leukodystrophies." J Child Neurol **19**(8): 559-570.

7. Barkovich, A. J. (2000). "Concepts of myelin and myelination in neuroradiology." American Journal of Neuroradiology **21**(6): 1099-1109.

8. Barkovich, A. J. (2005). "Magnetic resonance techniques in the assessment of myelin and myelination." J Inherit Metab Dis **28**(3): 311-343.

9. Barkovich, A. J., B. O. Kjos, et al. (1988). "Normal maturation of the neonatal and infant brain: MR imaging at 1.5 T." Radiology **166**(1 Pt 1): 173-180.

10. Bar-Or, A., E. M. Oliveira, et al. (1999). "Molecular pathogenesis of multiple sclerosis." J Neuroimmunol **100**(1-2): 252-259.

11. Barkovich AJ., Toxic and metabolic brain disorders, in Pediatric Neuroimaging. Philadelphia, Lippincott Willams & Wilkins; 2000.

12. Baslow, M. H. (2000). "Canavan's spongiform leukodystrophy: a clinical anatomy of a genetic metabolic CNS disease." J Mol Neurosci **15**(2): 61-69.

13. Baumann, N. and D. Pham-Dinh (2001). "Biology of oligodendrocyte and myelin in the mammalian central nervous system." Physiol Rev **81**(2): 871-927.

14. Bermel, R. A., R. Bakshi, et al. (2002). "Bicaudate ratio as a magnetic resonance imaging marker of brain atrophy in multiple sclerosis." Arch Neurol **59**(2): 275-280.

15. Bjartmar, C., X. Yin, et al. (1999). "Axonal pathology in myelin disorders." J Neurocytol **28**(4-5): 383-395.

16. Bjartmar, C. and B. D. Trapp (2001). "Axonal and neuronal degeneration in multiple sclerosis: mechanisms and functional consequences." Curr Opin Neurol **14**(3): 271-278.

17. Bjartmar, C., J. R. Wujek, et al. (2003). "Axonal loss in the pathology of MS: consequences for understanding the progressive phase of the disease." J Neurol Sci **206**(2): 165-171.

18. Black, J. A., J. D. Kocsis, et al. (1990). "Ion channel organization of the myelinated fiber." Trends Neurosci **13**(2): 48-54.

19. Boison, D., H. Bussow, et al. (1995). "Adhesive properties of proteolipid protein are responsible for the compaction of CNS myelin sheaths." J Neurosci **15**(8): 5502-5513.

20. Boison, D. and W. Stoffel (1994). "Disruption of the compacted myelin sheath of axons of the central nervous system in proteolipid protein-deficient mice." Proceedings of the National Academy of Sciences USA **91**(24): 11709-11713.

21. Bonekamp, D., L. M. Nagae, et al. (2007). "Diffusion tensor imaging in children and adolescents: reproducibility, hemispheric, and age-related differences." Neuroimage **34**(2): 733-742.

22. Bradl, M. and C. Linington (1996). "Animal models of demyelination." Brain Pathol **6**(3): 303-311.

23. Brady, S. T., A. S. Witt, et al. (1999). "Formation of compact myelin is required for maturation of the axonal cytoskeleton." J Neurosci **19**(17): 7278-7288.

24. Brenner, M., A. B. Johnson, et al. (2000). "Mutations in GFAP associated with infantile, juvenile, and adult forms of Alexander disease." Journal of Neurochemistry **74**: S4-S4.

25. Budde, M. D., J. H. Kim, et al. (2007). "Toward accurate diagnosis of white matter pathology using diffusion tensor imaging." Magn Reson Med **57**(4): 688-695.

26. Bradl, M. and C. Linington (1996). "Animal models of demyelination." Brain Pathol **6**(3): 303-311.

27. Cailloux, F., F. Gauthier-Barichard, et al. (2000). "Genotype-phenotype correlation in inherited brain myelination defects due to proteolipid protein gene mutations " Eur J Hum Genet **8**(11): 837-845.

28. Caon, C., M. Zvartau-Hind, et al. (2003). "Intercaudate nucleus ratio as a linear measure of brain atrophy in multiple sclerosis." Neurology **60**(2): 323-325.

29. Cassol, E., J. P. Ranjeva, et al. (2004). "Diffusion tensor imaging in multiple sclerosis: a tool for monitoring changes in normal-appearing white matter." Mult Scler **10**(2): 188-196.

30. Cercignani, M., M. Inglese, et al. (2001). "Mean diffusivity and fractional anisotropy histograms of patients with multiple sclerosis." <u>AJNR Am J Neuroradiol</u> **22**(5): 952-958.

31. Cheon, J. E., I. O. Kim, et al. (2002). "Leukodystrophy in children: A pictorial review of MR imaging features." <u>Radiographics</u> **22**(3): 461-476.

32. Ciccarelli, O., D. J. Werring, et al. (2003). "A study of the mechanisms of normal-appearing white matter damage in multiple sclerosis using diffusion tensor imaging--evidence of Wallerian degeneration." <u>J Neurol</u> **250**(3): 287-292.

33. Ciccarelli, O., D. J. Werring, et al. (2001). "Investigation of MS normal-appearing brain using diffusion tensor MRI with clinical correlations." <u>Neurology</u> **56**(7): 926-933.

34. Concha, L., D. W. Gross, et al. (2006). "Diffusion tensor imaging of time-dependent axonal and myelin degradation after corpus callosotomy in epilepsy patients." <u>Neuroimage</u> **32**(3): 1090-1099.

35. Davie, C. A., G. J. Barker, et al. (1995). "Persistent functional deficit in multiple sclerosis and autosomal dominant cerebellar ataxia is associated with axon loss [published erratum appears in Brain 1996 Aug;119(Pt 4):1415]." <u>Brain</u> **118**(Pt 6): 1583-1592.

36. Deluca, G. C., G. C. Ebers, et al. (2004). "The extent of axonal loss in the long tracts in hereditary spastic paraplegia." <u>Neuropathol Appl Neurobiol</u> **30**(6): 576-584.

37. De Stefano, N., P. M. Matthews, et al. (1998). "Axonal damage correlates with disability in patients with relapsing- remitting multiple sclerosis. Results of a longitudinal magnetic resonance spectroscopy study." <u>Brain</u> **121**(Pt 8): 1469-1477.

38. Demaerel, P., C. Faubert, et al. (1991). "MR findings in leukodystrophy." <u>Neuroradiology</u> **33**(4): 368-371.

39. Diehl, H. J., M. Schaich, et al. (1986). "Individual exons encode the integral membrane domains of human myelin proteolipid protein [published erratum appears in Proc Natl Acad Sci U S A 1991 Apr;86(6):617-8]." <u>Proc Nat Acad Sci Usa</u> **83**(24): 9807-9811.

40. Drobyshevsky, A., S. K. Song, et al. (2005). "Developmental changes in diffusion anisotropy coincide with immature oligodendrocyte progression and maturation of compound action potential." <u>J Neurosci</u> **25**(25): 5988-5997.

41. genic mouse model of Pelizaeus-Merzbacher disease." <u>EMBO Mol Med</u> **2**(2): 42-50.

42. Edgar, J. M., M. McLaughlin, et al. (2003). "Axonal pathology in proteolipid protein deficient mice." <u>Journal of Neurochemistry</u> **85**: 97-97.

43. Edgar, J. M., M. C. McCulloch, et al. (2010). "Demyelination and axonal preservation in a transgenic mouse model of Pelizaeus-Merzbacher disease." <u>EMBO Mol Med</u> **2**(2): 42-50.

44. Ellis, D. and S. Malcolm (1994). "Proteolipid protein gene dosage effect in Pelizaeus-Merzbacher disease " <u>Nature Genetics</u> **6**(4): 333-334.

45. Engelbrecht, V., A. Scherer, et al. (2002). "Diffusion-weighted MR imaging in the brain in children: Findings in the normal brain and in the brain with white matter diseases." <u>Radiology</u> **222**(2): 410-418.

46. Fazekas, F., R. Kleinert, et al. (1993). "Pathologic correlates of incidental MRI white matter signal hyperintensities." <u>Neurology</u> **43**(9): 1683-1689.

47. Filippi, M., M. Cercignani, et al. (2001). "Diffusion tensor magnetic resonance imaging in multiple sclerosis." <u>Neurology</u> **56**(3): 304-311.

48. Garbern, J. (1999). "PLP mutations in man." from http://www.med.wayne.edu/neurology/plp.html.

49. Garbern, J., F. Cambi, et al. (1999). "The molecular pathogenesis of Pelizaeus-Merzbacher disease." Arch Neurol **56**(10): 1210-1214.

50. Garbern, J. Y. (2005). "Pelizaeus-Merzbacher disease: pathogenic mechanisms and insights into the roles of proteolipid protein 1 in the nervous system." J Neurol Sci **228**(2): 201-203.

51. Garbern, J. Y., F. Cambi, et al. (1999). "Peripheral neuropathy caused by proteolipid protein gene mutations." Ann N Y Acad Sci **883**: 351-365.

52. Garbern, J. Y., F. Cambi, et al. (1997). "Proteolipid protein (PLP) expression is critical for PNS as well as CNS myelination: Molecular and pathological characterization of a family with a novel PLP mutation." Neurology **48**: 6093.

53. Garbern, J. Y., F. Cambi, et al. (1997). "Proteolipid protein is necessary in peripheral as well as central myelin." Neuron **19**(1): 205-218.

54. Garbern, J. Y., I. R. Griffiths, et al. (2000). "Proteolipid protein is necessary for axonal integrity." Journal of Neurochemistry **74**: S94-S94.

55. Garbern, J. Y., F. Cambi, et al. (1997). "Proteolipid protein (PLP) expression is critical for PNS as well as CNS myelination: Molecular and pathological characterization of a family with a novel PLP mutation." Neurology **48**: 6093.

56. Garbern, J. Y., D. A. Yool, et al. (2002). "Patients lacking the major CNS myelin protein, proteolipid protein 1, develop length-dependent axonal degeneration in the absence of demyelination and inflammation." Brain **125**(Pt 3): 551-561.

57. Gencic, S., D. Abuelo, et al. (1989). "Pelizaeus-Merzbacher disease: an X-linked neurologic disorder of myelin metabolism with a novel mutation in the gene encoding proteolipid protein." American Journal of Human Genetics **45**(3): 435-442.

58. Gieselmann, V. (2003). "Metachromatic leukodystrophy: recent research developments." J Child Neurol **18**(9): 591-594.

59. Gold, R., H. P. Hartung, et al. (2000). "Animal models for autoimmune demyelinating disorders of the nervous system." Mol Med Today **6**(2): 88-91.

60. Gow, A., C. M. Southwood, et al. (1999). "CNS myelin and sertoli cell tight junction strands are absent in Osp/claudin-11 null mice." Cell **99**(6): 649-659.

61. Gow, A., V. L. Friedrich, Jr., et al. (1994). "Intracellular transport and sorting of the oligodendrocyte transmembrane proteolipid protein." Journal of Neuroscience Research **37**(5): 563-573.

62. Gow, A., V. L. Friedrich, Jr., et al. (1994). "Many naturally occurring mutations of myelin proteolipid protein impair its intracellular transport." Journal of Neuroscience Research **37**(5): 574-583.

63. Gow, A. and R. A. Lazzarini (1996). "A cellular mechanism governing the severity of Pelizaeus-Merzbacher Disease." Nature Genetics **13**(4): 422-428.

64. Gow, A., C. M. Southwood, et al. (2002). "The unfolded protein response is activated in Pelizaeus-Merzbacher disease." Molecular Biology of the Cell **13**: 264A-264A.

65. Gow, A., C. M. Southwood, et al. (1998). "Disrupted proteolipid protein trafficking results in oligodendrocyte apoptosis in an animal model of Pelizaeus-Merzbacher disease." J Cell Biol **140**(4): 925-934.

66. Griffiths, I., M. Klugmann, et al. (1998). "Axonal swellings and degeneration in mice lacking the major proteolipid of myelin." Science **280**: 1610 - 1613.

67. Griffiths, I., M. Klugmann, et al. (1998). "Current concepts of PLP and its role in the nervous system." Microsc Res Tech **41**(5): 344-358.

68. Griffiths, I. R. (1996). "Myelin mutants: model systems for the study of normal and abnormal myelination." <u>Bioessays</u> **18**(10): 789-797.

69. Griffiths, I. R., A. Schneider, et al. (1995). "Transgenic and natural mouse models of proteolipid protein (PLP)-related dysmyelination and demyelination." <u>Brain Pathology</u> **5**(3): 275-281.

70. Harding, B., D. Ellis, et al. (1995). "A case of Pelizaeus-Merzbacher disease showing increased dosage of the proteolipid protein gene." <u>Neuropath Appl Neurobiol</u> **21**(2): 111-115.

71. Harsan, L. A., P. Poulet, et al. (2007). "Astrocytic hypertrophy in dysmyelination influences the diffusion anisotropy of white matter." <u>J Neurosci Res</u> **85**(5): 935-944.

72. Harsan, L. A., P. Poulet, et al. (2006). "Brain dysmyelination and recovery assessment by noninvasive in vivo diffusion tensor magnetic resonance imaging." <u>J Neurosci Res</u> **83**(3): 392-402.

73. Henry, R. G., J. Oh, et al. (2003). "Directional diffusion in relapsing-remitting multiple sclerosis: a possible in vivo signature of Wallerian degeneration." <u>J Magn Reson Imaging</u> **18**(4): 420-426.

74. Hodes, M. E., C. A. Blank, et al. (1997). "Nonsense mutation in exon 3 of the proteolipid protein gene (PLP) in a family with an unusual form of Pelizaeus-Merzbacher disease." <u>Am J Med Genet</u> **69**(2): 121-125.

75. Hoozemans, J. J., E. S. van Haastert, et al. (2007). "Activation of the unfolded protein response in Parkinson's disease." <u>Biochem Biophys Res Commun</u> **354**(3): 707-711

76. Hoozemans, J. J., R. Veerhuis, et al. (2005). "The unfolded protein response is activated in Alzheimer's disease." <u>Acta Neuropathol</u> **110**(2): 165-172.

77. Houtchens, M. K., R. H. Benedict, et al. (2007). "Thalamic atrophy and cognition in multiple sclerosis." <u>Neurology</u> **69**(12): 1213-1223.

78. Hudson, L. D. (2003). "Pelizaeus-Merzbacher disease and spastic paraplegia type 2: two faces of myelin loss from mutations in the same gene." <u>J Child Neurol</u> **18**(9): 616-624.

79. Hudson, L. D., C. Puckett, et al. (1989). "Mutation of the proteolipid protein gene PLP in a human X chromosome-linked myelin disorder." <u>Proc Natl Acad Sci U S A</u> **86**(20): 8128-8131.

80. Huppi, P. S. (2001). "MR imaging and spectroscopy of brain development." <u>Magn Reson Imaging Clin N Am</u> **9**(1): 1-17, vii.

81. Inoue, K., H. Osaka, et al. (1999). "Proteolipid protein gene duplications causing Pelizaeus-Merzbacher disease: molecular mechanism and phenotypic manifestations." <u>Ann Neurol</u> **45**(5): 624-632.

82. Inoue, K. (2004). "PLP1-related inherited dysmyelinating disorders: Pelizaeus-Merzbacher disease and spastic paraplegia type 2." <u>Neurogenetics</u>.

83. Inoue, K., H. Osaka, et al. (1996). "A duplicated *PLP* gene causing Pelizaeus-Merzbacher disease detected by comparative multiplex PCR." <u>American Journal of Human Genetics</u> **59**: 32-39.

84. Kagawa, T., K. Ikenaka, et al. (1994). "Glial cell degeneration and hypomyelination caused by overexpression of myelin proteolipid protein gene." <u>Neuron</u> **13**(2): 427-442. Karim, S. A., J. A. Barrie, et al. (2007). "PLP overexpression perturbs myelin protein composition and myelination in a mouse model of Pelizaeus-Merzbacher disease." <u>Glia</u> **55**(4): 341-351.

85. Klugmann, M., M. H. Schwab, et al. (1997). "Assembly of CNS myelin in the absence of proteolipid protein." <u>Neuron</u> **18**(1): 59-70.

86. Knapp, P. E., R. P. Skoff, et al. (1986). "Oligodendroglial cell death in jimpy mice: an explanation for the myelin deficit." <u>J Neurosci</u> **6**(10): 2813-2822.

87. Koeppen, A. H., K. D. Barron, et al. (1988). "Comparative immunocytochemistry of Pelizaeus-Merzbacher disease, the jimpy mouse, and the myelin-deficient rat." <u>Journal of the Neurological Sciences</u> **84**(2-3): 315-327.

88. Kohlschutter, A., A. Bley, et al. (2010). "Leukodystrophies and other genetic metabolic leukoencephalopathies in children and adults." <u>Brain Dev</u> **32**(2): 82-89.

89. Laule, C., E. Leung, et al. (2006). "Myelin water imaging in multiple sclerosis: quantitative correlations with histopathology." <u>Mult Scler</u> **12**(6): 747-753.

90. Le Bihan, D., J. F. Mangin, et al. (2001). "Diffusion tensor imaging: concepts and applications." <u>J Magn Reson Imaging</u> **13**(4): 534-546.

91. Losseff, N. A. and D. H. Miller (1998). "Measures of brain and spinal cord atrophy in multiple sclerosis." <u>J Neurol Neurosurg Psychiatry</u> **64 Suppl 1**: S102-105.

92. Mar, S. and M. Noetzel (2010). "Axonal damage in leukodystrophies." <u>Pediatr Neurol</u> **42**(4): 239-242.

93. Matalon, R. and K. Michals-Matalon (1999). "Recent advances in Canavan disease." <u>Adv Pediatr</u> **46**: 493-506.

94. McKinstry, R. C., A. Mathur, et al. (2002). "Radial organization of developing preterm human cerebral cortex revealed by non-invasive water diffusion anisotropy MRI." <u>Cereb Cortex</u> **12**(12): 1237-1243.

95. Melhem, E. R., P. B. Barker, et al. (1999). "X-linked adrenoleukodystrophy in children: review of genetic, clinical, and MR imaging characteristics." <u>AJR Am J Roentgenol</u> **173**(6): 1575-1581.

96. Merzbacher, L. (1910). "Eine eigenarige familiär-hereditare Erkrankungsform (Aplasia axialis extra-corticalis congenita)." <u>Zeitschrift für gesamte Neurologie und Psychiatrie</u> **3**: 1-138.

97. Miller, D. H., R. I. Grossman, et al. (1998). "The role of magnetic resonance techniques in understanding and managing multiple sclerosis." <u>Brain</u> **121 (Pt 1)**: 3-24.

98. Morita, K., H. Sasaki, et al. (1999). "Claudin-11/OSP-based tight junctions of myelin sheaths in brain and Sertoli cells in testis." <u>J Cell Biol</u> **145**(3): 579-588.

99. Nave, K. A., A. Schneider, et al. (1995). "Mutations of the proteolipid protein gene: loss and gain of function." <u>Journal of Neurochemistry</u> **65**: S.

100. Nave, K. A., C. Lai, et al. (1987). "Splice site selection in the proteolipid protein (PLP) gene transcript and primary structure of the DM-20 protein of central nervous system myelin." <u>Proc Natl Acad Sci U S A</u> **84**(16): 5665-5669.

101. Ono, J., K. Harada, et al. (1997). "Differentiation of dys- and demyelination using diffusional anisotropy." <u>Pediatr Neurol</u> **16**(1): 63-66.

102. Ono, J., K. Harada, et al. (1995). "Differentiation between dysmyelination and demyelination using magnetic resonance diffusional anisotropy." <u>Brain Research</u> **671**(1): 141-148.

103. Onuki, M., M. M. Ayers, et al. (2001). "Axonal degeneration is an early pathological feature in autoimmune- mediated demyelination in mice." <u>Microsc Res Tech</u> **52**(6): 731-739.

104. Osaka, H., C. Kawanishi, et al. (1995). "Novel nonsense proteolipid protein gene mutation as a cause of X-linked spastic paraplegia in twin males." <u>Biochemical and Biophysical Research Communications</u> **215**(3): 835-841.

105. Patay, Z. (2005). "Diffusion-weighted MR imaging in leukodystrophies." Eur Radiol **15**(11): 2284-2303.

106. Peled, S. (2007). "New perspectives on the sources of white matter DTI signal." IEEE Trans Med Imaging **26**(11): 1448-1455.

107. Pelizaeus, F. (1885). "Über eine eigenthümliche Form Spastischer Lähmung mit Cerebralerschinungen auf hereditärer Grundlage (Multiple Sklerose)." Archiv fur Psychiatrie und Nervenkrankheiten **16**: 698-710.

108. Pfeiffer, S. E., A. E. Warrington, et al. (1993). "The oligodendrocyte and its many cellular processes." Trends Cell Biology **3**: 191-197.

109. Pham-Dinh, D., O. Boespflug-Tanguy, et al. (1993). "Pelizaeus-Merzbacher disease: a frameshift deletion/insertion event in the myelin proteolipid gene." Human Molecular Genetics **2**(4): 465-467.

110. Phelan, J. A., L. H. Lowe, et al. (2008). "Pediatric neurodegenerative white matter processes: leukodystrophies and beyond." Pediatr Radiol **38**(7): 729-749.

111. Raskind, W. H., C. A. Williams, et al. (1991). "Complete deletion of the proteolipid protein gene (PLP) in a family with X-linked Pelizaeus-Merzbacher disease." American Journal of Human Genetics **49**(6): 1355-1360.

112. Ridha, B. H., V. M. Anderson, et al. (2008). "Volumetric MRI and cognitive measures in Alzheimer disease : comparison of markers of progression." J Neurol **255**(4): 567-574

113. Readhead, C., A. Schneider, et al. (1994). "Premature arrest of myelin formation in transgenic mice with increased proteolipid protein gene dosage." Neuron **12**(3): 583-595.

114. Rosenbluth, J., K. A. Nave, et al. (2006). "Subtle myelin defects in PLP-null mice." Glia **54**(3): 172-182.

115. Saugier-Veber, P., A. Munnich, et al. (1994). "X-linked spastic paraplegia and Pelizaeus-Merzbacher disease are allelic disorders at the proteolipid protein locus." Nature Genetics **6**(3): 257-262

116. Schiffmann, R. and M. S. van der Knaap (2009). "Invited article: an MRI-based approach to the diagnosis of white matter disorders." Neurology **72**(8): 750-759.

117. Schmithorst, V. J., M. Wilke, et al. (2002). "Correlation of white matter diffusivity and anisotropy with age during childhood and adolescence: a cross-sectional diffusion-tensor MR imaging study." Radiology **222**(1): 212-218.

118. Schneider, J. F., K. A. Il'yasov, et al. (2004). "Fast quantitative diffusion-tensor imaging of cerebral white matter from the neonatal period to adolescence." Neuroradiology **46**(4): 258-266.

119. Seitelberger, F. (1970). Pelizaeus-Merzbacher disease. Handbook of Clinical Neurology. P. J. Vinken and G. W. Bruyn. Amsterdam, North Holland Publishing Co. **10:** 150-220.

120. Seitelberger, F. (1984). "Structural manifestations of leukodystrophies." Neuropediatrics **15**(Suppl): 53-61.

121. Seitelberger, F. (1995). "Neuropathology and genetics of Pelizaeus-Merzbacher disease." Brain Pathology **5**(3): 267-273.

122. Sima, A. A., C. R. Pierson, et al. (2009). "Neuronal loss in Pelizaeus-Merzbacher disease differs in various mutations of the proteolipid protein 1." Acta Neuropathol **118**(4): 531-539.

123. Simons, M., E. M. Kramer, et al. (2002). "Overexpression of the myelin proteolipid protein leads to accumulation of cholesterol and proteolipid protein in endosomes/lysosomes: implications for Pelizaeus-Merzbacher disease." J Cell Biol **157**(2): 327-336.

124. Simons, M., E. M. Kramer, et al. (2000). "Assembly of Myelin by Association of Proteolipid Protein with Cholesterol- and Galactosylceramide-rich Membrane Domains." J Cell Biol **151**(1): 143-154.

125. Sistermans, E. A., R. F. de Coo, et al. (1998). "Duplication of the proteolipid protein gene is the major cause of Pelizaeus-Merzbacher disease." Neurology **50**(6): 1749-1754.

126. Sistermans, E. A., I. J. de Wijs, et al. (1996). "Duplication of the proteolipid protein gene (PLP) is a frequent cause of Pelizaeus Merzbacher disease." Am Soc Human Gen **59**: A10.

127. Skoff, R. P. (1976). "Myelin deficit in the Jimpy mouse may be due to cellular abnormalities in astroglia." Nature **264**(5586): 560-562.

128. Skoff, R. P., D. L. Price, et al. (1976). "Electron microscopic autoradiographic studies of gliogenesis in rat optic nerve. II. Time of origin." J Comp Neurol **169**(3): 313-334.

129. Snook, L., L. A. Paulson, et al. (2005). "Diffusion tensor imaging of neurodevelopment in children and young adults." Neuroimage **26**(4): 1164-1173.

130. Song, J., B. D. Goetz, et al. (2005). "His36Pro point-mutated proteolipid protein retained in the endoplasmic reticulum of oligodendrocytes in the Shaking pup." Glia.

131. Song, S. K., S. W. Sun, et al. (2003). "Diffusion tensor imaging detects and differentiates axon and myelin degeneration in mouse optic nerve after retinal ischemia." Neuroimage **20**(3): 1714-1722.

132. Song, S. K., S. W. Sun, et al. (2002). "Dysmyelination revealed through MRI as increased radial (but unchanged axial) diffusion of water." Neuroimage **17**(3): 1429-1436.

133. Song, S. K., J. Yoshino, et al. (2005). "Demyelination increases radial diffusivity in corpus callosum of mouse brain." Neuroimage **26**(1): 132-140.

134. Southwood, C. M., J. Garbern, et al. (2002). "The unfolded protein response is activated in Pelizaeus-Merzbacher disease." Glia: S23-S23.

135. Southwood, C. M., J. Garbern, et al. (2002). "The unfolded protein response modulates disease severity in Pelizaeus-Merzbacher Disease." Neuron **36**(4): 585-596.

136. Suzuki, K. (2003). "Globoid cell leukodystrophy (Krabbe's disease): update." J Child Neurol **18**(9): 595-603.

137. Tatar, C. L., S. Appikatla, et al. (2010). "Increased Plp1 gene expression leads to massive microglial cell activation and inflammation throughout the brain." ASN Neuro **2**(4).

138. Tievsky, A. L., T. Ptak, et al. (1999). "Investigation of apparent diffusion coefficient and diffusion tensor anisotrophy in acute and chronic multiple sclerosis

139. Trapp, B. D., L. Bo, et al. (1999). "Pathogenesis of tissue injury in MS lesions." J Neuroimmunol **98**(1): 49-56.

140. Trapp, B. D., J. Peterson, et al. (1998). "Axonal transection in the lesions of multiple sclerosis " N Engl J Med **338**(5): 278-285.

141. Trofatter, J. A., S. R. Dlouhy, et al. (1989). "Pelizaeus-Merzbacher disease: tight linkage to proteolipid protein gene exon variant." Proc Natl Acad Sci U S A **86**(23): 9427-9430.

142. Ulrich, J., R. Kohler, et al. (1983). "Immunocytochemical investigations of some human leukodystrophies." Acta Neuropathologica **60**(3-4): 199-206.

143. van der Knaap, M. S. (2001). "Magnetic resonance in childhood white-matter disorders." Dev Med Child Neurol **43**(10): 705-712.

144. van der Knaap, M. S., P. G. Barth, et al. (1997). "A new leukoencephalopathy with vanishing white matter." Neurology **48**(4): 845-855.

145. van der Knaap, M. S. and J. Valk (1995). <u>Magnetic resonance of myelin, myelination, and myelin disorders</u>. Berlin ; New York, Springer.

146. Werring, D. J., C. A. Clark, et al. (1999). "Diffusion tensor imaging of lesions and normal-appearing white matter in multiple sclerosis." <u>Neurology</u> **52**(8): 1626-1632.

147. Wolf, N. I., E. A. Sistermans, et al. (2005). "Three or more copies of the proteolipid protein gene PLP1 cause severe Pelizaeus-Merzbacher disease." <u>Brain</u> **128**(Pt 4): 743-751.

148. Woodruff, R. H., N. Tekki-Kessaris, et al. (2001). "Oligodendrocyte development in the spinal cord and telencephalon: common themes and new perspectives." <u>Int J Dev Neurosci</u> **19**(4): 379-385.

149. Woodward, K. J. (2008). "The molecular and cellular defects underlying Pelizaeus-Merzbacher disease." <u>Expert Rev Mol Med</u> **10**: e14.

150. Woodward, K. and S. Malcolm (2001). "CNS myelination and PLP gene dosage." <u>Pharmacogenomics</u> **2**(3): 263-272.

151. Yool, D. A., J. M. Edgar, et al. (2000). "The proteolipid protein gene and myelin disorders in man and animal models." <u>Hum Mol Genet</u> **9**(6): 987-992.

152. Yool, D. A., M. Klugmann, et al. (2001). "Myelin proteolipid proteins promote the interaction of oligodendrocytes and axons." <u>J Neurosci Res</u> **63**(2): 151-164

153. Zeman, W., W. DeMyer, et al. (1964). "Pelizaeus-Merzbacher disease: A study in nosology." <u>J Neuropath Exp Neurol</u> **23**: 334-354

154. Zivadinov, R., M. Stosic, et al. (2008). "The place of conventional MRI and newly emerging MRI techniques in monitoring different aspects of treatment outcome." <u>J Neurol</u> 255 Suppl 1: 61-74.

ABSTRACT

APPLICATION OF MAGNETIC RESONANCE IMAGING TO UNDERSTANDING THE PATHOGENESIS OF THE X-LINKED LEUKODYSTROPHY PELIZAEUS-MERZBACHER DISEASE

by

JEREMY JEROME LAUKKA

May 2011

Advisor: John Kamholz, M.D., Ph.D.

Major: Molecular Biology and Genetics

Degree: Doctor of Philosophy

Myelin is a multilamellar membrane structure surrounding axons in both the CNS and PNS that facilitates nerve conduction. In the CNS, myelin is synthesized by oligodendrocytes, while in the PNS; myelin is synthesized by Schwann cells. In the CNS, Proteolipid protein 1 (*PLP1*), an integral membrane protein, is the major protein component of myelin, constituting ~50% of myelin protein. Mutations of the *PLP1* gene in man cause a spectrum of neurological disease, ranging from the severe Pelizaeus-Merzbacher disease (PMD), that typically begins during infancy with nystagmus, seizures and hypotonia and evolves into spastic quadriparesis, cognitive impairment and ataxia, to 'pure' spastic paraparesis, that is characterized exclusively by leg spasticity and weakness. The predominant pathological abnormality in PMD consists of thinning to almost complete absence of myelin in the CNS. Gow and colleagues have proposed that the severity of mutations that alter the structure of PLP1 (typically missense mutations) correlates with the degree to which they cause protein misfolding, activate the unfolded protein

response, and cause oligodendrocyte apoptosis (Gow and Sharma, Neuromolecular Med 4:73, 2003). Implicit in this mechanism is that the degree of myelination should inversely correlate with the degree to which oligodendrocyte apoptosis is activated. We speculated that the early PMD phenotype predominantly is dictated by the effect on oligodendrocyte viability. In contrast, we have found that complete absence of PLP1 in both mice and humans is characterized by well-formed myelin, but late length-dependent pattern of axonal degeneration (Garbern et al. Brain 125:551, 2002). We speculate that progression of disease correlates with the rate of axonal damage. The goal of this study was to investigate whether non-invasive MR techniques to assess extent of myelination and degree of axonal disruption correlated with measures of clinical capacity. Furthermore we wanted to differentiate between axonal and myelin pathology using diffusion tensor imaging as a reliable imaging modality to assess the effects of *PLP1* mutations on water diffusion in central nervous system (CNS) white matter. The most dramatic difference between PMD patients and age-matched controls was increased $\lambda_\perp$, most marked in the corpus callosum. Moreover, this was most prominent in patients with *PLP1* null mutations. Increased radial diffusion has been reported in dysmyelinating rodents, including the myelin synthesis deficient rat (*md*) that has a severe *Plp1* missense mutation. Interestingly, $\lambda_{//}$ was also increased in the severely affected PMD patients, whereas in severely dysmyelinated rodents, the $\lambda_\perp$ is reported to be normal to decreased. $\lambda_{//}$ in patients with *PLP1* null mutations was relatively unaffected relative to controls. Since the degree of myelination is relatively preserved in PLP1 null myelin, the increased radial diffusion is not the result of thinner myelin sheaths. Therefore the increased radial diffusion is more likely due to increased myelin water, due to decreased compaction, and which may be in part due to the existence of a "radial component" to myelin,

described in *Plp1* null mice, created by aqueous channels that span the myelin sheath. Additional factors, such as astrocytosis, may also contribute to the increased radial diffusion.

Genetic abnormalities affecting the *PLP1* gene has been shown to cause axonal injury and significant early-onset dysmyelination and late-onset demyelination. The exact mutational mechanism remains to be described, although substantial progress had been made to make reasonable assessments that may provide a better understanding towards the disease pathogenesis. In the study involving autopsy tissue from genetically characterized patients has provided valuable information that describes the changes in the structural architecture of the tissue over time. These pathologic changes corroborate with the findings from the diffusion imaging making these two methods extremely reliable for describing the pathologic state as each patient experience a slightly different pathogenic course that is dependent on the exact *PLP1* mutation.

AUTOBIOGRAPHICAL STATEMENT

Jeremy J. Laukka

Education

2010   Ph.D. Molecular Biology and Genetics, Center for Molecular Medicine and Genetics, Wayne State University School of Medicine, Detroit, Michigan

2005   M.S. Basic Medical Science, Wayne State University School of Medicine, Detroit, Michigan

2003   B.S. Physiology, Michigan State University, College of Natural Science, East Lansing, Michigan

Certifications:

2008   Certified teacher of gross anatomy, Michigan State University, Department of Radiology, Division of Anatomy and Structural Biology

Publications:

Uhal BD., Wang R., Laukka J**.**, Zhuang J., Soledad-Conrad V., Filippatoa G. Inhibition of amiodarone-induced lung fibrosis but not alveolitis by angiotensin system antagonists. *Journal of Pharmacology and Toxicology*, in press for Vol 91, Issue 6 (Dec), 2002.

Uhal BD., Rayford H., Zhuang J., Li Xiaopeng. Laukka J**.**, Soledad-Conrad V. Apoptosis-dependent acute lung injury and repair after intratracheal instillation of norepinephrine in rats. In Press, *Journal of Experimental Physiology*, 2003.

Uhal BD, H. Rayford, X. Li, J. Laukka, J Zhaung and V Conrad. Alveolar epithelial apoptosis and acute lung injury by intratracheal instillation of norepinephrine. *Faseb*. J. 16:A412, 2002.

Presentations at Educational and Research Conferences

2009   International Society of Magnetic Resonance Imaging in Medicine. Honolulu, Hawaii. April 2009. Diffusion Tensor Imaging in Pelizaeus-Merzbacher disease

2006   International Society of Magnetic Resonance Imaging in Medicine. Seattle, WA. May 2006. Application of Magnetic resonance imaging to understanding pathogenesis of X-linked leukodystropy Pelizaeus-Merzbacher disease.

2005   The 5th Great Lake Glia meeting, Traverse City, Michigan. Neuroradiological correlates of clinical disability and progression in Pelizaeus-Merzbacher Disease.

2005   American Society of Neuroradiology. Toronto, Ontario Canada. May 21, 2005. Neuroradiological correlates of clinical disability and progression in Pelizaeus-Merzbacher Disease.